OSTEOINDUCTIVE MATERIAL DERIVED FROM DIFFERENTIATING EMBRYONIC STEM CELLS

A Dissertation
Presented to
The Academic Faculty

by

Ken Sutha

In Partial Fulfillment
of the Requirements for the Degree
Doctor of Philosophy in the
Wallace H. Coulter Department of Biomedical Engineering

Georgia Institute of Technology
May 2013

OSTEOINDUCTIVE MATERIAL DERIVED FROM DIFFERENTIATING EMBRYONIC STEM CELLS

Approved by:

Dr. Todd C. McDevitt, Advisor
Wallace H. Coulter Department of Biomedical Engineering
Georgia Institute of Technology

Dr. Barbara D. Boyan
Wallace H. Coulter Department of Biomedical Engineering
Georgia Institute of Technology

Dr. Robert E. Guldberg
George W. Woodruff School of Mechanical Engineering
Georgia Institute of Technology

Dr. Julie O'Connell
Amniox Medical

Dr. Zvi Schwartz
Wallace H. Coulter Department of Biomedical Engineering
Georgia Institute of Technology

Dr. Johnna S. Temenoff
Wallace H. Coulter Department of Biomedical Engineering
Georgia Institute of Technology

Date Approved: January 23, 2012

To my parents - Surachai and Rumpa

ACKNOWLEDGEMENTS

My time as a part of the Biomedical Engineering Department at Georgia Tech and Emory has allowed me to develop both scientifically and personally, preparing me for any challenges that may lie ahead. I could not have made it to where I stand today without the help and support of many people that I would like to take this opportunity to thank.

First, I would like to thank the members of my thesis committee for the invaluable support and feedback over the past years—Dr. Todd McDevitt, Dr. Barbara Boyan, Dr. Robert Guldberg, Dr. Julie O'Connell, Dr. Zvi Schwartz, and Dr. Johnna Temenoff. Their support and guidance has significantly impacted the success of my project, particularly through their push for scientific rigor. In addition to serving as liaison from my thesis committee to the MD/PhD Executive Committee, Dr. Boyan's expert knowledge in bone biology and direct, thought provoking questions always kept me thinking about how my work fit within the larger context. Dr. Schwartz always challenged me to re-evaluate my data and conclusions during our regular meetings, and I owe the success of my *in vivo* studies completely to his expert surgical skills. Together, their generosity in opening the expertise and resources of their lab was fundamental and directly impactful to every stage of my project. Dr. Guldberg's questions and comments during meetings also spurred me to think more critically about my work and to take a step back to see the bigger picture. Dr. Temenoff's feedback was always very useful, and she provided invaluable suggestions that helped me to improve the statistical rigor with which I was able to analyze my data. Though we have only met in person once or twice,

it was always a pleasure to talk to Dr. O'Connell on the phone, and I appreciated her encouragement and perspective from the industry side with respect to evaluations of DBM. Each of my committee members has been encouraging through the completion of my project while challenging me to become a better scientist, and I thank them all for their time and commitment to my training.

Of course, the single person who has contributed the most to my growth and development as a scientist has been my advisor, Todd. I first approached Todd to be my co-advisor back during my time in Dr. Marie Csete's lab at Emory. After a year and a half that included early morning meetings at Emory and supporting me through my qualifying exams, Todd stepped up to take me into his lab as a full time student when Marie left Emory to return to California. My graduate school experience was completely turned on end, but Todd guided me through the stress and uncertainty of completely changing labs and projects and has helped me find my way over the past several years (though it may have taken more than a few threats of shaking). Todd has challenged his students to do the best science possible with his attention to detail, but even as his lab has grown, he was always accessible and easy to reach out to with any new data or concerns that came up in the course of research. His dedication to his students is unparalleled, and I cannot imagine having a more outstanding mentor (other than the brief scare of becoming a lab orphan for a second time). Thank you Todd for you guidance, support, and encouragement in my growth as a scientist. I must also take a moment to thank his wonderful wife, Meg, for always looking out for us, Todd's students, by making sure to keep Todd in check as he pushed for the best from us and of course by providing us with delicious food.

There are also a number of individuals I would like to acknowledge, including collaborators from various other labs in the BME department and the IBB, who contributed to my project with their expertise, advice, and help. First, I would like to thank Dr. Rene Olivares-Navarrete and Sharon Hyzy from the Boyan/Schwartz Lab for their significant contributions to my work throughout this entire dissertation. In addition to their work on the vitamin D_3 studies, they performed several other protein assays included here and provided assistance and guidance through three iterations of the *in vivo* experiments. Countless times when I had to drop by their offices to ask them even the simplest of questions, they always welcomed me with a smile and helpful suggestions, even if I was not dressed in lab appropriate attire. Also from their lab, I thank Dr. David Deustch for his assistance with animal surgeries and troubleshooting histology, Chris Hermann for his help and advice with μCT analysis, and Rolondo Gittens for performing the material characterizations. I greatly appreciate the training and advice given to me in using μCT by Angela Lin of the Guldberg Lab. I would also like to thank the members of the Temenoff Lab, particularly Taymour Hammoudi, Peter Yang, and Jennifer Lei, for their help in teaching me more about statistics. Dr. Brani Vidokovic also provided additional valuable feedback for the statistical analyses in my project.

In the IBB, Sha'Aqua Asberry in the histology core was tremendously helpful in training and helping me to troubleshoot histological methods that were imperative to my research. Megan Richards, though she has not been around long, has always been quick to offer assistance with anything I asked of her. I would also like to thank Dr. Laura O'Farrell, the veterinary consultant for the *in vivo* studies. Dr. O'Farrell, along with Kim Benjamin, helped ensure that all the appropriate tools were in place and that the surgeries

ran as smoothly as possible. I also appreciated the friendliness and helpfulness of the rest of the PRL staff, who always helped keep things running efficiently for my work, particularly over winter breaks and even during the snow/ice storm of January 2011. I would also like to thank the BME academic advisors past and present - Beth Bullock Spencer, Shannon Oliver Sullivan, and Sally Gerrish; as well as the financial staff – Sandra Wilson, Penelope Pollard for their patience and helping me with all the paperwork over the years. Outside of Tech, I thank Dr. Nick Liu of Zimmer, who provided me with a lot of feedback and advice regarding the *in vitro* evaluation of DBM osteoinductivity.

There are many individuals at Emory that I would like to thank as well. Directly contributing to this project, I thank Jeanette Taylor of the Robert P. Apkarian Integrated Electron Microscopy Core for her assistance in acquiring the transmission electron microscope images. Many thanks go to the entire Emory Medical Scientist Training Program, including its students, staff, and administration, for their support through my many years in the program. I thank my fellow students, an amazing and inspiring group of people to be around socially and scientifically. I thank its staff, Sabrina Mallett, Rebecca Sandidge, and formerly Barbara Powley, for keeping the program running like a well oiled machine and constantly solving any problems that may have come up for us. I also thank its directors past and present, Mary Horton, Dr. Chuck Parkos, Dr. Kerry Ressler, Dr. Aron Lukacher, and Dr. Marie Csete, for their support and always being there to talk to about anything. A special thank you goes to Marie, who was also my original thesis advisor, for being such an amazing role model of all the things that a physician scientist can be, from the time she sat with me to help me revise my first abstract to when she was overseeing the administration of anesthesia during my

transplant. I thank the former members of the Csete lab for my introduction to the world of stem cell research during my first two years of graduate school, in particular my karaoke duet partner, Dr. Danielle Drury-Stewart, for the fun times we had while working together and since.

Though it was difficult to leave the Csete Lab behind, I was welcomed with open arms by the members of the McDevitt Lab, without whom I now cannot imagine having made it through graduate school. The McDevitt Lab has been such an amazing place to be for my growth scientifically and personally, and for that I thank its members past and present. The three senior students in the lab when I arrived full time, Dr. Rekha Nair, Dr. Rich Carpenedo, Dr. Carolyn Sargent, having been Todd's first guinea pigs, established an amazingly strong foundation that allowed the rest of us thrive and really set a high bar for what it meant to be a member of the lab, not only scientifically but also recreationally. Rekha, the trail blazer in the study of acellular EB matrices, was an inspiration with her work ethic, and I will always remember and appreciate her for making sure I had all my essential body parts intact after we hiked to the top of Mt. Si. Rich helped establish the high standard of scientific rigor in the lab by being the one to ask the tough questions in lab meeting but was also a role model in all things eating challenge, cycling, bacon, or crossword puzzle related. Carolyn was always approachable, helping me out and answering my stupid questions with a smile, and she really changed my life tremendously outside of the lab by encouraging me to become more active through the pilates and spin classes she taught at the CRC and by helping me to train for my first triathlon.

In addition to the original group, three more students were in the lab when I joined, Dr. Alyssa Ngangan Kitchel, Dr. Andres Bratt-Leal, and Dr. Barbara Nsiah.

Alyssa, in addition to being my fellow Thai, Infiniti-driving foodie, expanded upon Rekha's studies of acellular EB matrices and directly paved the way for my *in vivo* work with the techniques she developed. In addition to several other titles she has collected while being in the McDevitt lab, she has had the distinction of being my "workout wife," which I am glad is OK with her actual husband, Brandon, who I also thank for frequently serving as my fashion consultant. Andrés was one of my original BME classmates, and from the first time I sat next to him waiting for lunch on the first day of orientation, he has truly been a great friend and colleague. I am especially grateful that he was able share the experience of Camp Independence with me as my assistant counselor. Like Carolyn, Andrés was instrumental in getting me into better shape by serving as trainer for our early morning "Pumping Iron" crew, and we also had many fun, long bike rides together with Alyssa, Rich, Carolyn, and his girlfriend Erin Spinner (my fellow yogi, tri-training partner, classmate, and friend). Barbara, who would drop in from time to time for our workouts, also started full time in the lab shortly before I did. Unwavering, in the face of peer pressure, her independence has shined through in everything she has done. She has been a great person to be around both inside and outside of lab, always helping to keep me on track and motivating me by serving as a sounding board through the ups and downs of graduate school. Barbara has always looked out for me, whether she was bringing me food from her lunch seminars or providing me consultation on my wardrobe choices. Though it was often difficult to overcome her love of her bed and to get her out past her bedtime, Barbara was a great companion for late night excursions to Disney World and definitely knew her way around the dance floor! As we have progressed through graduate school together, I have been so fortunate to have such a group of peers

to motivate and support me. Each hurdle has seemed that much more doable because we were meeting the challenge together.

It was a little over a year before the next student, Melissa Kinney, entered the fold. As the baby of the lab for quite a while, we were always protective of her, but she has really come into her own as she has assumed the role of senior graduate student. Her dedication and hard work impressed me from the beginning, and she has only continued to surpass the high expectations set for her. Melissa and her boyfriend, Phil Keegan, have also been amazing hosts, and I appreciate them inviting us into their home for our lab Dexter viewing parties, even if it was only for me to fall asleep on the floor. After another dry spell, we welcomed Jenna Wilson, Anh Nguyen, and Doug White, and each has been a great addition to the lab, for both their scientific contributions and other qualities they bring, especially related to the many McDevitt Lab food traditions. I was lucky enough to be the beneficiary of Jenna's birthday cake baking skills, and I was happy to see the foodie streak in the lab will live on in Anh as she works her way through the Eater 38 list. Since Doug splits his time with the Kemp lab, I have not had as many opportunities to assess his cooking or eating skills, but after a strong showing at our last holiday cookie exchange, I am confident he is up to the challenge. I look to them to carry on all the things that make the McDevitt Lab such a great environment to work in, scientifically and gastronomically. I have also had less time to get to know the newest batch of students to join our lab family—Marian Hettiaratchi (newly minted American driver), Denise Sullivan (the maker of a mean banana pudding), Melissa Goude (heir to my role as lab photographer), and Josh Zimmermann (fellow sci-fi/comic/tv aficionado)—but based on all they have accomplished so far in their short time in lab, I

have no doubt they will continue on to outstanding and productive graduate student careers.

In addition to the graduate students, there are many others in the lab who have contributed to making it such a great place to work. The first post doc to join the lab was Dr. Priya Baraniak, and along with instituting the lab holiday cookie exchange, she has provided me with tremendous help with her feedback on experiments and writing. Dr. Ankur Singh and Dr. Krista Fridley both came to us from the Roy Lab at the University of Texas, and brought with them their great scientific minds and strong work ethics, which will no doubt continue to contribute to their success in our lab and beyond. As the lab has grown, its research technicians/lab managers/miracle workers past and present (Marissa Cooke, Jesse McClellan, Hallum Dickens, and Beth Krauth) have been a vital part of keeping the lab moving forward. A special thank you to Marissa whose hard work to keep things in order and running smoothly has always been accompanied by humor and a beautiful smile. I also thank Beth who performed the initial experiment that sparked the work leading to my dissertation. Though not actually a graduate student but an undergraduate researcher, Katy Hammersmith has been in the lab for so long and has worked so diligently that she has made it easy to forget she was not actually preparing to defend a PhD herself. Along with Barbara, she made for a fun and memorable night cavorting around the Magic Kingdom after hours. Last but most certainly not least from the lab, I would like to thank Lu Ling, an outstanding undergraduate researcher who has worked with me for the past two years and whose significant contributions to my work were critical to its completion. Lu has been an amazingly hard worker and thoughtful researcher, and I was very fortunate in having the opportunity to mentor her. With her

quiet and careful .work, she brought new perspectives and insights that helped to shape my project and the PFA studies in particular. Lu will no doubt continue to make major contributions to the lab as a new Petit Scholar, and I look forward to great things from her in the future.

I must also thank all of my friends—BME classmates, med school classmates, and those outside of school—for their constant support and for helping me to maintain balance in my life. With frequent trips to Buford Highway, shows at the Fox or Alliance, and game nights playing Wii, they kept me sane through the roller coaster ride of graduate school. A special thank you goes to Matt Barnett for letting me borrow his laptop AC adapter when mine died while writing my dissertation. Another group of people very important to my life since beginning graduate school has been the transplant community. Having started graduate school a few short months after receiving my kidney transplant, the two experiences are inextricably intertwined for me. I would like to thank all of the people I have met along my journey for what they have taught me about life and about living—my campers at Camp Independence, my teammates from Team Georgia and everyone from the Transplant Games, the children at Egelston, my fellow volunteers for the Georgia Transplant Foundation and Lifelink of Georgia, and those strangers whose negative opinions about organ donation I changed by sharing the story of my success. I would also like to thank the Georgia Transplant Foundation for the great honor of selecting me as its first Meg Jeffrey Memorial Scholarship recipient. I thank everyone with the Emory Transplant Center for the outstanding care I have received that has allowed me to continue on with my plans for graduate and medical school without having to miss a beat. I am especially thankful for their letting me set up my own personal work

station in the outpatient clinic while I worked on my dissertation. I also remember those from our community who have passed, in particular Mikey Leggett and Meg Jeffrey, as they remind me what this whole MD/PhD thing is ultimately for. Mikey, a heart transplant recipient, was my camper for four summers at Camp Independence, and his genuine excitement and innocence about everything always brought a smile to my face (particularly his short stint on the radio). Not a recipient herself, Meg ushered me into the transplant world as my first contact with the Emory Transplant Center while serving as a nurse coordinator. We became friends through our shared volunteer activities—pouring wine at fundraisers, handing out doughnuts while signing up organ donors, and playing bingo with the kids at CHOA—and seeing her wave at me from the audience during my Christmas concerts was something I looked forward to every year. She never met a stranger and was always there to offer a helping hand to all those she came across. Hers is an example by which I will always strive to live. I would also like to take this opportunity to thank all of the tissue donors from whom the DBM used for my studies was derived. As a transplant recipient, the magnitude of their gift in choosing to be organ and tissue donors has definitely not been lost on me.

Last and most importantly, I thank my family, without whom I would most certainly not be where I am today. My mom and dad, Dr. Rumpa Amornmarn and Dr. Surachai Sutha, as well as my grandparents, Che Peng and Me Cho Moy, and close extended family, Mittira Amornmarn, Anna Moy, Lina Amornmarn, Dr. Lulu Amornmarn, and Amy Amornmarn, have always loved and supported me. When I was a kid and got stuck on the first dungeon of Super Mario Bros, I was so frustrated and ready to give up, but my mom would not let me, telling me, “Don’t give up! You can do it.”

She was right, as moms always are. My dad has always showed me what no nonsense hard work can achieve. While my parents never pressured me and let me find my own interests and path in life, the knowledge that they were the top students in their country when they were growing up always pushed me to set a high academic standard for myself. My dad also happened to give me one of his kidneys, a gift for which I can never fully thank him. Thank you Mom and Dad for always pushing me towards excellence by your example!

TABLE OF CONTENTS

LIST OF TABLES

LIST OF FIGURES

LIST OF SYMBOLS AND ABBREVIATIONS

$1\alpha,25(OH)_2D_3$	1α,25-dihydroxyvitamin D_3
AA	ascorbic acid
AR	Alizarin red
βGP	β-glycerophosphate
BMP	bone morphogenetic protein
Coll-I	collagen type I
DBM	demineralized bone matrix
Dex	dexamethasone
EB	embryoid body
EBM	embryoid body material
ECM	extracellular matrix
EDS	energy dispersive spectroscopy
ERK 1/2	extracellular signal related kinase 1/2
ESC	embryonic stem cell
FTIR	Fourier transform infrared spectroscopy
GAPDH	glyceraldhyde-3-phosphate-dehydrogenase
H&E	hematoxylin and eosin
LIF	leukemia inhibitory factor
μCT	micro-computed tomography
MAPK	mitogen activated pathway kinase
MMAB	modified Mallory's Analine blue
MSC	mesenchymal stem cells

mESC	mouse embryonic stem cell
OCN	osteocalcin
OM	osteogenic medium
OPN	osteopontin
OPG	osteoprotegrin
OSX	osterix
PDIA3	protein disulfide isomerase family A, member 3
PFA	phosphonoformic acid
PKC	protein kinase C
Pi	inorganic phosphate
PiT-1	phosphate transporter 1
qRT-PCR	quantitative real time reverse transcription polymerase chain reaction
Runx-2	runt related transcription factor 2
SDS	sodium dodecyl sulfate
SEM	scanning electron microscopy
TEM	transmission electron microscopy
UHTP	ultra-high throughput
VDR	vitamin D receptors
VK	von Kossa
VEGF	vascular endothelial growth factor
XRD	x-ray diffraction

SUMMARY

With a growing elderly population, increased bone disease and decreased bone repair observed with aging are significant causes of morbidity and mortality. As a result, the investigation of novel strategies, including materials, used to promote bone growth and regeneration is an area of great interest and active investigation. One widely used and studied material is demineralized bone matrix (DBM). Since the discovery of its osteoinductivity, the ability to induce bone formation when implanted in ectopic sites, it is now used in various formulations for clinical applications to heal bony defects. The observed osteoinductive properties of DBM are attributed to its ability to capture in an acellular form the naturally regenerative microenvironment present within bone, including its collagenous matrix and associated growth factors, in particular bone morphogenetic proteins (BMPs). This material, however, is derived from allograft sources, and as such, is limited by donor availability and subject to donor to donor variability in potency and efficacy. As a result, the derivation of similar osteoinductive materials derived instead from a single cell source and generated *in vitro* remains an attractive goal to remove the variability associated with allograft tissue.

Stem or progenitor cells, which can differentiate to multiple cell types, are a promising candidate for use to derive such osteoinductive materials. Specifically, pluripotent embryonic stem cells (ESCs) can be directed to differentiate into a variety of phenotypes, including osteogenic cells. ESCs are commonly differentiated *in vitro* as embryoid bodies (EBs), three dimensional cellular aggregates that recapitulate many cellular and molecular aspects of early mammalian development. Therefore, ESCs,

specifically after directed osteogenic differentiation, may recreate a more regenerative, embryonic-like microenvironment that may be lacking from current adult allograft-based therapies, such as DBM. Taken together, harnessing the ESC microenvironment and the unique mixture of growth factors it contains in an acellular therapy may be an effective means to modulate cell behavior and tissue formation by delivering signals deficient in adult tissues, in particular for bone regenerative applications. Thus, the ***objective*** of this project was to examine the osteoinductive potential harbored within the embryonic microenvironment, *in vitro* and *in vivo*.

To better understand the osteoinductive potential harbored within the EB microenvironment, *in vitro*, the osteogenic differentiation of ESCs was characterized in response to administration of phosphate to cells in the form of β-glycerophosphate (βGP) (Chapter 4). In this work, the increasing presence of calcium phosphate mineralization was readily apparent throughout EBs differentiated for up to 14 days in the presence of βGP (starting at day 5), as evaluated by phase contrast microscopy, histological stains (von Kossa and Alizarin red), and micro-computed tomography (μCT). Coincident with EB mineralization, phenotypic markers of osteogenic differentiation (r*unx2, osteopontin, osteocalcin,* and *bone sialoprotein* expression and osteopontin and osteoprotegrin secretion) were significantly increased by βGP treatment (10 mM). Additionally, phosphate induced differentiation involved activation of ERK 1/2. As a further characterization of osteogenic phenotype, the expression and responsiveness of two 1α,25-dihydroxyvitamin D_3 (1α,25$(OH)_2D_3$) receptors were assessed, the classical vitamin D receptor (VDR) and a membrane 1α,25$(OH)_2D_3$-binding protein (protein disulfide isomerase family A, member 3 [PDIA3]). In order to determine if the observed

effects were specific to ESCs or a general property of osteogenic cells, both receptors were evaluated in mesenchymal stem cells. EBs expressed both VDR and PDIA3, but VDR increased as cells underwent osteogenic differentiation. Mesenchymal stem cells expressed PDIA3 at constant levels throughout differentiation, but VDR increased in cells treated with osteogenic medium. These results suggested that both $1\alpha,25(OH)_2D_3$ signaling mechanisms were important, with PDIA3 playing a greater role during early developmental events and VDR playing a greater role in later stages of differentiation. Taken together, the results of this *in vitro* work demonstrated that phosphate treatment was sufficient to induce osteogenic differentiation of EBs.

To further clarify the mechanism by which phosphate treatment induced osteogenic differentiation, the mineral deposits formed within osteogenic EBs were further characterized (Chapter 5). It was hypothesized that phosphate-induced differentiation was mediated through changes in the microenvironment induced by mineral deposit formation within differentiating EBs. The mineralization was evaluated and quantified by phase imaging, staining, and μCT, and further material characterization studies were undertaken to determine the mineral structure and composition by transmission and scanning electron microscopy, energy dispersive spectroscopy, Fourier transform infrared spectroscopy, and X-ray diffraction. Along with the observation that non-viable cells mineralized in βGP-containing media, additional material characterization suggested that the mineral present within EBs was comprised of calcium phosphate precipitation nucleated by non-viable cells and was not matrix mineralization. The relationship of calcium phosphate precipitates to the previously observed osteogenic differentiation was then further assessed. When precipitate formation was blocked by

addition of phosphonoformic acid (PFA, 0.5 mM), ERK 1/2 activation and downstream osteogenic differentiation were also blocked; however no inhibition of signaling or differentiation were seen if PFA treatment was delayed until after precipitate formation had begun, suggesting that the precipitates themselves were somehow initiating signaling and differentiation, a finding that was in agreement with recent studies in pre-osteoblasts and vascular smooth muscle cells. Finally, osteogenic matrix molecules and osteoinductive growth factors were found to be produced by EBs at varying levels, regardless of phosphate treatment. Taken together, further characterization of osteogenic differentiation, *in vitro* demonstrated that calcium phosphate precipitation under phosphate treatment altered the microenvironment of osteogenic cells within EBs, leading to differentiation.

Lastly, the ability to harness and deliver the osteoinductive microenvironment within osteogenic EBs as an acellular material (EBM) was evaluated *in vivo* in a mouse intramuscular osteoinduction assay (Chapter 6). EBM was found to retain several growth factors known to be important for the induction of bone formation and was particularly enriched in BMP-4. Osteogenic EB-derived EBM was determined to be osteoinductive *in vivo*, while EBM derived from spontaneously differentiating EBs was not osteoinductive, as evaluated by mineralized tissue formation visualized and quantified by X-ray and μCT, semi-quantitative scoring of osteoinduction, and histomorphometric quantification of new bone formed. Additionally, the EBM that was osteoinductive performed as well as active DBM positive controls, even though half the mass dose was delivered, which may have been explained by the abundant BMP-4 in EBM. In summary, the *in vivo* work demonstrated osteoinductivity of material derived from osteogenic EBs.

In conclusion, this work demonstrated that phosphate can induce osteogenic differentiation of EBs that modulates $1\alpha,25(OH)_2D_3$ receptor expression and activation, that this differentiation is mediated through alterations in the EB microenvironment created by the introduction of calcium phosphate precipitates within EBs, and that the osteoinductive microenvironment within osteogenic EBs can be harnessed to yield *in vivo* osteoinductivity. The *in vivo* study represents the first use of EBM for a tissue specific application after material derivation from ESCs undergoing directed differentiation. More broadly, the embryonic-like microenvironment of EBs undergoing directed differentiation can be harnessed in an acellular biomaterial for a tissue specific application, an approach that avoids the donor to donor variability that limits adult, allograft tissue-derived therapies, such as DBM. Furthermore, as methods are in place to direct the differentiation of ESCs to a variety of other cell types, such as endothelial cells, use of the same technique to derive other tissue specific EBMs may have a broad range of clinical applications beyond bone tissue engineering, such as promoting angiogenesis in ischemic myocardium following myocardial infarction. This work not only provides new insights into the dynamic microenvironments of differentiating stem cells but also establishes an approach for the development of additional ESC-derived, tissue specific therapies by deriving EBM after directed EB differentiation.

CHAPTER 1

INTRODUCTION

The ability of tissue to heal and regenerate changes over an animal's lifespan. Specifically, bone healing declines through development and aging, resulting in prolonged or incomplete fracture repair in aged animals; conversely, fetal animals heal defects that cannot be healed postnatally. The loss of regenerative capacity, from fetal to adult to aged animals, has been attributed not only to a decline in the function of cells involved in bone formation (i.e. osteoblasts, mesenchymal stem cells (MSCs)) but also to alterations in the bone microenvironment that occur through development and aging, including extracellular matrix (ECM) composition and growth/trophic factor content [1]. Clinical scenarios in which defect repair is the desired outcome must overcome the impaired healing ability resulting from these changes in the bone microenvironment in order to promote complete tissue regeneration. Consequently, a variety of therapies directed at serving as bone grafts or bone substitutes to augment incomplete bone repair and implant integration have been developed.

Autograft bone, the gold standard in bone defect repair, has been associated with significant donor site morbidity. Molecular approaches stimulating endogenous osteogenic repair have focused on administration of specific morphogens, such as bone morphogenetic proteins (BMPs), or on application of acellular matrices derived from adult tissue sources, such as demineralized bone matrix (DBM). However, single factor treatments lose the rich molecular complexity of acellular matrix-based approaches, making supraphysiologic doses of single growth factors required, while allograft bone-

derived treatments, including DBM, originate from cadaveric sources, lending inherent donor-to-donor and batch-to-batch variability. DBM osteoinductivity varies with donor characteristics and, specifically, is known to decrease with increasing donor age due to the changes in bone ECM composition that occur with aging [2]. Therefore, the development of alternative acellular therapies with not only high but also consistent osteoinductive potential remains a goal.

In the investigation of novel treatments for bone repair, one potential therapeutic goal is the restoration of a more regenerative microenvironment, as found during embryonic development. One approach to creating such a microenvironment is through the use of stem cells. In recent years, stem cells have emerged as a key element of regenerative medicine due to their inherent ability to differentiate into a variety of cell phenotypes, providing numerous potential cell therapies for an array of degenerative diseases and traumatic injuries. In addition to serving as a differentiated cell source, pluripotent stem cells, such as embryonic stem cells (ESCs), may possess the unique potential to modulate tissue environments via local production of ECM and growth factors that may be harnessed as an acellular therapy to promote functional tissue regeneration. Though such an approach to generate a naturally derived material has been employed successfully to deliver osteoinductive factors found within adult bone, in the form of DBM, the development of treatments derived instead from developing, more regenerative tissues or cells remains attractive. The derivation of regenerative therapies from an ESC source also presents the added benefit of eliminating donor to donor variability of adult, cadaveric tissue-derived materials, such as DBM. Thus, study of the microenvironment generated by embryonic cells, including growth factors produced and

retained within that environment, may provide insights into restorative, osteoinductive strategies to augment bone regenerative ability.

The ***objective*** of this project was to examine the osteoinductive potential harbored within the embryonic microenvironment, *in vitro* and *in vivo*. The ***central hypothesis*** of this work was that the embryonic microenvironment is rich in osteoinductive signals and that this microenvironment along with these signals, captured in a devitalized material, would harbor greater osteoinductive capacity or potency than adult tissue-derived matrices or materials. The ***rationale*** for this work was that, even in tissues, like bone, that regenerate and remodel readily, developing tissues regenerate more robustly than adult tissues and, furthermore, that the difference in regenerative ability is due in part to changes in the microenvironment, including growth factors present, which occur between embryonic and adult life. As such, embryonic stem cell-derived materials may possess enhanced inductive capabilities compared to ECM derived from adult tissues. The ***central hypothesis*** of the proposal was examined by completion of the following specific aims:

Specific Aim 1. Determine how modification of the embryonic microenvironment impacts osteogenic differentiation, *in vitro*. The hypothesis of this aim was that perturbations in ESC microenvironment, including the formation of calcium phosphate precipitates induced by phosphate treatment, would alter ESC phenotype to promote osteogenic differentiation. Differentiation was assessed by evaluation of gene and protein expression of osteogenic growth factors, extracellular and matrix molecules, as well as expression and activation of receptors and signaling molecules known to be important in

osteogenic differentiation, including two $1\alpha,25(OH)_2D_3$ receptors, VDR and PDIA3, and ERK 1/2.

Specific Aim 2. Compare the osteoinductive potential of the embryonic microenvironment from osteogenic and non-osteogenic embryonic cell sources, captured as an acellular biomaterial, with that of an adult tissue ECM, *in vivo*. The hypothesis of this aim was that material derived from ESCs undergoing osteogenic differentiation would exhibit greater osteoinductive capacity and potency than both material from spontaneously differentiating ESCs and adult DBM, *in vivo*, stimulating ectopic bone formation in a mouse intramuscular osteoinduction assay. Acellular materials derived from embryoid bodies (EBM) were implanted into the hindlimb of mice in order to assess ectopic bone formation *in vivo*, and osteoinductive capacity was compared with that of active and inactive DBM by mineralization formed, quantified by MicroCT, and histological assessments.

This research was *significant* because it demonstrated that the embryonic microenvironment of cells undergoing directed differentiation could be harnessed as an acellular biomaterial that impacted tissue formation *in vivo.* This work was *innovative* because it examined how the microenvironment of osteogenic cells, particularly mineralization, may impact further differentiation and because it evaluated the osteoinductive potential of ESC derived material. Characterization of the instructive factors and osteoinductive cues produced by embryonic stem cells while undergoing osteogenic differentiation have provided insights into interactions between osteogenic

cells and their microenvironment. Furthermore, identification and characterization of such factors has lead to the development of novel regenerative medicine therapy derived from stem cell sources that can improve not only bone repair but also the quality of life for many patients by reducing the morbidity and mortality associated with their own inadequate or incomplete bone healing.

CHAPTER 2

BACKGROUND

Bone Extracellular Matrix (ECM)

The ECM of bone provides structural support and presents cues that direct cell growth, differentiation, and mineralization. Illustrating their importance in bone development, mutations in bone extracellular matrix proteins lead to a variety of bone dysplasias in animal models and in humans [3]. During intramembranous bone formation, osteogenic mesenchymal cells undergo proliferation, matrix production, and then mineralization, after which the cells either become trapped as osteocytes or undergo apoptosis [4]. Endochondral bone formation proceeds through a cartilaginous intermediate, including a matrix rich in chondroitin sulfate and collagen type II that presents growth factors, particularly vascular endothelial growth factor, which promote vascular ingrowth [5]. Chondrocytes undergo hypertrophy, mineralization, and apoptosis, leaving a matrix that is then remodeled and further mineralized by infiltrating osteogenic cells [3]. The extracellular matrix of mature, native bone is comprised primarily of type I collagen, which constitutes nearly 90% of the organic material found in bone [6-8]. The collagen-I matrix itself is known to direct osteogenic differentiation. Osteoblast recognition of collagen-I by integrin binding has been shown to regulate early osteoblast differentiation and control the expression of key genes in osteoblastogenesis [9, 10]. Other important bone ECM molecules that have all been shown to regulate osteogenic differentiation and mineralization within developing bone include osteopontin [11, 12], osteocalcin [13], osteoprotegrin [14], bone sialoprotein [15], periostin [16], vitronectin

[17, 18], and fibronectin [4, 19]. In addition to providing signals that drive osteoblast growth and differentiation, individual ECM molecules may directly control mineralization by serving as nucleation points (e.g. bone sialoprotein) and inhibitors (e.g. osteopontin, osteocalcin) for hydroxyapatite formation [20]. Bone sialoprotein's role as a nucleation point for mineral deposition, in particular, is critical for *de novo* bone formation [4]. Osteoblast secreted factors, such as osteoprotegrin, also regulate bone turnover and remodeling through their effects on osteoclasts [14]. The bone matrix also harbors growth factors, in particular bone morphogenetic proteins (BMPs), which were discovered through the molecular characterization of bone ECM [21, 22].

Individual growth factors of particular relevance to bone forming ability include BMP-2 and VEGF. Since its first description in the 1960's, the osteoinductivity of demineralized bone matrix (DBM) has long been known to be due mostly to its BMP-2 content [22-24]. BMP-2 is directly osteoinductive, and as such, recombinant human BMP-2 has been employed clinically as a single factor therapy used to promote bone growth and regeneration, although at supraphysiologic doses in the milligram range [InFUSE; Medtronic Sofamor Danek, Memphis, TN] compared to nanogram amounts present in DBM used for similar applications [25]. When delivered with inactive DBM, BMP-2 induced robust new bone formation [24]. Smad signaling has been found to be activated by BMPs, leading to many of their osteoinductive effects [8, 26]. Though BMP-2 is the most potent factor in mediating new bone formation, resident within bone, other factors are important as well. The bone extracellular matrix also contains VEGF, which is vital to osteoinductivity, as it is required for endochondral bone formation and promotes neovascularization allowing for the recruitment of the mesenchymal progenitor cells that

are acted upon by BMPs to form new bone [5, 27, 28]. Additionally, VEGF acts directly on osteoblasts, increasing their chemotaxis [29], and, when used to supplement DBM, improves graft neovascularization and increases bone formation [30].

Another osteoinductive factor of interest but not abundant in native, adult bone is BMP-4. Like BMP-2, BMP-4 is directly osteoinductive, due to their high level of homology [31]. During endochondral ossification *in vivo*, knockout of either *Bmp2* or *Bmp4* was rescued by endogenous expression of the other, allowing for normal bone formation, suggesting interchangeable roles during osteogenesis; however, removal of both BMP-2 and BMP-4 together completely inhibited osteoblast differentiation and long bone development *in vivo* [32]. Although BMP-4 was found to be upregulated during fracture repair, a process related to bone growth [33, 34], it alone was not actually necessary for either long bone skeletogenesis or limb fracture healing[35]. However, BMP-4 was also determined to be critical during development and necessary for gastrulation and mesoderm formation [36].

Mineralization

Mineralization of the extracellular matrix is a cell mediated process resulting in the deposition of calcium phosphate as hydroxyapatite (HA - $Ca_{10}(PO_4)_6OH_2$), and this process requires alkaline phosphatase activity and a source of inorganic phosphate, such as β-glycerophosphate (βGP). Mineral accumulation occurs within membrane bound matrix vesicles before association with the collagenous matrix within bone [6, 37]. Mineralization can be assessed by several methods including stains for calcium (Alizarin Red) and phosphate (von Kossa) and, in three dimensional systems, can be demonstrated

by micro-computed tomography (μCT) due to its higher radio-opacity compared to other tissues and cellular material[38]. Though mineralization is often used as a readout of differentiation towards osteoblasts, several different cell types, primarily of the mesenchymal lineage, may be induced towards osteogenic differentiation and are capable of mineralization, including mesenchymal stem cells [39], skeletal myoblasts [40], and even fibroblasts [41, 42] and vascular smooth muscle cells [43] under certain physiological or pathological conditions.

In addition to being a process actively promoted within mineralizing tissues such as bone, it is one that is actively inhibited in non-mineralizing tissues. One factor promoting this inhibition is pyrophosphate (PPi), a naturally occurring, cell produced molecule that is present ubiquitously in soft tissues and known to be a potent inhibitor of mineralization both *in vivo* and *in vitro* [44-47]. Direct inhibition of crystal formation is one of the mechanisms by which it blocks precipitation and mineralization (Fig. 2.1) [47]. In mineralized tissues, alkaline phosphatase cleaves PPi to yield inorganic phosphate, thus removing inhibition and allowing for mineralization to occur [48].

Demineralized bone matrix (DBM)

The osteoinductive potential of demineralized freeze dried bone allograft, also commonly referred to as DBM, was first discovered in the 1960s [22], and it remains a leading molecular therapy to induce bone formation. DBM is an acellular matrix extracted from the native bone ECM, which has been found to be a natural material capable of harboring osteogenic growth factors and morphogens. Extraction of the mineral phase of bone by acid treatment yields a demineralized matrix comprised of

mostly collagen and associated growth factors, which may additionally have increased bioavailability after demineralization due to increased hydration [49], explaining why DBM is osteoinductive but non-demineralized allograft bone matrix is not [50]. Factors found to be present in DBM include primarily BMPs in combination with, but to a far lesser extent, other factors (e.g. TGFs, VEGF, FGFs) [31, 51].

The individual amounts of specific factors within DBM and overall osteoinductive bioactivity are confounded by donor and lot variability, making standardization difficult due to inconsistencies not only between preparations from different manufacturers but also independent batches of the same product formulation [25, 52, 53]}. The variability in DBM is due to the fact that allograft bone is used as the donor tissue source for the material and, as such, age, sex and other physiologically relevant parameters can affect DBM bioactivity [2, 25, 51, 54, 55]. Molecular characterization of DBM to identify key constituents imparting DBM with osteoinductive ability led to the discovery of BMPs [21-23, 56]. Thus, recombinant, single factor treatment has become a widely used approach for clinical applications, in particular, rhBMP-2 [InFUSE; Medtronic Sofamor Danek, Memphis, TN] and rhBMP-7/osteogenic protein-1 [Stryker Biotech, Hopkinton, MA]. Current approaches to deliver BMPs focus on administration of recombinant, singular factors in solution, within a carrier, commonly a collagen sponge [57]. One caveat of single factor treatment is the loss of the rich molecular complexity found in DBM and other acellular matrices, like porcine small intestinal submucosa [58].

The osteoinductive potential of demineralized bone matrices can be characterized by a variety of *in vitro* and *in vivo* techniques. *In vitro* characterization of DBM products

is usually based upon measuring the level of individual growth factors within DBM by ELISA, or comparable methods [52]. The evaluation of the *in vitro* osteoinductive capacity of DBM formulations has primarily been examined by cell seeding experiments [59]. Such studies have used a variety of cell types, including mesenchymal stem cells (MSCs) [39], myoblasts [40], and fibroblasts [42]; however, the choice of cell and predictive ability of *in vitro* cell assays for *in vivo* performance of DBM formulations remains arguable [60]. Compared to single cell types used to evaluate osteoinductivity *in vitro*, a complex mixture of multiple cell types and competing signals are present *in vivo*, leading to *in vitro* osteoinductivity not supported by *in vivo* osteoinductivity While some studies have demonstrated a correlation between single growth factor content and *in vivo* bioactivity [61], continued difficulty in identifying reliable predictors of *in vivo* osteoinductivity underscore the complex interplay between various factors contained in DBM [59]. Thus, the bulk of DBM characterization studies have utilized *in vivo* models, where osteoinduction, the ability to stimulate ectopic bone-like formation, is assessed either subcutaneously or intramuscularly. The latter method is currently accepted by the American Society of Testing and Materials (ASTM) International standards for the testing of DBM bioactivity [53, 62]. In the intramuscular model, it is believed that DBM particles recruit MSCs to the implantation site before inducing the formation of a cartilage intermediate and eventual bone, in a manner analogous to endochondral bone formation [26]. Measures of chondroinductive and osteoinductive potential, *in vivo,* can be assessed, including chondroitin sulfate production and ossicle formation [42, 63, 64]. In addition to its use in evaluating DBM, this model has also been used to evaluate the osteoinductivity of other types of ECM-based materials and formulations [65].

While successful isolation of DBM is routinely accomplished with acid treatment to remove the mineral phase of bone, the wide range of physical and chemical properties of different tissues indicates the need for a variety of decellularization processes to effectively yield tissue-specific bioactive acellularized products [66]. Most protocols generally involve a combination of physical and chemical means of disrupting cellular membranes and structure in order to effectively remove cellular elements. Physical methods can involve freeze-thaw, pressure, sonication, and lyophillization techniques [67-69]. Acellular biomaterials lack viable cells but retain natural ECM components, such as structural adhesive proteins, glycosaminoglycans and bioactive growth factors embedded within the native matrix from the tissue of origin [70-73]. Successful use of these materials has been demonstrated in soft and hard tissue repair, ranging from heart valves and nerve grafts to osteoinduction, demonstrating that acellular therapies retain bioactive molecules present within native tissue microenvironments and yield functional tissue regeneration.

Osteoinductive matrices

Similar to DBM, the ECM of osteogenic cells cultured *in vitro* have been found to be osteoinductive. Like DBM, the *in vitro* osteoinductivity of ECM generated by MC3T3-E1 pre-osteoblast cells has been attributed to BMP content and interactions of exogenously seeded cells with the collagenous matrix produced [74]. Such matrices have been used to direct the differentiation of ESCs [75]. Mesenchymal stem cells (MSCs) undergoing osteogenic differentiation have also been used to generate matrices for potential therapeutic purposes like DBM but have yielded mixed results with

demonstrated *in vitro* osteoinductivity not leading to *in vivo* osteoinductivity [65, 76, 77]. In a series of studies, MSCs were first differentiated in media containing dexamethasone, a common osteogenic media supplement, and then seeded onto titanium scaffolds for varying lengths of time before decellularization and rat intramuscular implantation. Though these matrices were found to induce osteogenic differentiation of MSCs *in vitro* [78], they were not found to be osteoinductive *in vivo* but instead were surrounded by a fibrous capsule [65], similar to results obtained in response to ectopic implantation of non-demineralized, allograft bone [50]. With the multiple, non-osteoprogenitor cell types present *in vivo* and in the absence of strong enough osteoinductive cues within the matrix, the fibrous tissue response trumped the response of the osteoprogenitor cell population to form new bone.

Developmental Changes in Bone Composition and Repair

Bone regenerative capacity is known to decline through development and aging, from the embryonic to adult and aged life of an animal. The decline in bone formation and healing ability in aged human populations is well demonstrated clinically [79]. The loss in regenerative capacity may be attributed to changes both in cellular function and in bone extracellular environment [1]. Cellular causes for this decline include a smaller pool of available MSCs [80], decreased proliferation of aged cells in response to matrix cues [81], and decreased expression of *Runx2*, an osteoblast transcription factor, resulting in decreased extracellular matrix production [82]. In contrast, fetal bone development and healing is augmented compared to that in adult animals. Fetal endochondral bone healing has been demonstrated to be a scar-free process. Fetal long bone fractures in sheep and

rabbits lack callus formation [83], and fractured embryonic chick radii heal without hematoma or callus formation typical after fracture [84]. Furthermore, fetal animals heal "critical-size" defects that would not be healed in postnatal animals [85]. Taken together, characteristics unique to the fetal/embryonic microenvironment promote improved bone regenerative ability compared to adult bone but are lost over the course of development towards and through adult life.

The difference in the bone-forming ability of children and adults has in part been attributed to differential expression of several growth factors such as BMPs, TGF-β1, TGF- β3, and FGF-2. Microarray analysis of calvarial regenerates from juvenile and adult mice demonstrated a marked upregulation of pro-osteogenic cytokines (such as BMP-2, -4, and -7, FGF-2, and IGF-2) and increased levels of markers for osteogenic differentiation (such as Sparc, osteonectin, and osteopontin) in juvenile samples. Additionally, increased levels of bone-related ECM proteins were seen in juvenile regenerates compared to adult. These included procollagens Col6a1, Col3a1, Col4a1, MMP-2, MMP-14, pleiotrophin, and cathepsin K [86]. Furthermore, the osteoinductivity of DBM declines with donor age, suggesting a decrease in the amounts of osteoinductive molecules present in bone with aging, specifically BMP-2 [2]. Though differences in composition have been found, direct comparisons of osteoinductivity between adult tissue-derived and embryonic-like or pluripotent cell-derived matrices have not been examined.

Pluripotent Stem Cells.

Embryonic stem cells (ESCs) are pluripotent cells derived from the inner cell mass of the blastocyst stage of development that are capable of self-renewal and differentiating into cells from all three germ layers (ectoderm, mesoderm and endoderm), as well as germ cells. ESCs can be used as a resource to experimentally probe mechanisms of early development and differentiation processes. In addition, the inherent plasticity of pluripotent ESCs suggests they could be effectively used as a robust cell source in regenerative medicine and tissue engineering applications for the treatment of a wide variety of degenerative diseases and traumatic tissue injuries. One additional advantage of ESCs compared to other multipotent stem cells, such as MSCs, is a significant capacity for self-renewal in a pluripotent state which readily permits the expansion of large numbers of cells. Successful derivation of ESCs from mouse blastocysts [87-89], eventually led to the ability to isolate ESCs from non-human primates [90, 91] and human embryos [92, 93]. The phenotypic and functional characterization of pluripotent stem cells paved the way for the recent ability to create "induced pluripotent" stem cells (iPSCs) from adult somatic cell types [94-97]. Though promising as a new tool in the development of regenerative therapies, particularly due to the potential for their derivation from autologous cell sources, many barriers must still be overcome before their clinical implementation [98]. Though much attention has been directed at evaluating the differentiation potential of these cells, with an eye towards cell-based therapies, like ESCs, the direct implantation of iPSC-derived cells presents the risk of teratoma formation. Consequently, the isolation of biomolecules, such as extracellular matrix and growth factors, isolated or extracted from pluripotent cells remains an attractive option.

ESCs are exquisitely sensitive to a variety of microenvironmental cues that regulate both self-renewal and differentiation. Differentiation of ESCs is influenced by soluble factors (produced endogenously or added exogenously), interactions with extracellular matrix components, cell-cell adhesions (both homotypic and heterotypic), and various combinations of these different types of stimuli [99]. Differentiation of ESCs *in vitro* can be induced in a variety of formats, the most common of which is via formation of cell aggregates in suspension culture referred to as "embryoid bodies" (EBs) [89, 100, 101]. EBs provide a three dimensional model of tissue morphogenesis that recapitulates many early aspects of embryological development and are an attractive format for tissue engineering and regenerative medicine applications because their production is intrinsically scalable due to suspension culture. However, transport limitations within EBs may limit the ability to yield a homogenous cell population when methods of directed differentiation are employed utilizing bulk administration of inductive factors to the media alone [102]. Additionally, if even a small population of undifferentiated, pluripotent cells persists within EBs, direct implantation of viable cells for therapeutic purposes will lead to teratoma formation.

Osteogenic Differentiation of Pluripotent Cells.

Based on MSC and osteoblast precursor studies, general protocols have been developed for the differentiation of ESCs to bone forming osteoblasts [103, 104]. In order to promote osteogenic differentiation, EBs are commonly treated with soluble factors (β-glycerophosphate (βGP), ascorbic acid, and dexamethasone or 1α,25-dihydroxy-vitamin D_3 ($1\alpha,25(OH)_2D_3$)), to encourage osteoblast maturation and matrix mineralization [105,

106]. Treatment with osteogenic supplements is usually initiated after the first five days of EB differentiation to allow for initial spontaneous induction of primitive mesodermal cells. βGP is necessary as a source of inorganic phosphate required for mineralization, though inorganic phosphate has also been found to induce osteogenic gene expression when administered alone [107]. Osteogenic differentiation cues are thought to be provided by supplementation with either dexamethasone or $1\alpha,25(OH)_2D_3$, which directly induce osteogenic gene transcription, while ascorbic acid (AA) is necessary for collagen fibril formation, which in turn promotes further osteogenic differentiation [9, 108, 109]. The influence of numerous other exogenous factors, including directly osteoinductive growth factor BMP-2, have also been investigated [104, 110-114], as well as osteogenic cell-derived matrices [75], highlighting the complexity of signals that may influence osteogenic differentiation and mineralization.

Phosphate Induced Osteogenic Differentiation

The ability of phosphate alone to induce mineralization and osteogenic differentiation has been demonstrated in multiple somatic cell types that exhibit the capacity to mineralize, including osteoblasts and vascular smooth muscle cells [43, 115], either by direct administration of inorganic phosphate or by addition of βGP. Both phosphate-induced mineralization and differentiation of these cells have been inhibited by blocking phosphate transport into cells, specifically through Type III Na,Pi co-transporters (PiT-1), using phosphonoformic acid (PFA), suggesting that phosphate needs to enter the cell for these phenotypic changes to occur (Fig. 2.1) [43, 115]. Additionally, phosphate-induced differentiation has been found to be mediated through activation of

the mitogen activated protein kinase (MAPK) pathway, specifically extracellular signal regulated kinase (ERK 1/2), in pre-osteoblast MC3T3-E1 cells [107, 116], and phosphate-induced ERK signaling in calcific vascular smooth muscle cells leads to upregulation of the gene encoding Runx-2 [43], an early osteoblast transcription factor that regulates the osteogenic phenotype [117]. Though it is ubiquitously expressed, *Pit-1* gene expression has been found to increase with osteoblast differentiation of MC3T3-E1 cells, coincident with the observation of mineralization, while *Pit-2*, which is also ubiquitously expressed, remains constant at an invariably low level, suggesting that PiT-1 but not PiT-2 is important in osteoblast phosphate transport [118]. At the protein level, phosphate transport through PiT-1 is increased by BMP-2 stimulation following upregulation of *Pit-1* expression and is required for BMP-2-induced matrix mineralization in MC3T3-E1 cells [119] and vascular smooth muscle cells [120]. Phosphate transport via PiT-1 has also been found to be important in chondrocyte differentiation and maturation using ATDC5 cells, a model of endochondral ossification [121-123].

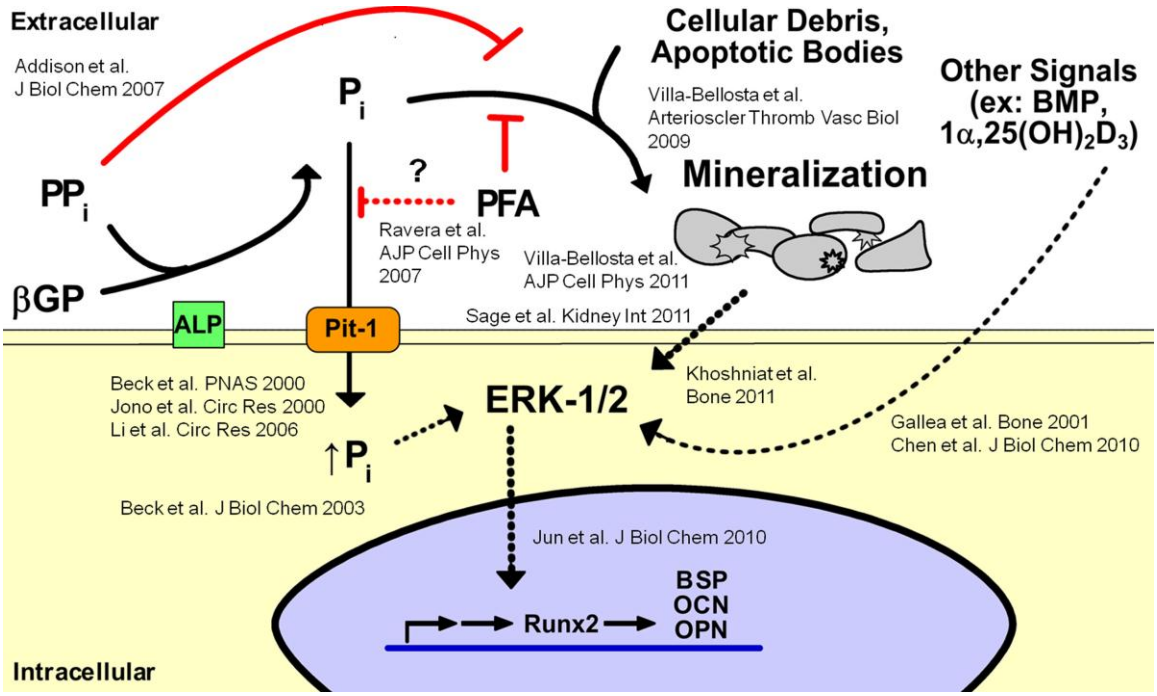

Figure 2.1. Phosphate-induced osteogenic differentiation. Phosphate-induced osteogenic differentiation of osteoblast [115] and vascular smooth muscle cells [43] was originally characterized to require transport of Pi into cells through type III Na, Pi co-transporters, PiT-1 [124] and activation of the ERK signaling pathway [116]. ERK signaling is activated by a variety of other pro-osteogenic signals [125, 126] and has been found to stabilize and activate Runx-2 [127]. Studies of phosphate-induced osteogenic differentiation found that ERK activation and subsequent differentiation were blocked with PFA treatment, thought to inhibit Pi uptake though PiT-1; however, more recent studies have suggested PFA may not block Pi transport at concentrations typically used [128]. Instead, PFA has been found to inhibit calcium phosphate precipitation directly [129], in a mechanism similar to that of PPi [47]. The presence of calcium phosphate precipitates have since been demonstrated to induce osteogenic differentiation independent of Pi concentration alone [130, 131] through activation of ERK signaling [132].

More recent electrophysiological studies of PiT-1 expressed exogenously in *Xenopus* oocytes have found that its transport of Pi was not actually blocked by PFA treatment at the concentrations typically used (0.5 mM), pointing towards another mechanism of action [128]. PFA is also an analogue of PPi, a natural inhibitor of extracellular mineralization that is known to directly interfere with calcium phosphate crystal formation, and additional studies of vascular smooth muscle cell calcification have suggested that PFA may inhibit mineralization by a similar mechanism [129] and therefore that the presence of extracellular mineral deposits, and not increased Pi concentrations, might actually induce osteogenic differentiation (Fig 2.1) [131, 132].

ERK Signaling in Osteoblast Differentiation

ERK 1/2 is an important signaling molecule in osteogenic differentiation, as ERK 1/2 signaling is activated by a diverse set of signals present within bone (Fig 2.1). It has been found to be activated by inorganic phosphate in a variety of mineralizing cell types, including, osteoblasts [116], chondrocytes [121], dental pulp cells [133], and vascular smooth muscle cells [134]. BMP-2 has also been found to activate ERK signaling by non-Smad pathway activity in osteogenic cells including the mesenchymal progenitor cell line C3H10T1/2 [135] and C2C12 skeletal myoblast cells [125]. BMP-2 induced ERK activation has additionally been demonstrated to increase Runx-2 transcriptional activity in concert with Smad activation [127] and to induce transcription and activity of Osterix [136]. ERK activation may also be induced by $1\alpha,25(OH)_2D_3$ [126].

Vitamin D and Receptors

Another important factor known to impact osteogenic differentiation and osteoblast maturation is $1\alpha,25(OH)_2D_3$. Effects of $1\alpha,25(OH)_2D_3$ in osteoblasts are mediated by two vitamin D receptors, the nuclear receptor (VDR) [137]and a membrane-associated $1\alpha,25(OH)_2D_3$-binding protein called protein disulfide isomerase A3 (PDIA3, also known as ERp60, ERp57, Grp58, and 1,25-MARRS) [138-140]. In classical VDR activation, $1\alpha,25(OH)_2D_3$ is recognized by cytoplasmic VDR, which then dimerizes with the retinoic acid receptor (RXR). This complex binds to vitamin D responsive elements (VDREs) in target genes and induces expression of osteoblast markers as such osteocalcin and Runx-2 [141, 142]. The interaction of $1\alpha,25(OH)_2D_3$ with PDIA3 in the membrane associated vitamin D receptor complex activates a rapid membrane-initiated signaling cascade that involves protein kinase C (PKC) and ERK activation, resulting in cellular events that modulate cell proliferation and differentiation [126, 143-146].

CHAPTER 3

GENERAL METHODS

Mouse Embryonic Stem Cell (ESC) Culture

Undifferentiated mouse ESCs (D3 line) were cultured in media containing DMEM (Mediatech, Herndon, VA) supplemented with 15% FBS (Hyclone, Logan, UT), 2mM L-glutamine (Mediatech), 1x non-essential amino acids (Mediatech), 100U/ml penicillin/ 100 μg/ml streptomyocin/ 0.25 μg/ml amphotericin (GIBCO, Carlsbad, CA), 0.1 mM β-mercaptoethanol (Fisher, Fairlawn, NJ), and 10^3 U/mL of leukemia inhibitory factor (LIF, Chemicon, Temecula, CA) on 0.1% gelatin coated tissue culture dishes. Media was changed at least every 2 days, and cells were passed every 2-3 days before reaching 70% confluency with 0.05% trypsin (GIBCO).

Embryoid Body (EB) Rotary Formation

Single cell suspensions of undifferentiated ESCs were inoculated into 100mm bacteriological grade Petri dishes at 2 x 10^5 cells/ml in 10 ml of ESC media without LIF and then cultured as EBs on rotary orbital shakers, as previously described by Carpenedo et al [147], at 40 rotations per minute of continuous shaking (Lab-Line Lab Rotator, Model #2314, Barnstead International, Dubuque, IA). For re-feeding every 2 days, EBs were collected by sedimentation, and 90% of media was exchanged with fresh ESC media.

EB Ultra-High Throughput (UHTP) Formation

Forced aggregation was used to generate individual EBs of identical cell number in 6 well cell culture plates [148]. ESCs were inoculated at 6 million cells per 1 ml of media (6 well plate). There were 6000 microwells for each microwell insert, corresponding to approximately 1000 cells per microwell. Plates were centrifuged 5 minutes at 200xg at 25°C to promote aggregation. After 24 hours of microwell culture, EBs were collected by wide bore pipette, transferred to 100 mm bacteriological Petri dishes (~2500 EBs/dish), and maintained on a rotary orbital shaker at 40 rotations per minute of continuous shaking Lab Rotator, Model #2314, Barnstead International, Dubuque, IA) in 10 ml of ESC media without LIF.

Histology

All samples collected for histology were dehydrated via an increasing series of ethanol and xylene rinses (Shandon Pathcentre Enclosed Processor), embedded in paraffin (Shandon Histocentre 2 Embedding System), cut into 5 μm-thick sections (Microm HM 355S Rotary Microtome), and placed on positively charged glass slides. Sections were deparaffinized in xylene, rehydrated in graded ethanol washes, and rinsed in deionized water (Leica AutoStainer XL) in preparation for staining. Tissue morphology was assessed by routine hematoxylin and eosin (H&E) staining (Leica AutoStainer XL), and digital brightfield images of stained slides were obtained using a Nikon 80i Upright Microscope and a Spot Flex camera (Diagnostic Instruments, Sterling Heights, MI).

For EB histology, EBs were collected, fixed in 10% formalin solution, rinsed in PBS, and embedded in Histogel™ (~200 EBs in 200 μl gel; Richard Allen Scientific,

Kalamazoo, MI). For von Kossa staining, deparaffinized sections were incubated in a 1% silver nitrate solution in water under UV for 15 min. Sections were rinsed in deionized water, transferred to 5% sodium thiosulfate for 5 minutes, rinsed in deionized water, and then counter stained for 5 minutes in 0.1% nuclear fast red stain before dehydration in graded ethanol, clearing in xylene, mounting in Cytoseal™ 60 (Richard-Allan Scientific), and cover-slipping. The number of EBs with positive staining (black) was quantified based on brightfield images.

Alizarin red staining was accomplished by incubating deparaffinized sections in a 2% Alizarin red solution in water for 2 minutes. Slides were blotted dry and then dehydrated in 100% acetone followed by an acetone-xylene solution (1:1) before clearing in 100% xylene, mounting with Cytoseal™ 60 mounting medium (Richard-Allan Scientific), and cover slipping. Brightfield images were acquired for quantification of positively stained EBs (red).

Quantitative Real Time Reverse Transcription Polymerase Chain Reaction (qRT-PCR)

For real-time PCR analysis, total RNA was extracted using the RNeasy Mini kit (QIAGEN, Valencia, CA). Complementary DNA was synthesized from 1 µg total RNA using the iScript cDNA synthesis kit (Bio-Rad, Hercules, CA), and quantitative PCR was performed with SYBR green technology on the MyiQ cycler (Bio-Rad). Amplification was performed using a two-step cycling program including 35 cycles, 1 minute/cycle. To assess EB osteogenic differentiation, primers for *osteocalcin, bone sialoprotein, osteopontin, collagen type I, osterix,* and *Runx-2* were used, in addition to housekeeping

gene *GAPDH*. MC3T3-E1 pre-osteoblast cells differentiated for 10 days with ascorbic acid were used as positive controls for primer validation and generation of standards. Gene expression was expressed as a fold change compared to undifferentiated ESCs and same day untreated EBs, calculated by the ΔΔCt method [149].

Table 3.1 Primer sequences used for qRT-PCR analysis

Gene	Forward	Reverse	Annealing Temp
osteocalcin	CCGGGAGCAGTGTGAGCTTA	TAGATGCGTTTGTAGGC GGTC	56°C
bone sialoprotein	CAGAGGAGGCAAGCGTCACT	CTGTCTGGGTGCCAACACTG	54°C
osteopontin	GATGCCACAGATGAGGACCTC	CTGGGCAACAGGGATGACAT	58°C
collagen type I	GCATGGCCAAAAGACATCC	CCTCGGGTTTCCACGTCTC	56°C
osterix	AGCCTCTGGCTATGCAAATGA	TGTAGACACTAGGCAGGCAGTCA	67°C
Runx-2	GTGCGTGCAAACTTTCTCC	AATGACTCGGTTGG TCTCGG	55°C
GAPDH	GCCTTCCGTGTTCCTACC	GCCTGCTTCACCACCTTC	60°C

Osteogenic Protein Expression

To measure alkaline phosphatase (ALP) specific activity, EB pellets were resuspended, vortexed, and incubated with substrate solution (3 mM p-nitrophenyl phosphate, 0.7 M 2-amino-2-methyl-1-propanol, 6.7 mM MgCl2, pH 10.3; Sigma, St. Louis, MO) for 30 min at 37 °C, and quenched by the addition of 0.2 M NaOH. The absorbance of reacted sample solutions were read at 405 nm wavelength on a Bio-Rad Benchmark plate reader, and the alkaline phosphatase specific activity was calculated using a standard curve generated with p-nitrophenol.

Osteocalcin protein concentration in EB media conditioned for 24 hours was measured by a competitive radioimmunoassay (Biomedical Technologies Inc, Stoughton, MA) according to manufacturer protocol. Briefly, conditioned media samples were incubated at room temperature with ^{125}I labeled osteocalcin and anti-osteocalcin antibody followed by secondary goat anti-rabbit IgG. After removing the supernatant, the radioactivity of the remaining pellet was measured and compared to a standard curve of known osteocalcin concentrations (1.5 – 200 ng/ml).

Enzyme Linked Immunosorbent Assay (ELISA)

For sandwich ELISAs, capture antibodies were adsorbed to wells of an immunosorbent 96-well plate. All samples (conditioned media or solubilized cell pellets) were centrifuged at 14,000 RPM for 5 minutes at room temperature to remove any insoluble material, and the supernatant was added to the antibody-adsorbed wells, followed by a biotinylated detection antibody and streptavidin-conjugated horseradish peroxidase (HRP). For the human BMP-4, human VEGF-A ELISAs, human

osteoprotegrin, and human osteopontin (R&D Systems, Minneapolis, MN), a chromogenic HRP substrate (3,3',5,5'-tetramethylbenzidine, TMB) was added and stopped by adding 1N sulfuric acid to produce a colorimetric result that was read at 450nm. For the human BMP-2 ELISA (PeproTech, Rocky Hill, NJ), the chromogenic substrate used was ABTS (2,2'-azino-bis(3-ethylbenzothiazoline-6-sulphonic acid), and color development was monitored at 405 nm with wavelength correction at 650 nm. Unknown values were compared to a standard curve generated from known concentrations of individual proteins in Tissue Protein Extraction Reagent (TPER, Pierce, Rockford, IL) buffer. Though the antibodies used were directed against human isoforms of each molecule, they are known to exhibit cross reactivity with their mouse counterparts as well.

Western Blotting

To assess extracellular signal-related kinase (ERK) signaling, EBs were collected at day 14 of differentiation for Western blot analysis, lysed by the addition of ice cold RIPA buffer (Pierce) supplemented with 500x protease inhibitor cocktail (Calbiochem, San Diego, CA) and 50x phosphatase inhibitor cocktail (Calbiochem), and stored at -80°C. The insoluble fraction was pelleted at 16,000g for 10 minutes, and the protein concentration of the supernatant was determined by use of the BCA Protein Quantification Kit (Pierce). Equal amounts of protein (20 μg) per sample were mixed with loading buffer containing 0.1 M Tris-HCl, SDS, glycerol, biomophenol blue, and 2-mercaptoethanol, incubated at 95°C for 5 minutes, and loaded on 4-20% Tris-HCl polyarcylamide precast gels (Bio-Rad) for electrophoresis. Proteins were transferred to

polyvinylidene fluoride (PVDF) membranes (Millipore, Billerica, MA) overnight at 4°C with 30V. Blots were stained using the Snap ID system (Bio-Rad). Membranes were blocked and with Near Infrared blocking medium (Rockland Immunochemicals, Gilbertsville, PA) and probed with anti-ERK, anti-pERK (1:250, Cell Signaling Technology, Danvers, MA), and anti-GAPDH (1:2000) antibodies overnight at 4°C before being pulled through by vacuum. Primary antibody incubation was followed by a continuous rinse under vacuum with 0.01% Tween-20 in PBS. Membranes were then incubated with infrared secondary antibody (1:5000, 800 anti-rabbit, Li-Cor Biosciences, Lincoln, NE) for 10 min at room temperature, rinsed, and imaged using the Odyssey Infrared Imager (Li-Cor). Blot images were converted to grayscale to obtain black protein bands on a white background in Image J (NIH, Bethesda, MD). Membranes were stripped prior to re-probing using 6 M guanidine HCl with 0.2% Triton-X and 0.1 M 2-mercaptoethanol at room temperature as described by Yeung and Stanley [150].

Micro-Computed Tomography (μCT) Evaluation of EB Mineralization

To evaluate the mineralization within EBs, approximately 200-500 EBs were suspended in 200 μl of Histogel™ (Richard Allen Scientific) in a 10 mm by 10 mm vinyl specimen mold (Sakura Finetek, Torrance, CA). Reference images of EB samples were taken using a dissecting stereomicroscope (Nikon SMZ1500) to determine EB distribution within the gel. The samples were scanned in air using a μCT 40 (Scanco Medical, Brüttisellen, Switzerland) at 45 kVp, 177 μA, 200-ms integration time, and a voxel size of 12 μm in a 12 mm scanning tube. Evaluation of μCT scans used sigma, support and threshold values set at 0.8, 1, and 70, respectively, setting for all samples

what was to be considered mineral volume. The total volume of mineralization within the entire Histogel-embedded samples was determined and normalized to estimated EB volume to calculate the average percentage of EB volume comprised of mineral. EB diameter was measured by phase contrast microscopy and used to calculate the average estimated volume of embedded EBs.

Statistical Analysis

Two-way ANOVA analysis, followed by Tukey's post-hoc test, was performed to determine statistical differences ($p<0.05$), using Systat 12™ statistical software unless otherwise noted. If data did not approximate a normal distribution when first examined by exploratory data analysis, including five number data summary and box and whisker plot, Box-Cox estimations were used to transform the data set to a normal distribution, as reviewed by Spitzer [151]. Outliers were identified by examination of studentized t-residuals. Based on power analysis after preliminary studies, sample sizes of n=3-8 were used as noted for individual assays. Results are reported as mean ± standard error of non-transformed data for a minimum of triplicate independent samples from each experiment after removal of outliers.

CHAPTER 4

PHOSPHATE INDUCED MINERALIZATION AND OSTEOGENIC DIFFERENTIATION OF MOUSE EMBRYONIC STEM CELLS*

Introduction

An important goal of regenerative medicine is to provide a source of cells with potential to proliferate, thereby increasing the available pool, and to differentiate into specific lineages of interest. Embryonic stem cells (ESCs) are pluripotent cells derived from the inner cell mass of a pre-implantation blastocyst [88, 92]. Not only can ESCs be maintained indefinitely as undifferentiated, self-renewing cells in culture under appropriate growth conditions without losing their pluripotent phenotype, but they have the unique ability to differentiate into cell types comprising all three germ lineages including osteoblasts (mesoderm), hepatocytes (endoderm), and neurons (ectoderm) [87, 152-154]. In addition to their use in tissue engineering and regenerative therapies [155-158], ESCs have also been used as an *in vitro* model to study early stages of cellular differentiation. ESCs spontaneously form three-dimensional cell aggregates called "embryoid bodies" (EBs) when grown in suspension culture conditions and differentiate into three lineages [89, 101, 159, 160]. EBs undergo morphogenic events similar to normal embryogenesis, and simultaneously yield cell types from endoderm, ectoderm, and mesoderm germ layers [161, 162]. Differentiation of ESCs and EBs to specific phenotypes can be induced by supplementing culture medium with specific stimulatory

Modified from:
R Olivares-Navarrete[†], K Sutha[†], SL Hyzy, DL Hutton, Z Schwartz, TC McDevitt, and BD Boyan. *Osteogenic Differentiation of Stem Cells Alters Vitamin D Receptor Expression.* **Stem Cells Dev**. 2011 Oct 28. In press. [†]Rene Olivares-Navarrete and Ken Sutha are co-first authors.

or inhibitory agents and molecules [99, 163, 164]. Alternatively, multipotent adult stem cells, such as mesenchymal stem cells (MSCs), may be used to provide cells of specific lineages, as they also have the capacity to divide and differentiate into several cell phenotypes and are found in diverse tissues or organs.

Although there are a number of protocols that promote the differentiation of ESCs and MSCs into osteoblasts, most studies indicate that this can be achieved by establishing an environment rich in phosphate, which results in formation of a mineralized extracellular matrix [165, 166]. The most commonly used osteogenic medium (OM) formulations contain β-glycerophosphate (*β*GP), dexamethasone, and ascorbic acid [167-169]. Specifically, βGP, an organic phosphate, is cleaved by extracellular alkaline phosphatase upon addition to the culture media, serving as a source of inorganic phosphate (Pi). The ability of phosphate alone to induce mineralization and osteogenic differentiation has been demonstrated in multiple somatic cell types that exhibit the capacity to mineralize, including osteoblasts and vascular smooth muscle cells [43, 115], either by direct administration of inorganic phosphate or by addition of βGP. Both phosphate-induced mineralization and differentiation of these cells have been inhibited by phosphonoformic acid (PFA), thought to block phosphate transport into cells, specifically through Type III Na, Pi co-transporters (PiT-1), suggesting that phosphate needs to enter the cell for these phenotypic changes to occur [43, 115]. Additionally, phosphate-induced differentiation has been found to be mediated through activation of the mitogen activated protein kinase (MAPK) pathway, specifically extracellular signal regulated kinase (ERK 1/2) [43, 107, 116],through activation of Runx-2, an early osteoblast transcription factor that regulates the osteogenic phenotype [117].

Some studies have also shown that addition of the vitamin D metabolite 1α,25-dihydroxy vitamin D3 [1α,25$(OH)_2D_3$] to osteogenic medium enhances osteoblastic differentiation of stem cells [170, 171]. 1α,25$(OH)_2D_3$ plays an important role in calcium and phosphate homeostasis and both catabolic and anabolic effects of this hormone have been demonstrated in bone cells [172]. Moreover, 1α,25$(OH)_2D_3$ regulates the expression of bone marker genes like *Runx-2*, collagen type I, osteocalcin (*Ocn*) and bone sialoprotein in osteoblasts [137, 173], indicating that it plays a role in their differentiation. Effects of 1α,25$(OH)_2D_3$ in osteoblasts are mediated by two vitamin D receptors, the nuclear receptor (VDR) [137]and a membrane-associated 1α,25$(OH)_2D_3$-binding protein called protein disulfide isomerase A3 (PDIA3, also known as ERp60, ERp57, Grp58, and 1,25-MARRS) [138-140].

Previous studies have focused primarily on directing differentiation of ESCs in two dimensional, adherent culture but more recently have attempted osteogenic differentiation of encapsulated cells [38, 174] and EBs [175-177]. Further investigation of the mineralization and differentiation processes as they occur in three dimensions, which more closely recapitulates *in vivo* environment, will provide a better understanding of bone development and regeneration not only as they occur *in utero* but also in emerging cellular therapies by identifying endogenous differentiation cues and cell-microenvironment interactions that are present. Therefore, additional characterization of the mineralization process as it occurs within the three dimensional and more primitive environment of EBs may provide insights into the initial differentiation associated with the earliest stages of bone development, which are not evident from studies employing more terminally differentiated pre-osteoblast and osteoblast-like cell lines.

The objective of this study was to assess the mineralization capacity of differentiating mouse ESCs and to examine the accompanying differentiation process induced by phosphate treatment. As further assessment of osteogenic phenotype, the response to exogenous $1\alpha,25(OH)_2D_3$ was also examined. To assess whether phosphate treatment can induce osteogenic differentiation of ESCs as has been observed in more committed cell types with osteogenic potential, EBs were cultured with βGP, a source of inorganic phosphate. First, mineralization was evaluated and quantified given this minimal substrate based on phase images, histological staining, and micro-computed tomography. Next, to evaluate accompanying osteogenic differentiation in the presence of the mineralization process, ERK 1/2 signaling in response to phosphate treatment was evaluated, and the expression of specific osteogenic marker genes activated downstream of this signaling was quantified. In addition, we characterized how this phosphate induced differentiation was associated with differential expression and responsiveness of two $1\alpha,25(OH)_2D_3$ receptors, PDIA3 and VDR. In this study, EBs provide a model for interrogating the interplay between differentiating cells and their microenvironment, including mineralization, extracellular matrix, and associated growth factors, during the earliest stages of bone development, lending novel insights into the potential interactions between the processes of mineralization and differentiation.

Materials and Methods

Mouse ESC culture and EB formation

Undifferentiated mouse ESCs (D3 line) were grown and maintained in the undifferentiated state on tissue culture dishes coated with 0.1% gelatin with the addition

of leukemia inhibitory factor (LIF). EBs were formed from single cell suspensions of 2 x 10^5 cells/ml in ESC medium without LIF and formed on rotary orbital shakers at 40 rotations per minute as described previously (see Chapter 3 – General Methods) [147].

EB osteogenic differentiation

EBs were supplemented with 0, 2.5, 5, and 10 mM βGP from day 5 of suspension culture onward (MP Biomedical, Solon, OH). Phase images of EBs in each βGP treatment group were taken throughout the duration of the experiments (up to 14 days of differentiation) and were analyzed using Metamorph™ software (v. 7.5, Molecular Devices, Sunnyvale, CA). Mineral deposits were visualized as dark, irregularly shaped deposits compared to surrounding cells and media by phase contrast. EBs exhibiting characteristics of mineral deposition were identified by the software based on brightness, and the percentage of EBs containing mineral accumulation was determined.

Histology

EBs were collected, fixed in 10% formalin solution, rinsed in PBS, and embedded in Histogel (~200 EBs in 200 µl gel; Richard Allen Scientific, Kalamazoo, MI) before paraffin processing and embedding. Mineralization was assessed by von Kossa and Alizarin red staining. Slides were imaged using a Nikon 80i Upright Microscope, and digital brightfield images were acquired for quantification of positively stained EBs (see Chapter 3 – General Methods).

Micro-computed tomography (µCT)

Approximately 200-500 day 14 EBs were suspended in 200 µl of Histogel™ (Richard Allen Scientific). Reference images of EB samples were taken, and samples were scanned in air using a µCT 40 (Scanco Medical, Brüttisellen, Switzerland) at 45 kVp, 177 µA, 200-ms integration time, and a voxel size of 12 µm in a 12 mm scanning tube. Evaluation of µCT scans used sigma, support and threshold values set at 0.8, 1, and 70, respectively. The total volume of mineralization within each entire Histogel-embedded sample was determined and normalized to estimated EB volume to calculate the average percentage of mineralization (see Chapter 3 – General Methods).

Quantitative real-time polymerase chain reaction (qRT-PCR)

For real-time PCR analysis, total RNA was extracted from undifferentiated ESCs or EBs after 7 and 14 days of differentiation. Complementary DNA was synthesized, and quantitative PCR was performed with SYBR green technology on the MyiQ cycler (Bio-Rad). Primers for *osteocalcin, bone sialoprotein, collagen type I, osterix,* and *Runx-2* were used to assess osteogenic differentiation, in addition to housekeeping gene *GAPDH* (see Chapter 3 – General Methods, Table 3.1). Gene expression was examined to determine if levels of mRNA for several other key proteins were sensitive to osteoblastic differentiation. VDR and PDIA3 are receptors for $1\alpha,25(OH)_2D_3$; osteoprotegerin (OPG) is secreted by differentiated osteoblasts [178]; osteopontin is a $1\alpha,25(OH)_2D_3$-sensitive extracellular matrix protein that possesses a VDRE [179] and is regulated via PDIA3 [126]; and α2β1 integrin expression is associated with osteoblast differentiation through collagen type 1 recognition [9, 10]. Expression of mRNA was measured for mouse *Vdr*, *Pdia3*, *Tnfsf11* (the gene that codes for osteoprotegerin), osteopontin (*Opn*), integrin

alpha 2 (*Itga2*), and integrin beta 1 (*Itgb1*) (primer sequences listed in Table 4.1). *Pit-1* expression was verified by conventional PCR of cDNA samples with 35 cycles using GoTaq Flexi DNA Polymerase (Promega, Madison, WI).

Table 4.1. Primer sequences used in qRT-PCR analysis.

Vdr	F	AGG CAG GCA GAA GAG ATG AG
	R	AGG GAT GAT GGG TAG GTT GTG
Pdia3	F	CCA ATG ATG TGC CTT CTC
	R	TGT GCC TTC TTC TTC TTC
Tnfsf11	F	CGC CAA CAT TTG CTT TCG
	R	TGC TCC CTC CTT TCA TCA
Opn	F	AAC TCT TCC AAG CAA TTC C
	R	TCT CAT CAG ACT CAT CCG
Itga2	F	ACT GTT CAA GGA GGA GAC
	R	GGT CAA AGG CTT GTT TAG G
Itgb1	F	ATT ACT CAG ATC CAA CCA C
	R	TCC TCC TCA TTT CAT TCA TC
Gapdh	F	TTC AAC GGC ACA GTC AAG G
	R	TCT CGC TCC TGG AAG ATG G
Pit-1	F	CAC CCA TAT GGC TTC TGC TT
	R	CAG GAA TTC ATA GCC CAG GA

Immunohistochemistry

Immunohistochemistry was performed to assess the distribution of PDIA3 and VDR in the EBs. EBs were fixed in 10% formalin, embedded in Histogel (Richard Allen Scientific, Kalamazoo, MI), processed, and embedded in paraffin. For each sample, 5µm sections were taken every 50µm and affixed to positively charged glass slides. Deparaffinized slides were used for staining. Samples were stained with antibodies

against PDIA3 and VDR, with Alexa Fluor 488 phalloidin (Invitrogen) to stain actin filaments, and DAPI to stain the nucleus (Invitrogen).

Osteogenic protein production

In addition to verifying that the EBs expressed mRNAs for proteins associated with osteoblastic differentiation, immunoassay was used to quantify production of secreted proteins. After 14 days culture in control medium or medium supplemented with *β*GP, EBs were treated for 24h with 10 nM $1\alpha,25(OH)_2D_3$ (Enzo Life Sciences, Plymouth Meeting, PA). The dose of $1\alpha,25(OH)_2D_3$ was based on previous studies examining the effects of the vitamin D metabolite on differentiation of ESCs into mineralizing osteoblasts [105]. Osteocalcin in the conditioned medium was measured using a commercially available radioimmunoassay (Biomedical Technologies, Inc., Stoughton, MA). Osteoprotegerin and osteopontin in the conditioned media were measured using commercially available ELISAs, according to manufacturer's specifications (DuoSet, R&D Systems, Minneapolis, MN,).In EBs, levels of secreted proteins in conditioned media were normalized to total DNA content (Quant-iT PicoGreen Assay, Invitrogen). EBs were then lysed in 0.05% Triton X-100 and alkaline phosphatase specific activity was measured as the release of *p*-nitrophenol from *p*-nitrophenylphosphate at pH 10.2. Alkaline phosphatase specific activity in the cell pellet was normalized to total protein content (Pierce BCA Protein Assay, Thermo Fisher, Rockford, IL) [180].

Protein Kinase C assay

PKC activity was measured in response to $1\alpha,25(OH)_2D_3$ in order to determine if PDIA3 was functional. EBs were cultured as above until day 14. Based on previous studies showing that 10 nM $1\alpha,25(OH)_2D_3$ causes rapid PDIA3-dependent activation of PKC in mouse osteoblasts within 9 minutes [126], both cell types were then treated for 9 minutes with either 0.01% ethanol (vehicle) or 10 nM $1\alpha,25(OH)_2D_3$. After incubation, EBs were spun for 3m at 2000x*g*, the medium removed, and lysed in 1ml cold RIPA buffer (20mM Tris-HCl, 150mM NaCl, 5mM disodium EDTA, 1% Nonadet P-40). PKC activity was measured using a commercially available assay kit (GE Biosciences, Piscataway, NJ) and results normalized to total protein content of the lysates as described above.

Human mesenchymal stem cells

The expression of receptors for $1\alpha,25(OH)_2D_3$ in EBs was compared to expression in human mesenchymal stem cells (MSCs, Lonza Walkersville, Walkersville, MD) during osteoblastic differentiation. MSCs were cultured in MSC growth medium (GM, Lonza Walkersville) or hMSC Osteogenic BulletKit (OST, Lonza Walkersville) for 14 days. Western blots were performed for VDR, PDIA3, and GAPDH as described above. Effects of $1\alpha,25(OH)_2D_3$ on differentiation were assessed as a function of alkaline phosphatase specific activity, and osteocalcin and osteoprotegerin production. MSCs cultured for 14 days in GM or OST. $1\alpha,25(OH)_2D_3$ (10 nM) was added to the cultures for an additional 24h and the conditioned medium was collected. Enzyme activity was measured in cell lysates. Secreted proteins were normalized to total cell number (Z2 Cell Counter, Beckman Coulter, Hercules, CA).

Presence of functional PDIA3 was determined by assessing $1\alpha,25(OH)_2D_3$-dependent PKC activity. MSCs were cultured in growth medium until confluence. Cells were treated with $1\alpha,25(OH)_2D_3$ for 15 minutes, and lysed in RIPA immediately after treatment. PKC was assayed as described above.

Western blotting

EBs were collected at day 14 of differentiation for western blot analysis of ERK pathway activation. Membranes were probed with anti-ERK, anti-pERK (1:250, Cell Signaling Technology, Danvers, MA), and anti-GAPDH (1:2000) antibodies. Membranes were then incubated with infrared secondary antibody (1:5000, 800 anti-rabbit, Li-Cor Biosciences, Lincoln, NE), and imaged using the Odyssey Infrared Imager (Li-Cor) (see Chapter 3 – General Methods).

Additional Western blots of VDR and PDIA3 were performed to validate the presence of these proteins in the EBs. Treated EBs were lysed in 300µl RIPA buffer and resolved on 4-20% Tris glycine gels (LongLife, NuSep, Bogart, GA) using gel electrophoresis. Proteins were transferred from the gel onto a nitrocellulose membrane using the iBlot® Dry Blotting transfer method (Invitrogen, Carlsbad, CA). Membranes were then incubated overnight using specific primary antibodies against PDIA3 (sc-18620, Santa Cruz Biotechnology, Santa Cruz, CA), VDR (sc-1008, Santa Cruz Biotechnology) or glyceraldehyde 3-phosphate dehydrogenase (GAPDH, MAB374, Millipore, Billerica, MA). After primary antibody incubation, membranes were then incubated in 1% BSA in PBS with either goat anti-rabbit or goat anti-mouse horseradish peroxidase-conjugated secondary antibodies (Bio-Rad Laboratories) for one hour. Blots

were developed using SuperSignal West Pico Chemiluminescent System (Thermo Fisher Scientific, Rockford, IL). Membranes were imaged using VersaDoc imaging system (Bio-Rad Laboratories). Pixel intensity of bands was quantified using Quantity One Software (Bio-Rad Laboratories) and normalized to pixel intensity of GAPDH.

Statistical analysis

Two-way ANOVA analysis, followed by Tukey's post-hoc test, was performed to determine statistical differences ($p<0.05$), using Systat 12™ statistical software unless otherwise noted. Results are reported as mean ± standard error of the mean for a minimum of triplicate experiments from each experiment unless otherwise noted; a minimum of two independent experiments were analyzed by each of the assays described.

For $1\alpha,25(OH)_2D_3$ experiments, each data point is the mean $\pm$ standard error for six independent cultures, with the exception of the mRNA expression experiment, where n=4. The data shown for the mRNA analyses are ratios of the mRNA for the gene of interest to *Gapdh* rather than treatment/control ratios to enable analysis of experimental variability. Data were analyzed by analysis of variance and significant differences between groups determined using Bonferroni's modification of the Student's t-test. $P<0.05$ was considered to be significant.

Results

Mineralization within EBs

D3 ESC derived EBs were cultured in media supplemented with 10 mM βGP as a phosphate substrate to assess the endogenous mineralization capacity of differentiating EBs. Small von Kossa positive foci of mineral deposits were apparent by day 10 of differentiation within βGP treated EBs, but were not readily apparent in untreated cultures, and the mineral accumulations increased in size and number per EB through day 14, while untreated samples exhibited little positive staining (Fig. 4.1 A). EBs cultured with lower concentrations of βGP (1, 2.5, and 5 mM) were additionally examined and each dose exhibited an increase in mineralization throughout the EB populations over the 14 day differentiation, but less prominent than at 10 mM, with smaller mineralized regions and fewer mineral deposits per EB, assessed by light microscopy (Fig. 4.2 A). Therefore, all subsequent experiments were carried out comparing untreated EBs with 10 mM βGP treated EBs, which was also equivalent to concentrations used in common osteogenic differentiation methods for both mesenchymal stem cells and ESCs [105, 108, 181]. The presence of calcium phosphate, as seen in bone, was verified by staining serial sections of EBs with von Kossa and Alizarin red. Previous studies have suggested that the use of one characterization technique alone may not be sufficient to demonstrate calcium phosphate deposition *in vitro* since each stains independently for either calcium (Alizarin red) or phosphate (von Kossa) species [37]. EBs at day 14 contained overlapping areas that stained positive for both von Kossa (in black) and Alizarin red (in red), therefore indicating that the mineral deposits were composed of calcium and phosphate (Fig. 4.1 B). Equivalent percentages of βGP-treated EBs contained regions of positive staining for each stain (60.2 ± 15.6% von Kossa positive, 40.0 ± 17.6% Alizarin

red positive), with minimal staining (< 7%) present in untreated samples ($p<0.001$, t-test) (Fig. 4.1 C). To test whether the formation of mineral deposits was limited to the ESC cell type used (D3), another mouse ESC line (R1) was used, and similar mineralization was also observed (Figure 4.2 B). Based on histological analysis, βGP treated D3 EBs produce calcium phosphate mineralization that increases throughout differentiation, however further quantification of mineralization was undertaken because histological techniques do not fully capture the three dimensional extent and distribution of deposits within EBs.

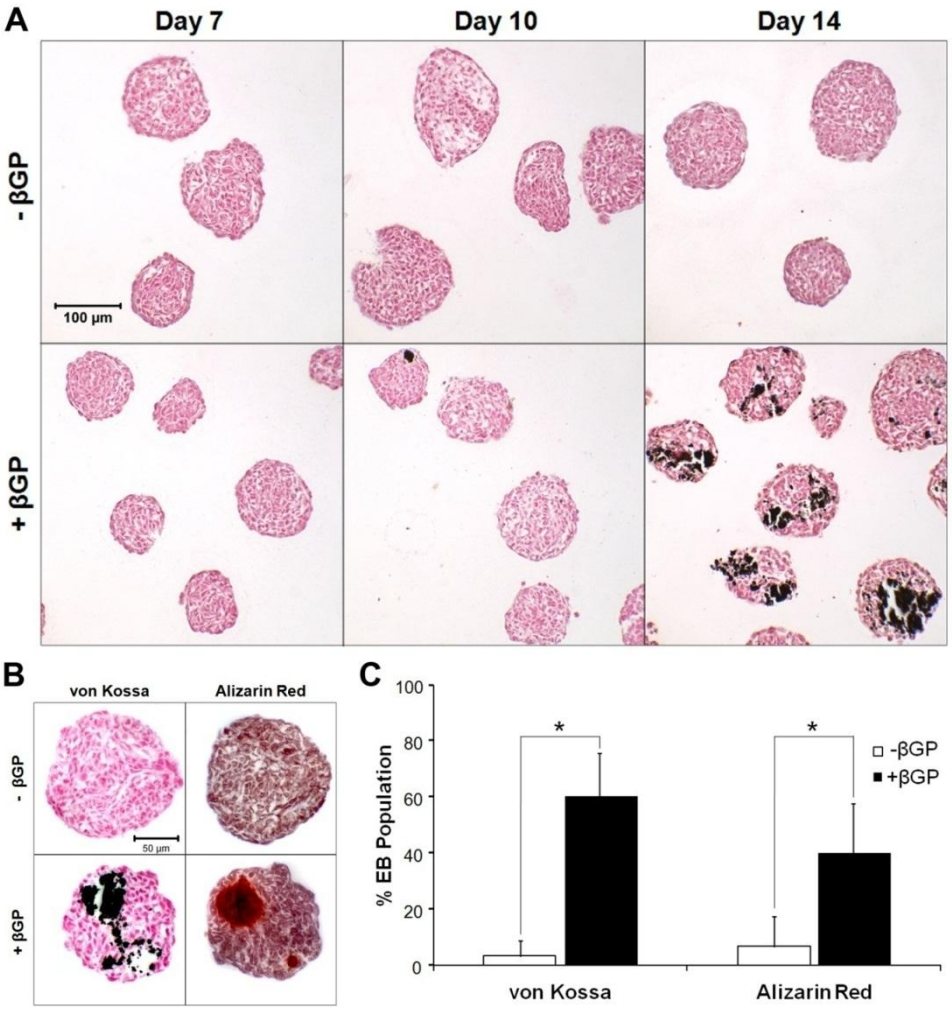

Figure 4.1. Calcium phosphate deposition within EBs. Von Kossa staining of EBs differentiated with βGP increased in EBs/ population and per EB compared to untreated samples (A). Further histological analysis of serial sections of untreated and treated embryoid bodies demonstrated that the deposits stained positively by both von Kossa and Alizarin red staining (B). Quantification of both von Kossa and Alizarin red staining by image analysis demonstrated equivalent increases in both stains with treatment at day 14 (C) (n=3 cultures, t-test, *p<0.001). (Scale bar in A = 100 µm, B = 50 µm, C = 500 µm).

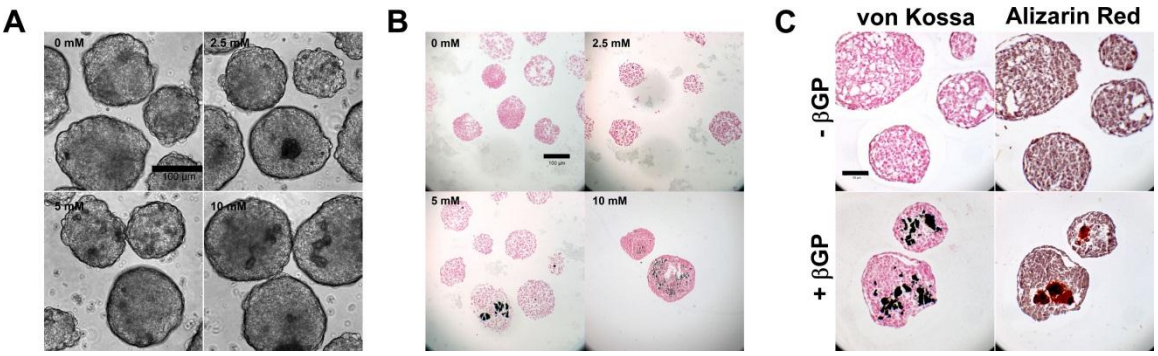

Figure 4.2. Mineral deposits within EBs. Phase imaging and von Kossa staining of EBs differentiated with varying concentrations of βGP demonstrated a dose response with increasing βGP (A). Mineral deposit formation occured with 10 mM βGP treatment of R1 line mouse ESCs, similar to that observed in D3 line ESCs used primarily in this study. (Scale bar in A and B = 100 μm, C = 50 μm).

The overall mineralization within EB populations was further analyzed by quantifying the percentage of EBs with regions of mineralization. Mineralization was observed by phase contrast as dark, irregularly shaped regions within treated EBs (Fig. 4.3 A, B). The overall mineral deposition at day 10 throughout the treated EB population was greater than had been apparent based on histological analyses. The percentage of EBs with mineral deposits significantly increased in βGP treated EBs at days 10 (75.5 ± 3.9%, $p<0.001$) and 14 (84.3 ± 3.8%, $p<0.001$) compared to untreated samples (<10%) (Fig. 4.3 A, C). This was in good agreement with the histological analysis (Fig. 4.1 A). Based on the distribution of EB sizes, measured in Metamorph™ image analysis software, βGP treated EBs were slightly smaller than untreated EBs (22.2 ± 1.6 x 10^3 μm^2 treated vs. 29.5 ± 1..2 x 10^3 μm^2 untreated, $p<0.001$, t-test) (Fig. 4.3 D, E). The degree of mineralization of EBs, defined as the number of mineralized EBs compared to total number of EBs of the same size, remained at this same level across the distribution of EB sizes, with between 70-100% of treated EBs containing mineral deposits at any given size (Fig. 4.3 D, E). However, the presence of mineralization within untreated EBs remained low (<15%) across all EB sizes. Based on stains for calcium and phosphate and phase images of differentiating EBs, mineralization occurs within EBs with βGP treatment, and mineral deposits increase in size and number through the duration of treatment in this study.

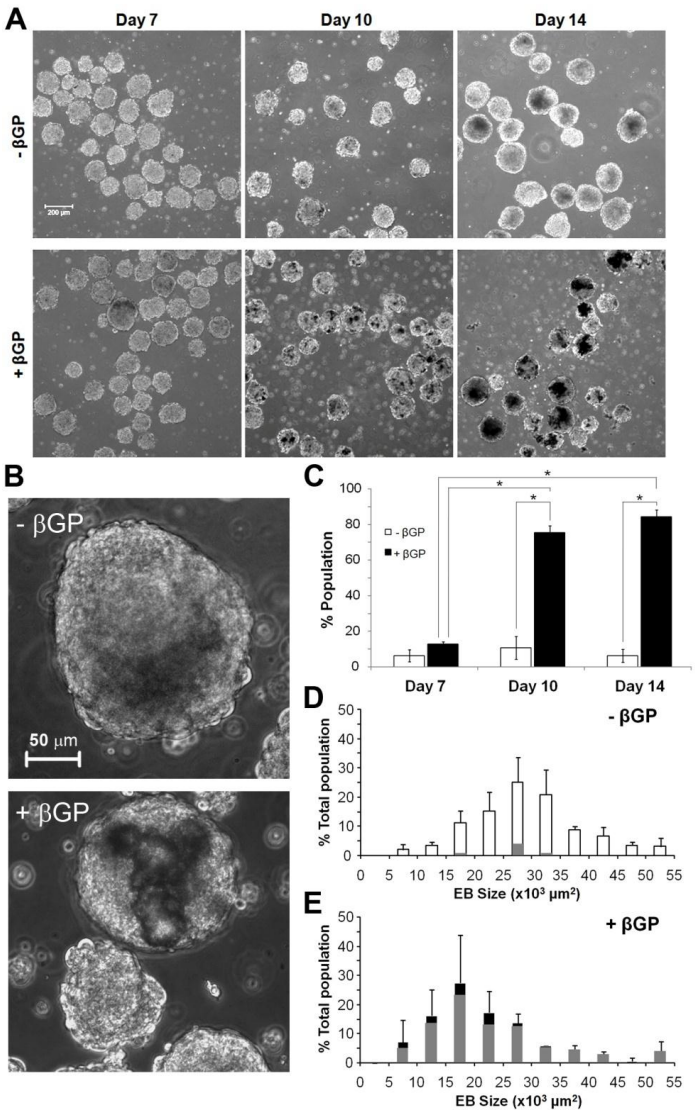

Figure 4.3. Quantification of mineralization. βGP treated EBs accumulate mineral deposits much more readily and abundantly than untreated samples based upon phase contrast images (A). EBs were treated with 10 mM βGP from day 5-14 of differentiation. Mineral accumulation within the EBs, visualized by phase contrast as dark regions within EBs, were observed abundantly in treated EBs but not untreated EBs (B). The percentage of the total, treated population with mineral accumulation increased significantly by day 10 of EB culture (n=3 cultures, two-way ANOVA, Tukey's post-hoc test, $p<0.001$) (C). The percentage of EBs that exhibited mineral accumulation (grey overlay bars) within treated EBs was consistent across the distribution of EB sizes observed, though average EB size was smaller with treatment (n=3 cultures, t-test, $p<0.001$) (D,E). (Scale bar in A = 200μm, scale bar in B = 100 μm)

μCT analysis of mineral deposition

While the histological assessments used have allowed for the identification and localization of the EB mineralization, μCT allows for the quantification of mineralization volume in three dimensions [182]. μCT also provided the added benefit of enabling one easily to assess the mineralization within an entire population and to quantify this volume of mineralization for comparison across treatment groups in a non-destructive manner. This imaging technique has been routinely used to assess mineralization and bone formation within *in vivo* applications [183]. μCT analysis was performed on day 14 of differentiation because previous histological and phase analyses illustrated that mineral deposits were present within the resolution of μCT. Images of the Histogel™-embedded EBs were first taken using a stereomicroscope to verify comparable numbers of EBs were loaded in each sample and to determine the distribution of the EBs within the gels (Fig. 4.4 Ai, Aiii). The volume of mineralization determined by μCT was normalized to the total calculated volume of EBs loaded into each gel. Treatment with βGP resulted in a greater amount of radio-opaque material than in untreated samples, as seen by scans of day 14 EB samples (Fig. 4.4 Aii, Aiv). Abundant mineralization was evident in EBs with βGP treatment (31.06 ± 9.66%), but was significantly less in EBs without supplementation (0.06 ± 0.02%) ($p<0.05$, t-test). The mineral deposits from μCT images at higher magnifications (regions indicated within boxes) overlapped within the respective regions containing EBs imaged by stereomicroscopy (Fig. 4.4 B). μCT provided visualization and quantitative analysis of the mineralization deposits within EBs in three-dimensions, and in this study, presented further evidence of the calcium phosphate mineralization process occurring within βGP treated EBs.

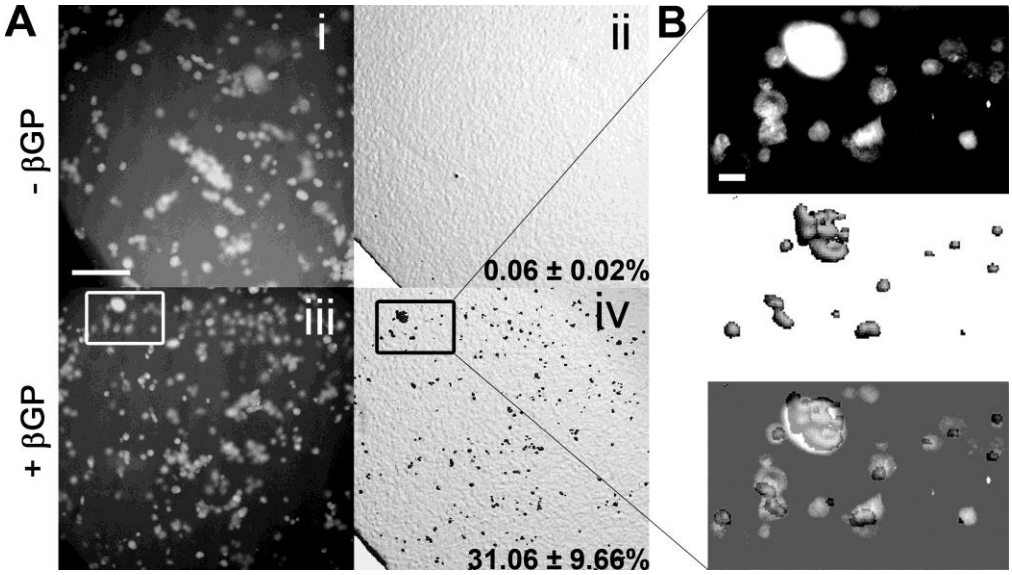

Figure 4.4. Quantification of mineralization by µCT. An equivalent number of Histogel embedded, day 14 EBs, first imaged by stereomicroscope (-βGP (A i) and +βGP (A iii), were analyzed by µCT to assess degree of mineralization. The percentages of mineralized volume, normalized to EB volume, were found to be 31.06 ± 9.66% for treated EBs (A ii) vs. 0.06 ± 0.02% for untreated EBs (A iv) (t-test, $p<0.05$, n = 3 samples). EBs and mineral deposits overlap in stereoscope (B top) and µCT (B middle) images (regions indicated by boxes) (merge – B bottom). (Scale bar in A = 1mm, scale bar in B = 100 µm)

Phosphate induced signaling

Because phosphate transport has been suggested to be necessary for matrix mineralization and to induce osteogenic differentiation, the gene level expression of the Na, Pi co-transporter PiT-1 was assessed. *Pit-1* has been found to be ubiquitously expressed at the message level, but its expression and not that of the related Na,Pi co-transporter, *Pit-2,* has been demonstrated to be increased during the course of osteoblast differentiation in MC3T3-E1 cells [118]. Additionally, phosphate transport through PiT-1 is required for matrix mineralization to occur [119, 120, 124]. Undifferentiated ESCs express mRNA for *Pit-1,* and maintain expression through day 14 of EB differentiation, regardless of βGP treatment (Fig. 4.5 A). qRT-PCR for *Pit-1* was also performed and confirmed that gene expression remained constant throughout EB differentiation and was the same as differentiated MC3T3-E1 controls (Fig. 4.5 B).

Phosphate induced osteogenic differentiation, which accompanies mineralization in response to phosphate treatment, has been found to occur through ERK 1/2 pathway signaling [107, 116], so ERK phosphorylation in βGP treated EBs was assessed. βGP treated EBs exhibited an increase in the ratio of phosphorylated to non-phosphorylated ERK at day 14 compared to untreated EBs. The finding by Western blot was in good agreement with the increased mineralization observed earlier, suggesting enhanced signaling and activation of the ERK pathway (Fig. 4.5 C).

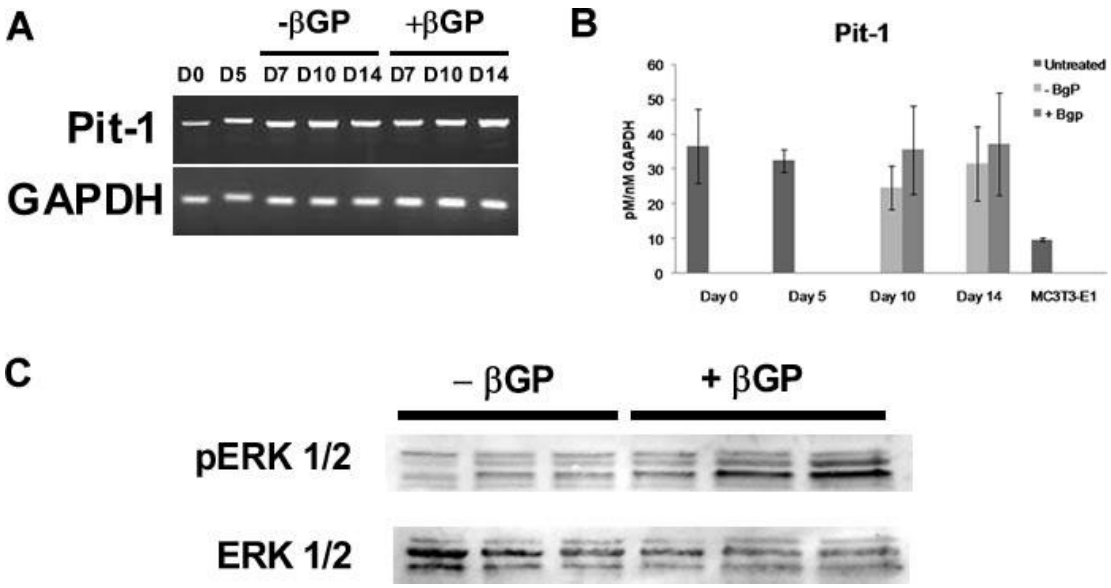

Figure 4.5. **Phosphate transport and signaling.** At the gene level, ESCs differentiated as EBs express the Type III Na,Pi co-transporter, *Pit-1*, which permits the entry of Pi into cells (A). No difference in *Pit-1* expression was observed by qRT-PCR throughout EB differentiation with or without βGP compared to MC3T3-E1 cells (n=3, two-way ANOVA, Tukey's post-hoc test). When βGP was provided in the culture media, the ratio of pERK to ERK was increased (C). Western blot samples were collected at day 14 of EB differentiation and are shown in triplicate.

Osteogenic gene expression

Based on the observed time course for mineralization within differentiating EBs, osteogenic marker gene expression was assessed at days 7 and 14 of differentiation. Previous work in our lab has demonstrated that by day 5 of EB suspension culture, the expression of mRNA for Brachyury T, an early, transient mesoderm transcription factor, was increased compared to undifferentiated ESCs, confirming initial mesoderm differentiation, corresponding to the time when βGP administration was initiated in this study [184]. At day 7 of EB culture (two days after beginning βGP supplementation), no significant changes in the gene expression of osteogenic markers were found with βGP supplementation compared to both undifferentiated ESCs and untreated EBs. However by day 14 of EB differentiation, the expression level of several osteogenic marker genes were significantly increased with βGP treatment, in conjunction with the observed increase in EB mineralization and ERK phosphorylation (Fig. 4.6). The expression level of osteogenic transcription factor *Runx-2* increased 9-fold with βGP treatment compared to untreated EBs ($p<0.05$), and since mineralization was known to be mediated by interactions with the extracellular matrix, the expression of genes encoding several osteogenic matrix proteins was also quantified. The gene expression was increased for *bone sialoprotein* (14-fold, $p<0.05$), and *osteocalcin* (9-fold, $p<0.05$) in βGP treated EBs compared to untreated EBs (Fig. 4.6). However, the expression of *collagen-I* and *osterix*, an osteogenic transcription factor expressed downstream of *Runx-2*, did not increase with treatment over the 14 day time course of this experiment. Additionally, the observed increase in osteogenic gene expression corresponded with the increases in mineralization

and ERK signaling activation also observed at day 14 of differentiation with βGP treatment.

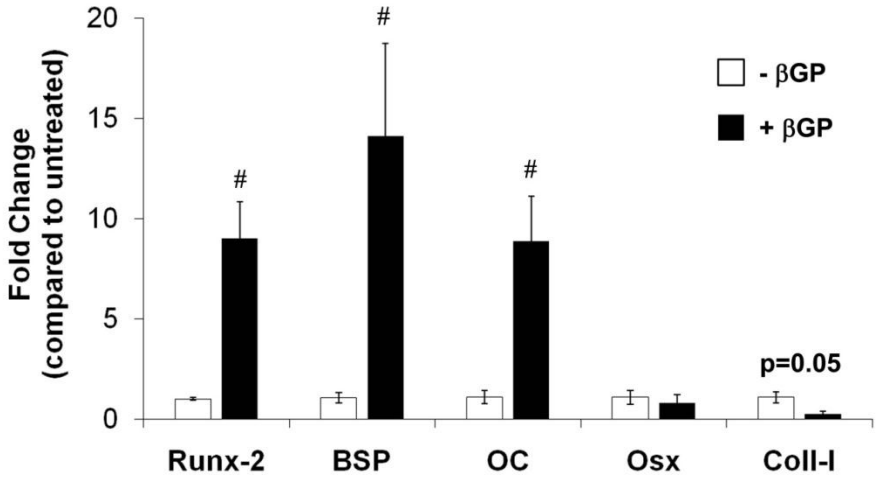

Figure 4.6. Osteogenic gene expression. The expression of several osteoblast marker genes was assessed by RT-PCR. The expression of the gene for the osteoblast transcription factor, RUNX-2, along with genes encoding several bone matrix proteins, including bone sialoprotein (BSP) and osteocalcin (OCN), were increased with βGP treatment by day 14. Osterix (OSX), and collagen-I (Coll-I) were unchanged. No differences between treated and untreated EBs were observed at Day 7 (t-test, # $p<0.05$, n = 3 samples).

Vitamin D receptor expression

To further characterize the osteogenic differentiation, vitamin D receptor expression at the gene and protein levels were then determined. EBs expressed mRNAs for VDR and PDIA3 and expression of each receptor mRNA was differentially regulated (Fig 4.7). After 7 days of differentiation, expression of *Vdr* was higher in EBs cultured in medium supplemented with *β*GP when compared to control medium (Fig. 4.7 A); this effect was more pronounced after 14 days. Expression of *Pdia3* was similar at days 0 and 7 in both media (Fig. 4.7 B). After 14 days, expression of *Pdia3* in control cells was higher than at day 0 or day 7, but 14 days of culture in the presence of *β*GP decreased expression of *Pdia3*.

The presence of both vitamin D receptors was confirmed using Western blot (Fig. 4.7 C). The ratio of VDR/GAPDH increased from day 0 to day 14 in both control and *β*GP culture groups (Fig. 4.7 C, D). In contrast, PDIA3/GAPDH decreased at 14 days in cultures grown in medium containing *β*GP compared to day 0 (Fig. 4.7 C, E). The presence of PDIA3 and VDR was also demonstrated by immunofluorescence staining (Fig. 4.7 F). VDR and PDIA3 were distributed throughout the cell aggregates in control cultures after 14 days (Fig. 4.7 F, left panels). However, EBs cultured with *β*GP had more VDR staining and less PDIA3 staining (Fig. 4.7 F, middle panels), an effect more evident at higher magnification (Fig. 4.7 F, right panels; 100x).

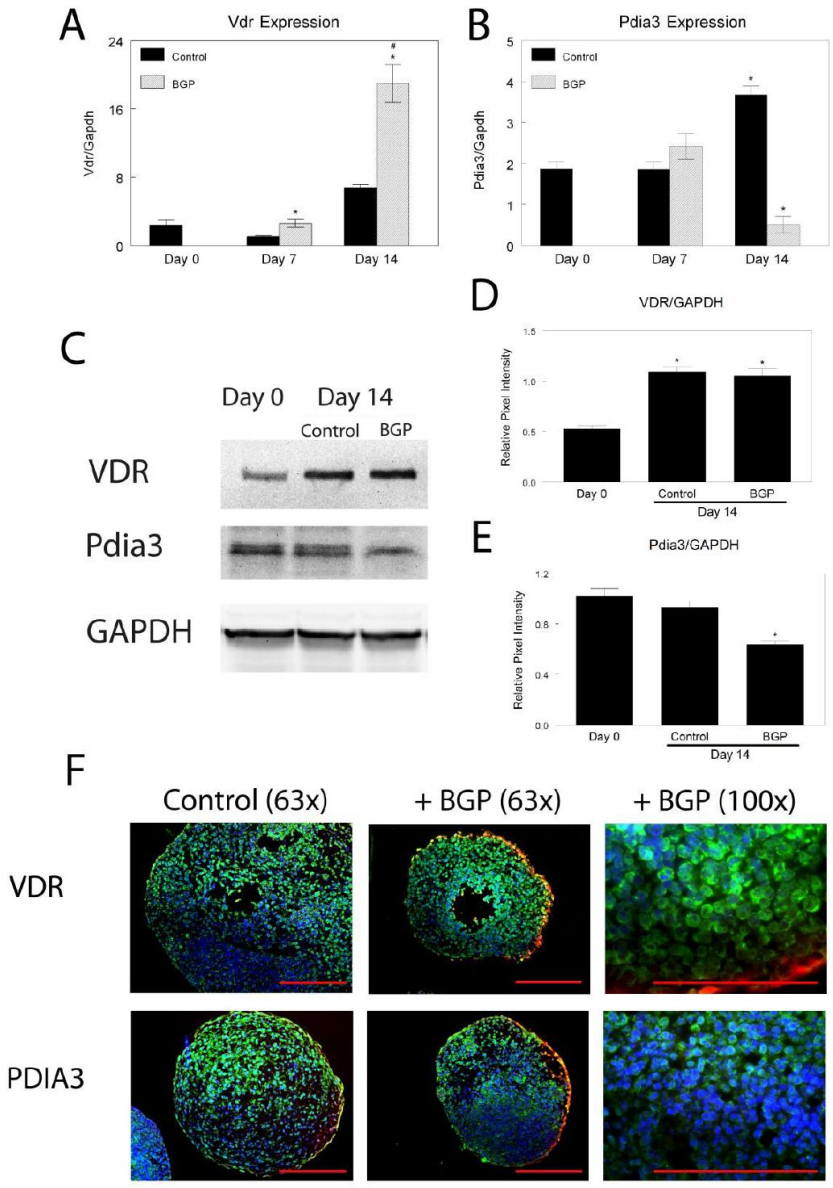

Figure 4.7. Evaluation of vitamin D receptors in mouse EBs. Embryoid bodies were cultured with control medium or medium supplemented with β-glycerophosphate (*B*GP). Real-time qPCR was performed on samples at embryoid body formation (day 0), or after 7 or 14 days in culture. mRNA expression of Vdr (A) and Pdia3 (B) were measured and are presented as normalized to GAPDH. *p<0.05, vs. day 0; #p<0.05, vs. control. VDR and Pdia3 proteins were analyzed by Western blot using GAPDH as a reference (C). Ratios of VDR/GAPDH (D) and PDIA3/GAPDH (E) were calculated using pixel intensity of Western blot bands. *p<0.05, vs Day 0. Immunofluorescent staining of embryoid bodies was performed for VDR and Pdia3 after 14 days culture in control medium or medium supplemented with *B*GP (F). Cells were stained for β-actin (red), DAPI nuclear staining (blue) and antibodies against either VDR or Pdia3 (green) and imaged at 63x or 100x magnification.

Responsiveness to 1α,25$(OH)_2D_3$ stimulation

Changes in markers associated with osteogenic differentiation showed that EBs cultured in medium containing *β*GP exhibited an osteoblast-like phenotype and were more responsive to 1α,25$(OH)_2D_3$ than untreated cells. DNA content of EBs was similar among groups, independent of treatment (Fig. 4.8 A). In cells cultured in control medium, alkaline phosphatase specific activity was unaffected by 1α,25$(OH)_2D_3$ treatment (Fig 4.8 B). However, culture with *β*GP stimulated alkaline phosphatase specific activity, and this effect was enhanced by 1α,25$(OH)_2D_3$ (Fig. 4.8 B). Osteocalcin (Fig. 4.8 C), osteoprotegerin (Fig. 4.8 D), and osteopontin (Fig. 4.8 E) were equally stimulated by 1α,25$(OH)_2D_3$ or *β*GP treatment alone. Culture with *β*GP followed by 1α,25$(OH)_2D_3$ treatment stimulated greater osteocalcin and osteopontin secretion than 1α,25$(OH)_2D_3$ alone.

This treatment regime also affected expression of other genes. In EBs cultured in control medium, *Tnfsf11* mRNA expression was upregulated after 1α,25$(OH)_2D_3$ treatment in comparison to control cultures (Fig. 4.9 A). This effect was more robust when cells were cultured in medium containing *β*GP. *Opn* expression was not affected in cells cultured in medium with *β*GP or in control cultures treated with 1α,25$(OH)_2D_3$ (Fig. 4.9 B). However, expression increased when EBs that had been grown in osteogenic medium were treated with 1α,25$(OH)_2D_3$. *Itga2* mRNA was higher in cells cultured with *β*GP and treated with 1α,25$(OH)_2D_3$ than control cells (Fig. 4.9 C). 1α,25$(OH)_2D_3$ stimulated *Itgb1* expression in control medium and expression was also higher in osteogenic medium compared to control medium. There was a synergistic increase in expression in cultures grown in osteogenic medium and then treated with the vitamin D

metabolite (Fig. 4.9 D). With respect to phosphate treatment alone, osteogenic marker and matrix proteins were upregulated by βGP treatment, paralleling results observed in gene level assessments, suggesting that providing the minimal substrate to induce mineralization was sufficient to alter and influence differentiation but that additional inductive signals were required for more directed commitment to the osteogenic lineage by cells within EBs.

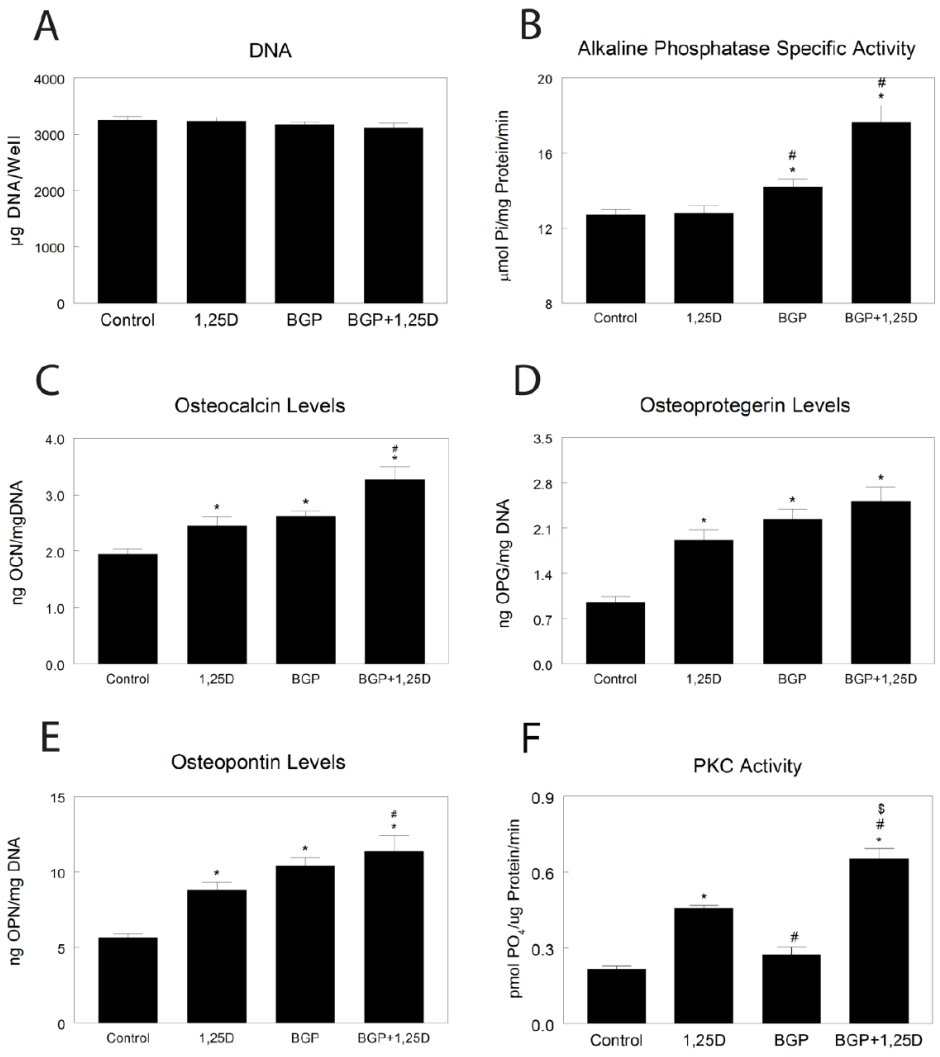

Figure 4.8. Osteogenic phenotype of mouse EBs. Embryoid bodies were cultured for 14 days in medium or medium supplemented β-glycerophosphate (*B*GP). EBs were then treated with 0.01% ethanol or 1α,25$(OH)_2D_3$ for 24h. DNA content (A) and alkaline phosphatase specific activity (B) were measured in cell lysates. Secreted osteocalcin (C), osteoprotegerin (D), and osteopontin (E) were measured in the conditioned medium. *p<0.05, vs. control; #p<0.05, vs. 1α,25$(OH)_2D_3$. To assess rapid, membrane-initiated signaling, protein kinase C activity was measured in EBs treated with 0.01% ethanol or 1α,25$(OH)_2D_3$ for 9 minutes. *p<0.05, vs. control; #p<0.05, vs. 1α,25$(OH)_2D_3$; $p<0.05, vs. *β*GP.

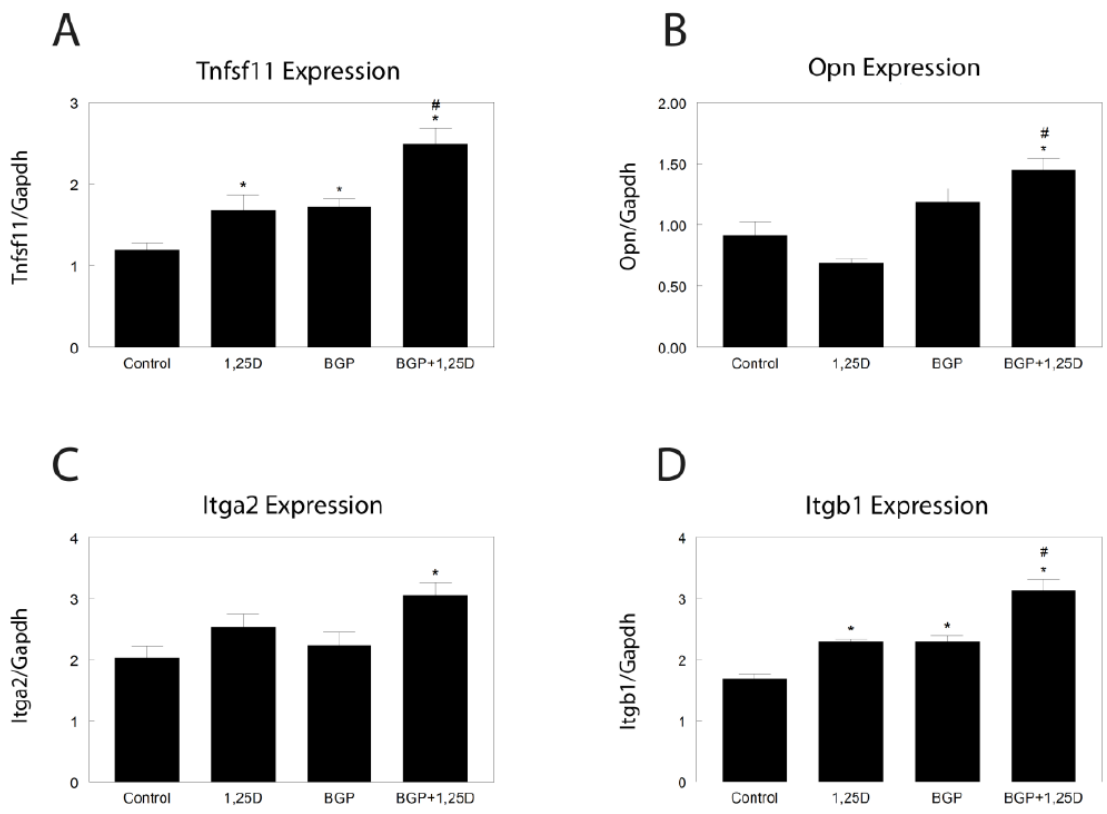

Figure 4.9. Osteogenic gene expression of mouse EBs. Embryoid bodies were cultured for 14 days in medium or medium supplemented with β-glycerophosphate (*B*GP). EBs were then treated with 0.01% ethanol or $1\alpha,25(OH)_2D_3$ for 12h. Expression of *Tnfsf11* (A), osteopontin (*Opn*, B), *Itga2* (C), and *Itgb1* (D) were measured by real-time qPCR. Gene expression was normalized to expression of Gapdh mRNA per 1 ug RNA. *$p<0.05$, vs. control; #$p<0.05$, vs. $1\alpha,25(OH)_2D_3$.

Finally, to evaluate whether the effects of $1\alpha,25(OH)_2D_3$ on EBs were a general property associated with multipotent cell osteogenic differentiation, receptor expression and responsiveness to $1\alpha,25(OH)_2D_3$ were tested in MSCs. Human MSCs exhibited differential levels of VDR and PDIA3 when cultured in GM or OST in a manner comparable to EBs. VDR in cell lysates was higher in cells cultured in OST than in GM (Fig. 4.10 A, B) and PDIA3 was similar in cells cultured in GM and OST (Fig. 4.10 A, C). Levels of alkaline phosphatase specific activity (Fig. 3.11 A), osteocalcin (Fig. 4.11 B), and osteoprotegerin (Fig. 4.11 C) were higher in cells cultured in OST than in cells cultured in GM.

PDIA3 was functional in both EBs (Fig. 4.8 F) and in MSCs (Fig. 4.11 D). PKC activity was comparable in control EB cultures and in EB cultures grown in medium containing βGP. $1\alpha,25(OH)_2D_3$ treatment caused a rapid increase in PKC activity in EBs cultured in both medium but the effect was 50% greater when EBs were grown in osteogenic medium. Similarly, $1\alpha,25(OH)_2D_3$ treatment caused a rapid increase in PKC activity in cultures of MSCs.

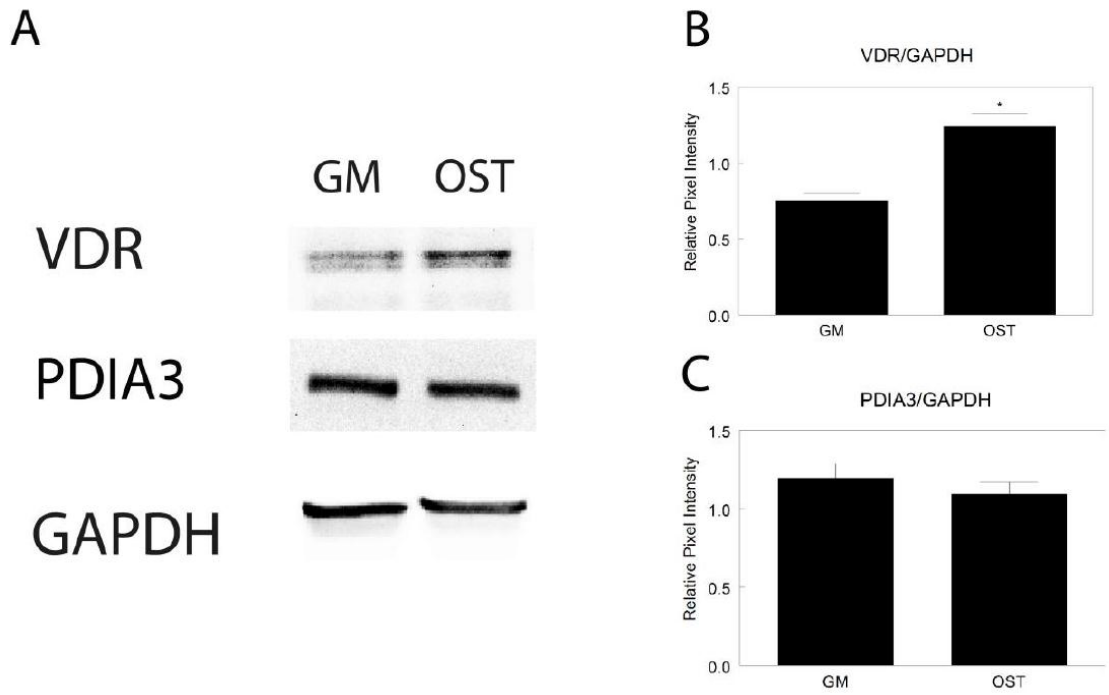

Figure 4.10. Western blot of Vitamin D receptors in human MSCs. MSCs were cultured with growth medium (GM) or osteogenic medium (OST) for 14 days as described. Western blots against VDR and PDIA3 were performed. (A) Western blots of MSC lysates against VDR, PDIA3, and GAPDH. Calculated ratios of VDR/GAPDH (B) and PDIA3/GAPDH (C) using pixel intensity of Western blot bands. *p<0.05, vs. GM.

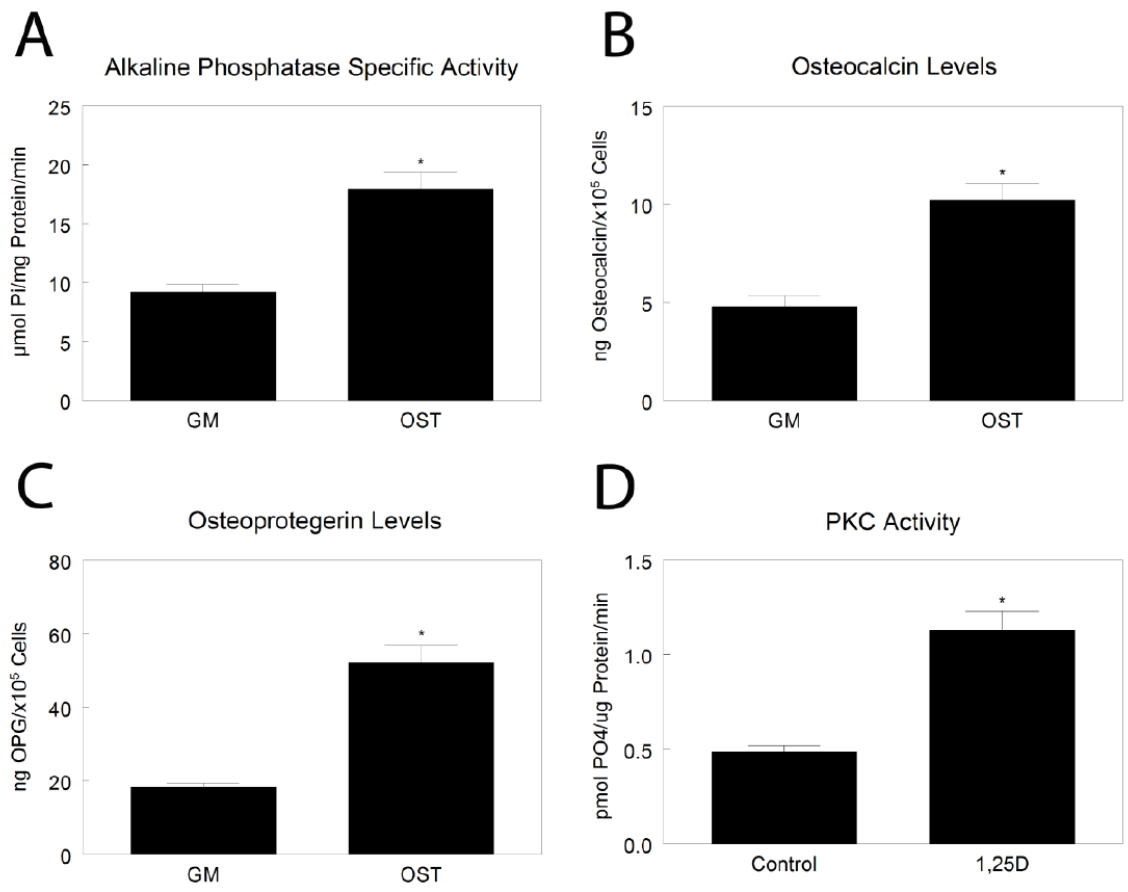

Figure 4.11. Osteogenic phenotype of human MSCs. MSCs were cultured in growth medium (GM) or osteogenic medium (OST) for 14 days. MSCs were treated with fresh medium for 24h. Alkaline phosphatase specific activity (A) was measured in the cell lysates. Levels of secreted osteocalcin (B) and osteoprotegerin (C) were measured in the conditioned medium. *$p<0.05$, vs. control**;** *$p<0.05$, vs. GM. To assess rapid, membrane-initiated signaling, protein kinase C activity was measured after 9 minutes treatment with 0.01% ethanol or $1\alpha,25(OH)_2D_3$ (D). *$p<0.05$, vs. control; #$p<0.05$, vs. $1\alpha,25(OH)_2D_3$.

Discussion

This study demonstrated that ESCs mineralize and undergo osteogenic differentiation when cultured with an inorganic phosphate source and that the observed differentiation was characterized by changes in vitamin D receptor expression and responsiveness. Though previous studies have suggested enhanced osteogenic differentiation in adherent, two dimensional culture systems [185, 186], βGP treated EBs produced mineralization, which was also accompanied by an induction of ERK signaling and osteogenic differentiation, demonstrated at the message and protein levels.

Calcium phosphate containing mineral deposits were formed in βGP treated EBs, as demonstrated by von Kossa and Alizarin red staining, the combination of which provide stronger evidence for calcium-phosphate deposition, as opposed to precipitation of calcium or phosphate individually out of solution [37]. Phase contrast microscopy and μCT were used to more thoroughly quantify the observed mineralization in addition to histological analysis. Analysis of mineralization by phase contrast also allowed for the study of the correlation between EB size and mineralization. The rotary culture method of EB formation method employed here can be used to form EBs of more uniform size than static culture, limiting variability in EB size that may impact differentiation [147]. The size distribution of EBs with mineral deposits matched that of the entire EB population, suggesting no tendency for EBs of a particular size being more or less likely to mineralize. However, it was noted that EB size within the entire βGP treated population was significantly smaller than in the untreated EB population. Potentially, this observation mimics *in vivo* and *in vitro* osteoblast differentiation, in which a shift to matrix production and matrix mineralization results in decreased proliferation[4]. Additionally, μCT was used as an added method to assess mineralization in three

dimensions to fully capture the three dimensional architecture, including size, shape, and distribution, of the mineralization occurring within three dimensional EBs. The volume of mineralization was significantly increased in βGP treated EBs, and overlays of μCT and stereoscope images confirmed histological and phase imaging findings of multiple mineral deposits per EB throughout most of the population of treated EBs.

ESCs differentiated as EBs expressed *Pit-1* at levels similar to differentiated MC-3T3-E1 cells, suggesting a route for phosphate uptake by differentiating ESCs, and βGP treated EBs exhibited an increase in ERK 1/2 signaling compared to untreated EBs that was not associated with increased PKC activity. Both ESCs and osteoblasts maintain high levels of alkaline phosphatase activity, suggesting that the handling of phosphate is important to key functions in both cell types. Phosphate transport into cells via PiT-1 has been demonstrated to be necessary for BMP-2 induced mineralization [119, 120], but its role in the accompanying ERK signaling and osteogenic differentiation is not as clear. Numerous studies in cell types including osteoblasts [116], dental pulp cells [133], and vascular smooth muscle cells [134] have suggested that phosphate induced activation of the ERK 1/2 pathways leads to osteogenic gene transcription and differentiation. Many previous studies of phosphate induced ERK signaling and osteogenic differentiation have employed treatment with phosphonoformic acid (PFA), thought to inhibit phosphate transport into cells, specifically through PiT-1, suggesting that phosphate needs to enter the cell for these phenotypic changes to happen [43, 107]. However, more recent electrophysiological studies of PiT-1 expressed exogenously in *Xenopus* oocytes have found that its transport of Pi was not actually blocked by PFA treatment at the concentrations typically used (0.5 mM), pointing towards another mechanism of action

[128]. PFA is also an analogue of pyrophosphate (PPi), a natural inhibitor of extracellular mineralization that is known to directly interfere with calcium phosphate crystal formation. Additional studies of both osteoblast and vascular smooth muscle cell calcification have suggested that PFA may inhibit mineralization by a similar mechanism to PPi [129] and therefore that the presence of extracellular mineral deposits, and not increased Pi concentrations, might actually lead to changes in the cellular microenvironment that induce ERK signaling followed by osteogenic differentiation [131, 132]. This alternate mechanism was explored further within the context of EB osteogenic differentiation in Chapter 5. Regardless of the mechanism of induction, phosphate treatment of EBs, provided in the form of βGP, induced ERK signaling leading downstream to osteogenic differentiation.

Phosphate induced mineralization and ERK signaling activation in EBs was accompanied by robust osteogenic differentiation, demonstrated at both the transcriptional and protein levels (Fig. 4.6, 4.8, 4.9). βGP treatment alone was sufficient to induce osteogenic differentiation within EBs. Upon establishing the ability of differentiating cells within βGP treated EBs to robustly mineralize, coincident osteogenic differentiation was demonstrated by increased expression of *Runx-2*, an early osteogenic transcription factor that controls the expression of most genes characteristic of the osteogenic phenotype [117], along with genes encoding extracellular matrix molecules. Additionally, vitamin D receptor expression and responsiveness were also characterized as additional assessments of osteogenic differentiation. These results revealed that embryonic stem cells expressed mRNA and protein for both receptors for $1\alpha,25(OH)_2D_3$, VDR and PDIA3, and they continued to be present as ESCs differentiated in the form of

EBs. Interestingly, the expression of *Vdr* increased in EBs at 14 days after βGP treatment, while *Pdia3* expression decreased during the same period. The presence of both receptors in adult stem cells was also examined. The results showed that osteogenic induction increased VDR whereas levels of PDIA3 remained stable after osteogenic induction. These results demonstrated that expression levels of these receptors were modulated during the course of osteogenic differentiation of stem cells. However, it is not known if changes in mRNA were required to initiate a change in osteoblast differentiation state or if they were a consequence of that state.

The results also indicated that EBs were sensitive to $1\alpha,25(OH)_2D_3$ at all stages of embryonic development, but effects were more robust in cultures induced to differentiate along an osteoblast lineage. This was correlated positively with increased expression of VDR and, not surprisingly, there was an increase in genes and proteins that possess VDREs including *Opn* and osteocalcin. Similar results were found by zur Nieden et al when ESCs were cultured in a osteogenic induction media containing ascorbic acid, β-glycerophosphate and $1\alpha,25(OH)_2D_3$. In that study, the authors found an increase in alkaline phosphatase, osteocalcin, bone sialoprotein, osteopontin, osteonectin, collagen type 1, and Runx-2 after treatment with $1\alpha,25(OH)_2D_3$[105].

The increase in the classical VDR may have been due to the cells differentiating into osteoblasts, which require a microenvironment higher in calcium in order to mineralize their extracellular matrix. This is supported by the observation that VDR knockout mice do not exhibit rickets until they are weaned and no longer have high serum calcium provided by their mother [187]. This suggested that at least some of the early $1\alpha,25(OH)_2D_3$-dependent differentiation is via PDIA3 and later osteoid production

and mineralization were dependent on VDR. The differential roles of VDR and PDIA3 are not exclusive, however, as VDR is required for development of growth plate tethers, even in Ca^{++}-replete mice [188].

$1\alpha,25(OH)_2D_3$ caused a dose-dependent rapid increase in PKC in the EBs, indicating that PDIA3 was functional as a receptor for the vitamin D metabolite. $1\alpha,25(OH)_2D_3$ induces PKC activation via a membrane-associated rapid-response mechanism and downstream gene expression in a number of cell types [126, 139, 189]. This effect is abolished in PDIA3-knockdown cells, indicating that PDIA3 mediates the $1\alpha,25(OH)_2D_3$ membrane response [126]. The PDIA3 knockout mouse is embryonically lethal by day E10.5 [190], confirming the importance of this protein in stem cell differentiation and embryonic development. In addition, PDIA3 deficiency in $PDIA3^{+/-}$ mice results in skeletal anomalies that affect trabecular and cortical bone [190]. Interestingly, the stimulatory effect of the $1\alpha,25(OH)_2D_3$ on PKC activity was greater in both EBs and MSC cultures grown in osteogenic medium. These results suggested that $1\alpha,25(OH)_2D_3$ may have diverse effects in stem cell differentiation and embryogenesis. It is not clear if cells with a more differentiated osteoblastic phenotype have higher affinity to $1\alpha,25(OH)_2D_3$ or if PDIA3 and VDR form a complex that trigger the rapid membrane response.

EBs also exhibited increased expression of mRNAs for α2 and β1 integrin subunits in cultures grown in osteogenic medium. Moreover, $1\alpha,25(OH)_2D_3$ caused a further increase in expression and this was particularly evident in the levels of β1. Integrin receptors recognizing collagen type I have been shown to regulate early osteoblast differentiation and control the expression of key genes in osteoblastogenesis

[9, 10]. We have observed that maturation of osteoblasts on microtextured biomaterial surfaces are dependent on signaling by α2β1 [191] and that expression of β1 is regulated by $1\alpha,25(OH)_2D_3$ [192, 193]. This suggests that α2β1 expression may play a similar role in EB differentiation.

Conclusions

In conclusion, minimal manipulation of the EB environment by the addition of βGP was sufficient to induce mineralization, ERK 1/2 signaling pathway activation, and subsequent osteogenic differentiation within EBs, characterized at both the gene and protein levels. Furthermore, taken together, our results demonstrate for the first time that $1\alpha,25(OH)_2D_3$ caused rapid activation of PKC in embryonic stem cells and this activation increased during osteogenic differentiation. In addition, $1\alpha,25(OH)_2D_3$ also induced PKC activation in adult stem cells. The two receptors for this vitamin D metabolite were expressed differentially during osteoblastic differentiation, with increased Vdr expression in osteogenic medium. These results correlated with an increase in the expression of genes containing VDREs. Although there was a decrease in PDIA3 in EBs cultured in βGP containing medium, PKC activity in these cells was sensitive to $1\alpha,25(OH)_2D_3$ demonstrating that the receptor was still functional. These data indicated the important role of $1\alpha,25(OH)_2D_3$ signaling in osteogenic differentiation of embryonic and mesenchymal stem cells.

CHAPTER 5

CALCIUM PHOSPHATE PRECIPITATES FORMED ENDOGENOUSLY WITHIN EMBRYOID BODIES PROMOTE OSTEOGENIC DIFFERENTIATION

Introduction

Pluripotent cells, such as embryonic stem cells (ESCs), are promising for many potential applications in tissue engineering and regenerative medicine, including for bone repair. ESCs are a renewable source of cells derived from the inner cell mass of blastocyst stage embryos, and various directed differentiation protocols have been reported to derive diverse cellular populations from ESCs, including neural, cardiovascular, and musculoskeletal cells [103, 194-196]. One common method of inducing ESC differentiation is as cell aggregates, referred to as embryoid bodies (EBs), which recapitulate many of the morphogenic events in three dimensions that occur during embryogenesis [89, 100, 101]. Recently, work in our lab has demonstrated control of the cellular microenvironment within EBs through the incorporation of biomaterial microparticles, which may be used to recapitulate and study cell-microenvironment interactions found in development [99, 102, 197]. Using such techniques, ESCs present not only great potential for use in regenerative medicine applications but also a readily accessible model system of early development and differentiation processes.

Specifically, EBs may be used as a model for early bone formation events as osteogenic differentiation of ESCs and the accompanying mineralization observed *in*

Modified from
K Sutha, L Ling, R Olivares-Navarrete, RE Guldberg, Z Schwartz, BD Boyan, and TC McDevitt. *Endogenous Mineralization within Embryoid Bodies Promotes Osteogenic Differentiation by Mouse Embryonic Stem Cells,* **in preparation.**

vitro parallels bone development *in vivo*, progressing in order through stages of proliferation, matrix production, and mineralization [105]. β-glycerophosphate (βGP) is typically provided as part of the commonly used cocktails as a source of inorganic phosphate (Pi) required for mineralization [106, 185, 198]. The most common protocols for the osteogenic differentiation of mouse ESCs include supplementation with not only βGP but also ascorbic acid and dexamethasone [103, 110, 198], but phosphate is required for production of a mineralized matrix. ESCs express membrane alkaline phosphatase that can cleave organic phosphates such as βGP and liberate Pi, which is then available as the substrate necessary for mineralization [199, 200], and cells maintain this activity as they spontaneously differentiate within EBs (see Chapter 4).

Within the context of physiological mineralization of bones, calcium phosphate precipitation occurs in a controlled manner locally and is deposited on a collagen-I rich matrix [37]. Mineralization of the extracellular matrix during bone development is a cell mediated process resulting in the deposition of calcium phosphate (CaP) as hydroxyapatite (HA - $Ca_{10}(PO_4)_6OH_2$) and requires alkaline phosphatase activity to cleave organic phosphate sources in the cellular environment, yielding the free, inorganic phosphate needed to mineralize [199, 200]. Matrix vesicles release high concentrations of calcium (Ca) and Pi locally allowing for matrix mineralization, while osteogenic matrix proteins produced by resident bone forming cells, osteoblasts, regulate this mineralization process [20].

Pyrophosphate (PPi), produced by all cells and present ubiquitously, serves to modulate mineralization by acting as a direct inhibitor of CaP precipitation and mineralization [44, 201]. In bone, alkaline phosphatase cleaves PPi, thus removing the

inhibition of local CaP crystal formation and allowing for mineralization to proceed [46-48]. In non-mineralizing tissues, inhibitors of mineralization produced by cells, including PPi, are present in the cellular microenvironment, but under pathological conditions, mineralization can occur either because of loss of these inhibitory factors, as seen in dystrophic calcification, or because of an increase in conditions that promote CaP precipitation, such as increased Ca and Pi concentrations as seen in metatstatic calcification [202]. Decrease in PPi within microenvironment can occur either because live cells express phosphatase activity to cleave PPi or because non-viable cells within that region are unable to produce PPi

Phosphate treatment, administered either directly in the form of Pi or indirectly cleaved from βGP by alkaline phosphatase, induces mineralization and osteogenic differentiation of osteoblast like cells (MC3T3-E1) [115], vascular smooth muscle cells [43], and ESCs (See Chapter 4). Both osteoblasts and ESCs maintain high alkaline phosphatase activity, further suggesting that Pi is an important molecule for cellular functions in both cell types. Phosphate induced differentiation involves activation of mitogen-activated protein kinase (MAPK)/ extracellular-signal related kinase (ERK 1/2) signaling cascade with increased ERK 1/2 phosphorylation [107, 116]. Phosphate induced differentiation and mineralization may be blocked by treatment with phosphonoformic acid (PFA) [43, 115]. Though the exact mechanism of inhibition remains unclear, PFA has a similar structure to PPi and so is thought to act similarly by inhibiting crystal formation [129]. Given this more recently understood mechanism of PFA action, newer studies have suggested that induction of osteogenic differentiation only requires the presence of extracellular CaP deposits, independent of Ca and P

concentrations individually, and in fact, exogenous CaP administration has been found to induce ERK phosphorlyation and subsequent osteogenic gene expression in MC3T3-E1 and vascular smooth muscle cells [130-132].

After establishing the ability of mouse ESCs differentiated as EBs to form mineral deposits and undergo osteogenic differentiation in response to phosphate treatment (see Chapter 4), here the deposits formed were further characterized to determine if they were forming through a controlled, cell mediated process, as in bone, or were precipitates of CaP. Then, in light of osteogenic differentiation of other, more commited cell types directly induced by CaP precipitation, the relationship of these endogenously formed mineral deposits with the observed phosphate-induced ERK signaling and osteogenic differentiation was investigated by inhibiting mineral formation with PFA treatment, and subsequent changes in osteogenic gene expression were observed. Finally, to further assess the induced osteogenic differentiation, as well as to shed light upon a potential mechanism by which CaP induced changes could create an osteoinductive microenvironment *in vitro*, osteogenic protein expression, including production of matrix molecules and osteoinductive growth factors, was assessed. As a model for early bone formation, studying mineralization by differentiating ESCs in EBs would provide an avenue to investigate the potential interrelationship between differentiation and mineralization and how manipulating the microenvironment of cells can alter their differentiation.

Materials and Methods

Mouse ESC culture, EB formation, and osteogenic differentiation

Undifferentiated mouse embryonic stem cells (D3 line) were cultured as described in Chapter 3 – General Methods. Forced aggregation was used to generate individual EBs of identical cell number in 6 well cell culture plates with approximately 1000 cells/ microwell [148] as described in the General Methods, and EBs were supplemented with 10 mM βGP (MP Biomedical, Solon, OH) from day 5 of suspension culture onward to promote mineral deposit formation.

Phase images of EBs in each treatment group were taken throughout the duration of the experiments (up to 14 days of differentiation) and were analyzed using Metamorph™ software (v. 7.5, Molecular Devices, Sunnyvale, CA) to measure EB size. Mineral deposits were visualized as dark, irregularly shaped deposits compared to surrounding cells and media by phase contrast. For studies including PFA treatment (Sigma, St. Louis, MO), samples were treated from day 5 through 14 of EB differentiation with 10 mM βGP alone (+βGP), 0.5 mM PFA alone (+PFA), both βGP and PFA starting at day 5 (+βGP +D5 PFA), or left untreated. EBs receiving "Day 10 PFA treatment" were treated from day 5 through 14 with βGP and then supplemented with PFA from day 10 through 14 only (+βGP +D10 PFA).

In separate experiments, the effects of osteogenic supplements and EB size on calcium phosphate precipitation were evaluated. For additional osteogenic supplement studies, EBs were formed by the rotary method described in Chapter 3 – General Methods with a cell seeding concentration of $2x10^5$ cells per 1 ml of media in 10 ml. EBs were supplemented with 10 nM dexamethasone, 50 μg/ml ascorbic acid, and 10 mM βGP from day 5-14 of differentiation, individually or in combination (DAG). For the EB size experiment, the UHTP, forced aggregation method was used to form EBs as described in

Chapter 3 – General Methods, and the cell seeding concentration was varied to 3 million cells and 9 million cells per 1 ml of media in order to achieve EBs of 500 and 1500 cells per EB respectively, in addition to the 1000 cells per EB used throughout the remainder of the study. EBs of the three different sizes were cultured with 10 mM βGP from day 5-14. EBs from both of these experiments were evaluated for calcium phosphate precipitate formation by phase contrast and von Kossa staining described in the General Methods.

Histology and fluorescence imaging

Preparation of EBs for histological evaluation were performed by embedding in Histogel, and mineral deposits were stained by von Kossa and Alizarin red, as described in Chapter 3 - General Methods.

To investigate the association of non-viable cells with mineral deposit formation, LIVE/DEAD® staining was used (Molecular Probes, Eugene, OR). Day 14 EBs were incubated in serum free, phenol free media containing 1 μM calcein AM and 2 μM ethidium homodimer I at 4°C for 30 min. EBs were washed three times in PBS, transferred onto glass coverslips, and imaged using a Zeiss LSM/NLO Multi-photon microscope. To assess the ability of non-viable cells or cellular debris to nucleate calcium phosphate precipitation under EB culture conditions, non-viable EBs were maintained in rotary culture with ESC media for 14 days, with supplementation with 10 mM βGP from day 5-14 of culture. Non-viable EBs were derived from untreated EBs collected at either day 5 or 10 of EB differentiation and were devitalized by overnight lyophilization as previously described [69]. Non-viable EBs were collected at day 14, fixed, and processed

as described above, and mineralization by calcium phosphate precipitation was evaluated by von Kossa and Alizarin red staining.

Masson's Trichrome stain was employed to visualize collagen composition within EBs (stained in blue). Briefly, deparaffinized slides were incubated in Bouin's solution for 1 hour at 56°C, and after cooling to room temperature, they were incubated in Weigert's hematoxylin (2 minutes), Bierbrich's scarlet acid fuchsin (5 minutes), phosphotungsic-phosphomolybdic acid (1 minute), aniline blue (5 minutes), and 1% acetic acid (5 minutes), with intermittent water rinses between incubations. Slides were dehydrated, cleared, and cover-slipped before imaging.

For immunofluorescent staining, histological sections were deparaffinized before being permeabilized and blocked using a 0.05% Triton X-100/2% goat serum solution. Slides were incubated with the primary antibody directed against either collagen-I (1:200) or collagen-II (1:200) at 4ºC overnight in the blocking solution. Samples were then incubated (1 hour, room temperature) with the fluorescently-tagged secondary antibody and rinsed in PBS (3x, 5 minutes). Nuclei were counterstained using Hoechst fluorescent dye and cover-slipped.

Micro-computed tomography (μCT)

Evaluation of the formation of mineral deposits within EBs was also performed by μCT, described in detail in Chapter 3 - General Methods. The total volume of mineralization within the entire Histogel-embedded samples was determined and normalized to estimated EB volume to calculate the average percentage of EB volume

containing calcium phosphate precipitates. EB diameter was measured by phase contrast microscopy and used to calculate estimated volume of embedded EBs.

Mineralization analysis

EBs were fixed at day 14 of differentiation in 2% glutaraldehyde in 0.1M sodium cacodylate buffer and postfixed in 1% osmium tetroxide for one hour at room temperature (Electron Microscopy Sciences, Hatfield, PA). Transmission electron microscopy (TEM) samples were dehydrated by a series of graded ethanol washes, embedded in epoxy resin medium (Fluka, St. Louis, MO), and sectioned with a RMC MT-7000 ultra-microtome using a diamond knife (Boeckeler, Tucson, Ariz.). Thin sections (60-80 nm thick) were collected on 200 mesh copper grids, and post-stained with 5% Uranyl Acetate and Reynold's Lead Citrate stains. The imaging was achieved using a JEOL JEM-1210 TEM set to 80 KV accelerating voltage. For scanning electron microscopy, samples were dehydrated in graded acetone washes, dried in liquid CO_2 (31.58°C, 1100 psi) using an E3000 series critical point dryer (Quorum Technologies, ON, Canada), and mounted on aluminum stubs (Electron Microscopy Sciences) before sputter coating in gold for 90 s in a Polaron Sputter Coater SC 7640 (Quorum Technologies) and imaging with a Hitachi S-800 Field Emission Gun Scanning Electron Microscope (SEM) with iXRF EDS2004 image acquisition software.

Samples were prepared from day 14 EBs for X-ray diffraction (XRD), energy dispersive X-ray spectroscopy (EDS), and Fourier transform infrared spectroscopy (FTIR). EBs were collected in deionized water and frozen at -80°C, before being placed under vacuum in a lyophillizer (Labconco, Kansas City, MO) overnight. Surface structure

was first qualitatively evaluated before EDS using an Ultra 60 field emission (FE) SEM (Carl Zeiss SMT Ltd., Cambridge, UK). Lyophillized EBs were imaged directly using a 5 kV accelerating voltage and 30 µm aperture. The SEM equipment was coupled with an INCA EDS (Oxford Instruments, Bucks, UK) used for non-surface-sensitive analysis of elemental composition of samples. For XRD, crystal structure of the samples was identified using an X'Pert PRO Alpha-1 diffractometer (PANalytical, Almelo, The Netherlands). XRD scans were collected using 1.8 kW Cu Kα radiation. A 1° parallel plate collimator, ¼ divergence slit and a 0.04 rad soller slit were used for controlled axial divergence. Bragg-Brentano parafocusing setup was used to analyze samples. Infrared spectroscopy in attenuated total internal reflection mode (ATR) (Pike Technologies, Madison, WI) was performed using a Nexus 870 FT-IR bench (Nicolet Instrument Corporation, Madison, WI). Each spectrum was the mean of 64 acquisitions (between 1800 and 400 cm-1) with a spectral resolution of 4 cm^{-1}. Sample disks were placed on top of the transmission crystal and pressed with the sample holder. Two spectra were collected per sample analyzed. Observed spectra were compared to references for pure hydroxyapatite crystal, as well as sodium (NaCl) and potassium (KCl) salts.

Western blotting

EBs were collected at day 14 of differentiation for western blot analysis of ERK phosphorylation, as described in Chapter 3 - General Methods.

Quantitative real-time polymerase chain reaction (qRT-PCR)

For real-time PCR analysis (see Chapter 3 - General Methods), total RNA was extracted from undifferentiated ESCs or EBs after 10 and 14 days of differentiation. Primers for *osteocalcin, bone sialoprotein, osteopontin, collagen type I, osterix,* and *runx2* were used, in addition to housekeeping gene *GAPDH*. Gene expression was expressed as a fold change compared to same day untreated EBs, calculated by the ΔΔCt method [149].

Osteogenic protein expression

Alkaline phosphatase (ALP) activity was determined at day 14 in EB cell pellets, with and without βGP treatment. Day 14 EB conditioned media was also assayed by sandwich ELISA (enzyme linked immunosorbent assay) for osteopontin and osteoprotegrin (DuoSet, R&D Systems, Minneapolis, MN), and EB cell pellets at day 14 of differentiation were solubilized in T-Per Tissue Protein Extraction Reagent (~2 mg/ml T-Per; Pierce) and assayed by sandwich ELISA for BMP-4 (bone morphogenetic protein; DuoSet, R&D Systems), and BMP-2 (PeproTech, Rocky Hill, NJ) protein levels. Measurements were normalized to total protein for alkaline phosphatase specific activity and either total DNA content or total protein for the other assays (See Chapter 3 - General Methods).

Statistical analysis

Two-way ANOVA analysis, followed by Tukey's post-hoc test, was performed to determine statistical differences ($p<0.05$), unless otherwise noted. If data did not approximate a normal distribution when first examined by exploratory data analysis,

Box-Cox estimations were used to transform the data set to a normal distribution, as reviewed by Spitzer [151]. Outliers were identified by examination of studentized t-residuals. Results are reported as mean ± standard error of the mean of non-transformed data for a minimum of triplicate experiments from each experiment unless otherwise noted; a minimum of two independent experiments were analyzed by each of the assays described.

Results

Calcium phosphate precipitation within EBs

EBs were cultured with βGP, ascorbic acid, and dexamethasone supplements individually and in combination in order to test whether βGP was the minimal essential component of this cocktail required for the formation of mineral deposits within EBs. After culture with these supplements from day 5-14 of EB differentiation, mineral deposits were visible by phase contrast microscopy in only EBs treated with βGP: the group receiving all three supplements and the group treated with βGP alone (Fig. 5.1 A). The extent and distribution of the mineral deposits was then further examined by von Kossa staining of the two treatment groups containing mineral deposits (Fig 5.1 B). The addition of dexamethasone and ascorbic acid did not appear to alter the mineral deposits formed in response to βGP treatment (in black). Because the goal of this study was to investigate the influence of calcium phosphate precipitates and mineralization on osteogenic differentiation, βGP treatment alone was used for all subsequent experiments in order to remove any confounding effects or bias towards osteogenic differentiation that may have been introduced by the addition of dexamethasone and ascorbic acid, both of which are known to promote osteogenic differentiation.

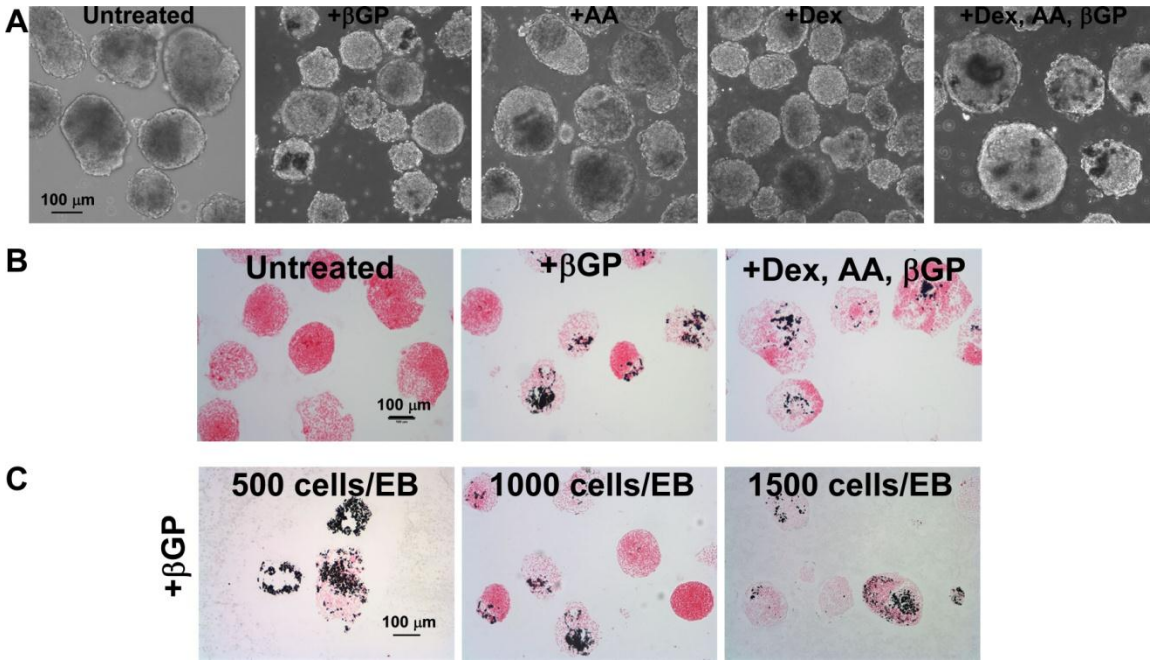

Figure 5.1. Effects of osteogenic supplements and EB size on mineral deposit precipitate formation. Calcium phosphate precipitates form when βGP is provided in the culture media, regardless of starting EB size. EBs were treated from day 5-14 of differentiation with βGP, ascorbic acid (AA), and dexamethasone (Dex), either individually or in combination. Mineral deposits were visible by phase contrast at day 14 only in those cultures supplemented with βGP (A) and stained positively by von Kossa staining (B). In a separate experiment, EBs of different sizes, formed by forced aggregation, were all found to contain mineral deposits by day 14 after culture with βGP (C). Scale bars = 100 μm.

Next, to remove variability in mineral deposit formation and osteogenic differentiation that may arise from heterogeneity in the EB starting population [97, 203, 204], experiments were undertaken employing techniques to control EB size. Though the rotary formation method used in Chapter 4 lead to increased EB homogeneity and some control of EB size compared to static formation methods [147], forced aggregation EB formation techniques have allowed more finely tuned manipulation of EB size by control of the number of cells used to form each EB, leading to improved homogeneity [148]. Previous data examining the size distribution of EBs with βGP induced mineral deposition did not reveal any bias for EBs of a particular size to contain mineralization (See Chapter 4, Fig. 4.3 E). To confirm the result that mineral accumulation was independent of size, EBs of different sizes were formed by forced aggregation and cultured with βGP. Mineral deposits formed in EBs of each of the three sizes examined, those formed from 500, 1000, and 1500 cells per EB. When evaluated by von Kossa staining at day 14, qualitatively similar amounts of mineral were present in the 1000 and 1500 cell formed EBs; however, a larger portion of each 500 cell formed EB was found to be comprised of mineral deposits (Fig. 5.1 B). As had been observed in highly mineralized populations of rotary formed EBs, the increased mineralization in the 500 cell EBs also lead to increased agglomeration, and coupled with the decreased EB size with βGP treatment (Fig. 4.3 E), resulted in low EB yield. To maximize EB yield and to reduce the possibility of transport limitations that might be experienced in the larger, 1500 cell EBs, EBs formed at 1000 cells per EB were used for all subsequent experiments.

Using 1000 cells/EB, the ultra-high throughput, forced aggregation method of EB formation yielded EBs of uniform starting size that remained homogeneous through the initiation of βGP treatment at day 5, thus reducing intraexperimental variability before βGP was introduced that may have confounded the results and allowing for differences arising directly from βGP treatment to be more easily interpreted. EBs were visualized at day 7, 10, and 14 by phase contrast microscopy, and mineral deposits were noted to be visible in βGP treated samples beginning at day 7 (Fig. 5.2 A). Mineralization was observed by phase contrast as dark, irregularly shaped regions within treated EBs (Fig. 5.2 B). Both untreated and βGP treated EBs decreased in size over the 14 day time period ($p<0.005$), but by day 10, +βGP EBs were 17% smaller than untreated ($p<0.005$) and 32% smaller by day 14 ($p<0.005$) (Fig. 5.2 C). Overall, mineral deposit formation assessed by phase contrast microscopy was enhanced in phosphate treated EBs but not untreated EBs.

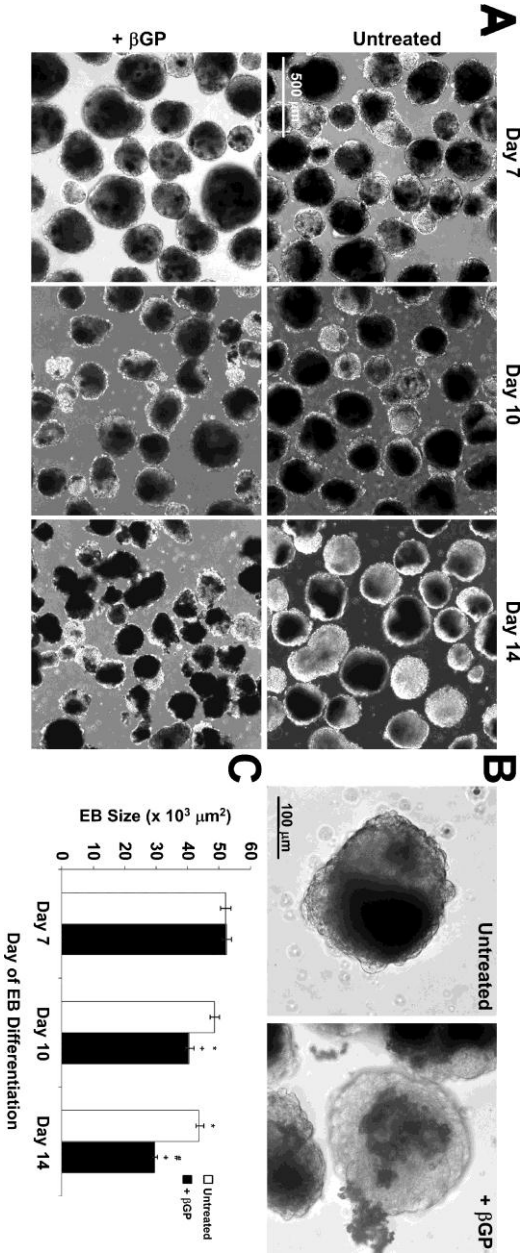

Figure 5.2. Mineral accumulation within βGP treated EBs. EBs were treated with 10 mM βGP from day 5-14 of differentiation. βGP treated EBs accumulated mineral deposits much more readily and abundantly than untreated samples based upon phase contrast images (A). Mineral accumulation within the EBs, visualized by phase contrast as dark regions with irregular borders within EBs, were observed abundantly in treated EBs but not untreated EBs at day 14 (B). The size of EBs decreased over the 14 day EB differentiation time course, but βGP treatment caused a larger decrease in size. (C). (Scale bar in A = 500 µm, scale bar in B = 100 µm). n=3 cultures, two-way ANOVA, Tukey's post-hoc, +$p<0.005$ compared to same day untreated, *$p<0.005$ compared to Day 7 untreated and Day 7 +βGP, # $p<0.005$ compared to Day 7 untreated, Day 7 +βGP, Day 10 untreated, and Day 10 +βGP.

The mineral deposits were next stained by von Kossa and Alizarin red to assess the composition of the mineral and to visualize their size and distribution within EBs. The presence of calcium phosphate (CaP) containing deposits was assessed by staining serial sections of EBs at days 7, 10, and 14 with von Kossa and Alizarin red (Fig. 5.3). In untreated EBs, positive von Kossa staining (in black) was found at day 14 that did not correspond with regions of positive Alizarin red (in red) staining in adjacent sections (Fig. 5.3 A). In fact, when the populations of day 14 untreated EBs stained by von Kossa and Alizarin red were quantified and compared, significantly more stained positively by von Kossa (18.3 ± 10.6% Alizarin red vs. 64.8 ± 1.4% von Kossa, $p<0.05$) (Fig. 5.3 B). In +βGP EBs, few, small foci of positive staining for both von Kossa and Alizarin red were observed at day 7 that increased in size and number at days 10 and 14 (Fig 5.3 A). By day 14, nearly the entire cross sectional area of some EBs was comprised of positive staining. Quantitatively, the percent of EBs stained positively for both stains increased over time and in βGP treated EBs compared to untreated EBs at days 7 and 10 by both von Kossa and Alizarin red ($p<0.005$) (Fig. 5.3 B). At day 14, however, only von Kossa staining was significantly increased within βGP treated EBs ($p<0.05$). The amount of mineral deposits was quantified to increase over time with phosphate treatment, supporting observations based on phase contrast imaging.

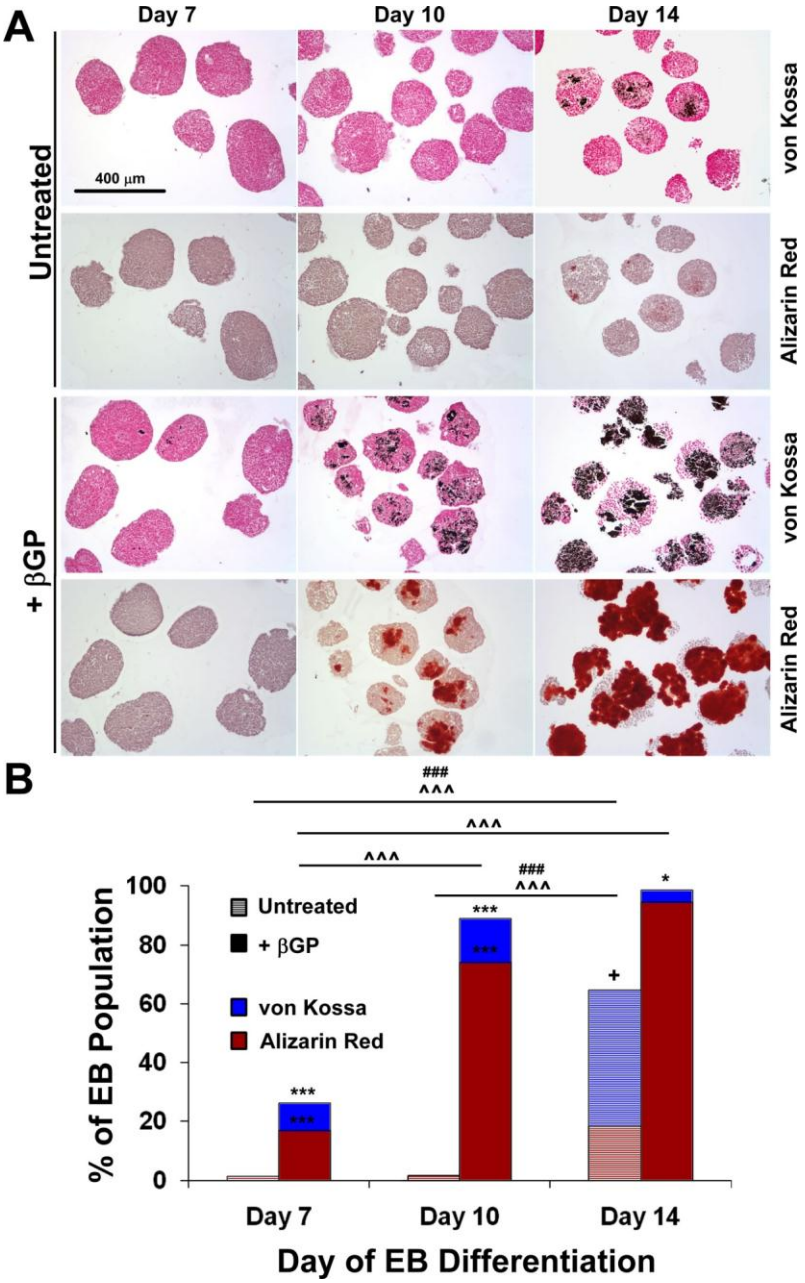

Figure 5.3. Calcium phosphate mineral deposits within EBs. Mineral deposits within EBs stained positively by von Kossa and Alizarin red stains in adjacent sections, indicating a composition of both phosphate and calcium; were present more in βGP treated EBs; and increased in size and distribution over the 14 day time course of EB differentiation (A). Quantification of von Kossa and Alizarin red stains confirmed significant increases in the number of EBs (% of total EB population) containing calcium phosphate precipitates with βGP treatment over 14 days. n=3 cultures, Box-Cox transformation, three-way ANOVA, Tukey's post-hoc test, ***$p<0.005$, *$p<0.05$ comparing treatment at same day with same stain, +$p<0.05$ comparing stain with same treatment and day, ^^^$p<0.005$ for marked comparison of Alizarin red stain, ###$p<0.005$ for marked comparison of von Kossa stain.

The measurement of percent population containing mineral, determined from staining, did not fully capture the increases in size and number of mineral deposits apparent from looking at the deposits within EBs, therefore additional volumetric quantification of mineral accumulation was used. Volume of CaP mineral deposits within intact EBs was quantified in three dimensions by μCT and was measured to increase over time in βGP treated EBs while remaining low in untreated EBs. EBs at day 7, 10, and 14 were embedded in Histogel, imaged by stereomicroscope to determine EB distribution within the gels, and scanned by μCT to quantify the mineral volume. Based on previous EB size measurements (Fig. 5.2 C) and the number of EBs loaded per gel, estimates of total EB volume were obtained and used to normalize the mineral volume quantified per gel sample, giving the percentage of total EB volume comprised of calcium phosphate deposits. At day 14, the percent mineral deposit volumes were found to be 16.72 ± 1.47% for treated EBs (Fig. 5.4 A iii) compared with 0.02 ± 0.01% for untreated EBs (A iv) ($p<0.001$). Overlay of stereoscope and uCT images demonstrated that CaP mineral visualized by uCT was contained within βGP treated EBs (Fig. 5.4 B). Quantitatively, the percent mineral volume remained unchanged in untreated EBs and increased with βGP over time and compared to untreated EBs ($p<0.001$) (Figure 5.4 C). Taken together, mineral deposits form upon βGP treatment, increase during the treatment period, and may be quantified based on histological and μCT based measures, supporting findings obtained by both phase contrast and von Kossa and Alizarin red staining.

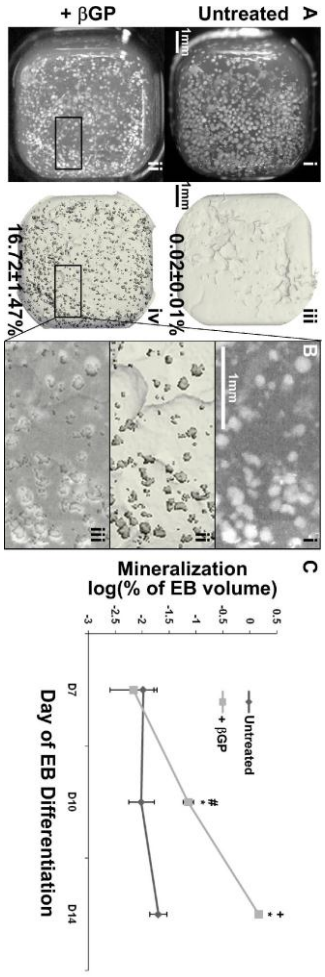

Figure 5.4. Quantification of calcium phosphate mineral deposits by µCT. Day 7, 10, and 14 EBs were analyzed by µCT to quantify degree of mineralization based on volume of calcium phosphate mineral deposits. An equivalent number of Histogel embedded day 14 EBs were also imaged by stereomicroscope (-βGP (A i) and +βGP (A ii)). The percentage volume comprised of calcium phosphate deposits at day 14, normalized to EB volume, were found to be 16.72 ± 1.47% for treated EBs (A iii) vs. 0.02 ± 0.01% for untreated EBs (A iv) ($p<0.001$, n = 3 samples). EBs and mineral deposits overlapped in stereoscope (B i) and µCT (B i) images (regions indicated by boxes) (merge – B iii). Degree of mineralization, calculated from the % of total EB volume comprised of calcium phosphate deposits and plotted as mean ± relative error, was then compared across time and treatment groups and found to increase over time in βGP treated EBs compared to untreated EBs (C). Scale bar in A = 1mm, scale bar in B = 1 mm. n=3 samples, Box-Cox transformation of % of EB volume mineralized, two-way ANOVA, *$p<0.001$ compared to same day untreated, #$p<0.001$ compared to Day 7 untreated and Day 7 +βGP, +$p<0.001$ compared to Day 7 untreated, Day 7 +βGP, and Day 10 untreated.

Characterization of mineral deposition

Though mineral deposits were demonstrated by phase contrast, von Kossa and Alizarin red staining, and μCT, none of these assessments distinguished between CaP precipitation and biologically mineralized matrix, as found in bone. Therefore, additional material characterizations were required to distinguish between these processes. CaP mineral deposits within day 14 βGP treated EBs were visualized using electron microscopy techniques to further evaluate the mineral deposition process occurring within EBs. Transmission electron microscopy further elucidated the organization and distribution of mineral deposits within EBs. Mineralization was not found in untreated samples (Fig. 5.5 A) but was visible both intra- (B) and extracellularly (C) in treated EB samples. Higher magnification images demonstrated that βGP treated EBs contained a poorly crystalline mineralization lacking clear collagen fibrils and matrix vesicles but containing material suggestive of cellular debris (Fig. 5.5 D). Regions of mineralization within βGP treated EBs were also visualized by scanning electron microscope and were noted to be present extracellularly as numerous globular structures with flattened surfaces (Fig. 5.5 E, F).

To identify the composition and structure of the mineral deposits, energy dispersive X-ray spectroscopy (EDS), Fourier transform infrared spectroscopy (FTIR), and X-ray diffraction (XRD), were used to analyze devitalized, day 14 EBs, a mixture of cellular, organic material and calcium phosphate mineral deposits. EDS demonstrated the presence of increased calcium and phosphate in βGP treated samples when compared to untreated samples, however the calcium phosphate ratio (0.75) did not match the ratio of pure hydroxyapatite (10 Ca/6 P = 1.67). Along with FTIR, these data suggested that the

mineral composition was distinct from that found in hydroxyapatite of native bone (Fig. 5.5 G, H). Additionally, XRD did not demonstrate the ordered crystalline structure of hydroxyapatite within either the βGP treated or untreated samples (Fig. 5.5 I). βGP treated EBs exhibit calcium and phosphate accumulation not found in untreated samples but with differences in structure and composition to bone hydroxyapatite. Taken together with electron microscopic findings, phosphate treatment enhanced mineral deposit formation, and the structure and composition of these depositesse results were suggestive of CaP precipitates. In combination with the previous data, phosphate treatment quantifiably increases the formation of CaP precipitates within EBs.

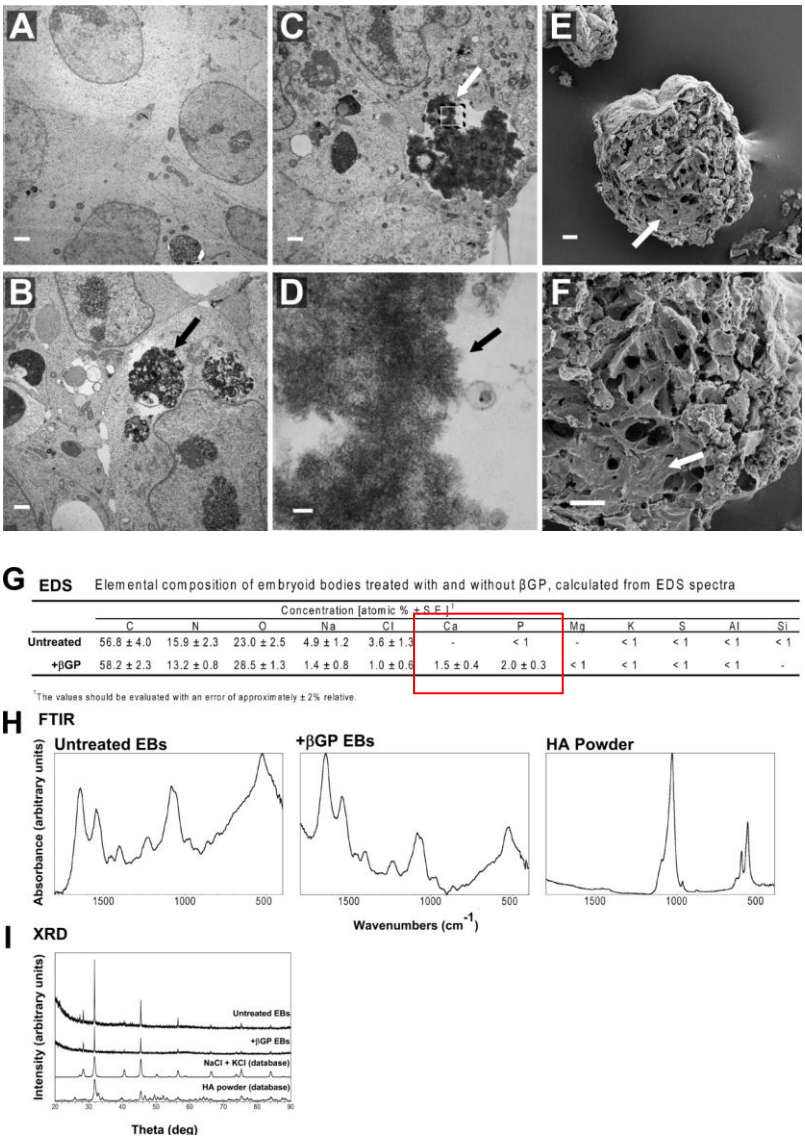

Figure 5.5. **Characterization of calcium phosphate precipitates.** Transmission electron microscope images of untreated EBs (A) did not contain electron dense material present both intra- (B) and extracellularly (C, higher magnification view - D) in βGP treated EBs. Scanning electron microscope views of the interior of representative βGP treated EBs revealed regions of calcification within EBs (E, F) (Scale bar in A-C = 1 μm, D = 100 nm, E, F = 10 μm). Lyophilized preparations of day 14 EBs with βGP treatment, a mixture of cellular organic material and calcium phosphate precipitates, were further analyzed to characterize the mineral content. Calcium and phosphate content, calculated from EDS, were enriched in βGP EBs compared to untreated EBs, but the calcium phosphate ratio (0.75) did not match that of native bone hydroxyapatite (HA) (1.67) (G). Further analysis of EBs containing calcium phosphate precipitates confirmed distinct mineral composition and crystal structure than purified HA by FTIR (H) and XRD (I), respectively.

Because of the visualization by TEM of material suggestive of cellular debris within the CaP precipitates, Live/Dead staining was used to investigate if dead cells were associated with the precipitates. The component of the stain which demonstrates dead cells is ethidium homodimer, which binds to exposed DNA from non-viable cells in non-intact cells or cellular debris. Positive dead staining (red) in day 14 βGP treated EBs (Fig. 5.6, top) overlayed with CaP precipitates visualized by phase contrast (Fig. 5.6, bottom), while portions of the βGP treated EBs not containing the CaP precipitates exhibited similar viability to untreated EBs. One possible explanation for the strong ethidium homodimer staining of the CaP deposits, supported by the TEM findings, was the presence of cellular debris within the precipitates themselves, as cellular debris may have acted as a nucleation point for CaP precipitation. Increased amounts of cellular debris and single cells were noted by phase imaging outside of EBs in +βGP cultures, particularly by day 14 (Fig. 5.2 A). Alternatively, CaP precipitates may have non-specifically bound the ethidium homodimer. To further investigate the possibility that cellular debris present in +βGP cultures and EBs was able to nucleate the formation of CaP precipitates, non-viable EBs were maintained under the same culture conditions used to promote mineral formation within viable EBs. After addition of βGP to the non-viable EB culture from day 5-14, extensive calcium phosphate precipitation was observed as demonstrated by positive von Kossa and Alizarin red staining throughout all of the non-viable EBs collected (Fig. 5.7). In fact, the mineral deposition was far greater and extensive than typically seen within viable EBs, in agreement with previous studies of non-viable cell mineralization [129, 131]. The same observations were made when non-viable EBs devitalized at day 5 and day 10 were used. In combination, the data suggested that the

βGP induced mineral formation observed in EBs occured through a process of CaP precipitation. The precipitates contained and were nucleated by cellular debris, and their formation was not dependent upon viable cells.

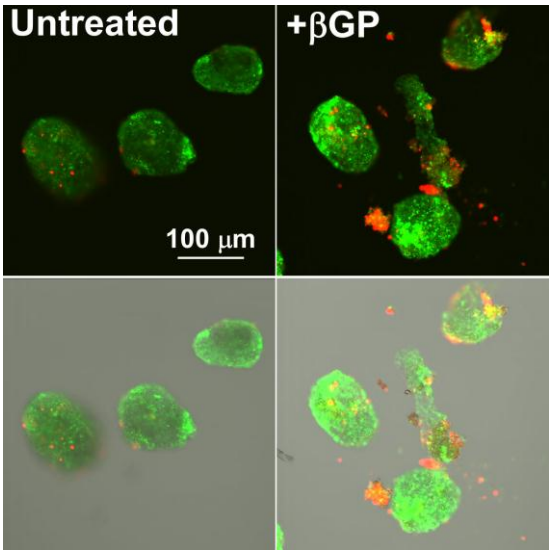

Figure 5.6. Live/Dead staining of calcium phosphate precipitates formed in EBs. Calcium phosphate precipitates contained dead cellular material. Day 14 EBs with and without βGP treatment were stained with ethidium homodimer, a stain used to demonstrate dead cells in red, and calcein, to demonstrate viable cells in green, and imaged by confocal microscopy. Calcium phosphate precipitates within EBs, visible by phase contrast within βGP treated EBs (overlay, bottom), stained strongly positive for the presence of dead cells while the remainder of the EB stained similarly to untreated EBs. Scale bar = 100 μm.

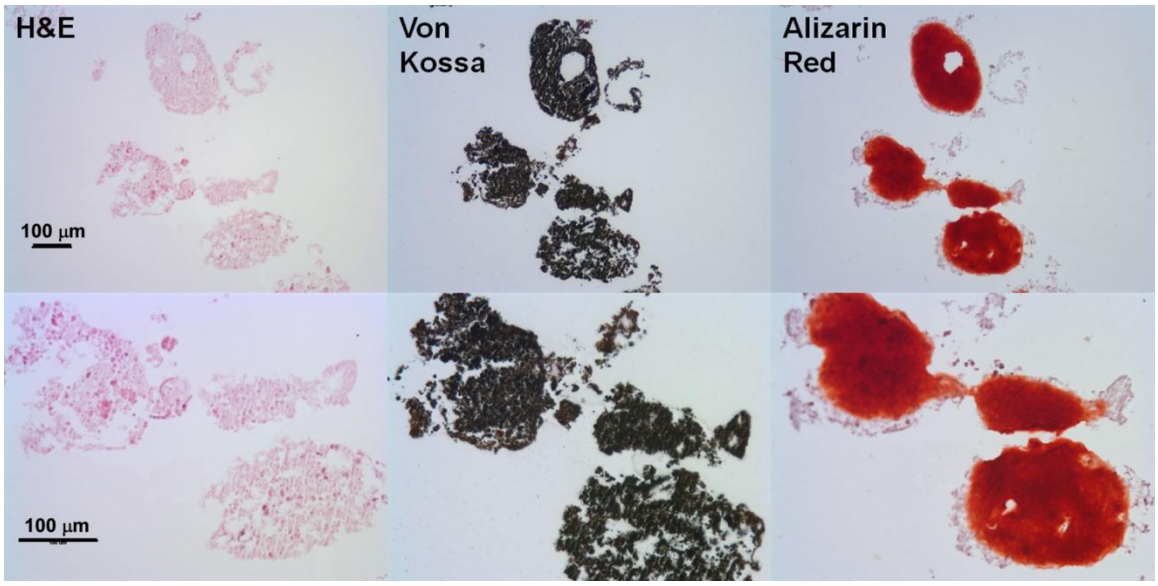

Figure 5.7. Mineralization of devitalized EBs. Calcium phosphate precipitates formed in non-viable EBs maintained under EB culture conditions. Devitalized EBs (lyophilized, untreated Day 10 EBs) were cultured under the same conditions as viable EBs with βGP treatment from day 5-14 of culture and became mineralized by calcium phosphate precipitates by day 14 as demonstrated by von Kossa and Alizarin red stains of adjacent sections. Scale bars = 100 μm.

ERK 1/2 activation and osteogenic gene expression

Regardless of the structure and composition of the mineral deposits, the alterations in the EB microenvironment brought about by their presence alone were previously found to be sufficient to induce osteogenic differentiation (see Chapter 4). To test whether the osteogenic differentiation in response to phosphate treatment was in fact due to the formation and presence of CaP precipitates, studies blocking precipitation using PFA were performed. Here, PFA treatment initiated at day 5, concurrently with βGP administration, completely inhibited the CaP precipitates, visible by phase contrast and von Kossa staining, formed by day 14 with βGP treatment alone (Fig. 5.8 A). However, when blocking with PFA was delayed until day 10, after CaP formation had

begun (+βGP +D10 PFA), the amount and size of CaP precipitates was maintained at levels observed in day 10 +βGP samples. All groups receiving phosphate treatment were observed to have increased amounts of cellular debris. Next, ERK 1/2 activation was assessed by Western blot for phosphorylated and non-phosphorylated ERK. Phosphorylated ERK was increased at day 14 in samples containing CaP precipitates, both +βGP alone and +βGP +D10 PFA (Fig. 5.8 B). Since Runx-2 activation and osteogenic differentiation occur downstream of ERK activation [205], osteogenic gene expression was then examined.

The expression of several key osteogenic genes was increased in a coordinated manner at day 14 in response to the presence of CaP precipitates within EBs. *Runx-2* expression was increased in EBs treated with βGP (4.25 fold compared to untreated, $p<0.05$) (Fig. 5.8 C). This upregulation was inhibited with PFA treatment beginning at day 5 but not when it was begun at day 10 (8 fold compared to untreated, $p<0.005$), correlating with the presence of CaP precipitates and ERK phosphorylation. The expression of *Bsp* and *Opn* responded similarly to *Runx-2* expression after βGP and PFA treatments, not surprisingly, as Runx-2 is an early osteogenic transcription factor known to control the expression of several osteogenic genes [117]. Not all osteogenic genes assayed were regulated in this coordinated manner. Interestingly, the expression of two late osteogenic marker genes for osteocalcin and osterix were actually increased in all PFA treated groups (10-20 fold compared to untreated), and there was a synergistic increase in both groups treated with both βGP and PFA (+βGP +D5 PFA and +βGP +D10 PFA). *Coll-I* expression was not increased with βGP treatment but was decreased compared to untreated cells with PFA treatment from day 5, both with and without

concurrent βGP treatment (3 fold and 5 fold decrease compared to untreated, $p<0.005$). Additionally, *Coll-I* expression was also decreased in +βGP EBs when they were treated with PFA that began only at day 10 ($p<0.005$). No significant changes in gene expression were seen between treatment groups except for decreases in *Runx-2* expression for both PFA treated samples (+βGP +D5 PFA and +PFA) compared to untreated and +βGP samples ($p<0.05$). Taken as a whole, these data demonstrated that CaP precipitates induced by phosphate treatment were associated with activated ERK 1/2 and osteogenic gene expression. ERK phosphorylation and osteogenic differentiation were abolished when CaP precipitation was blocked completely with PFA treatment but not when CaP precipitates were allowed to form before PFA inhibition, suggesting that the precipitates themselves were altering the phenotype of the EBs.

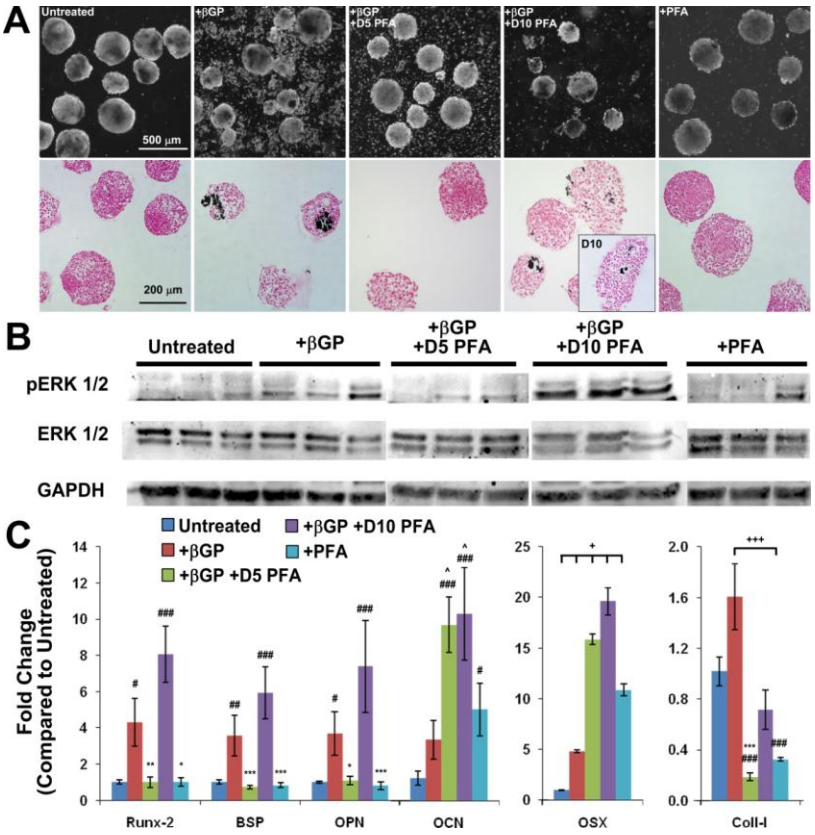

Figure 5.8. Effect of PFA on CaP precipitation, ERK 1/2 signaling, and osteogenic gene expression. EBs were treated with βGP from day 5-14 of EB differentiation to promote the formation of calcium phosphate precipitates, visualized by phase contrast and von Kossa staining at day 14 (A). Precipitate formation was completely inhibited when PFA treatment was initiated at day 5 (+βGP +D5 PFA), arrested at amounts present at day 10 when PFA treatment began at day 10 (+βGP +D10 PFA), and not observed in untreated and PFA only controls. ERK 1/2 phosphorylation at day 14 was assayed by Western blot to investigate activation of the ERK 1/2 signaling cascade (B). ERK 1/2 activation was correlated with the presence of calcium precipitates and increased in +βGP and +βGP +D10 PFA samples. The expression of the genes for osteoblast transcription factors, Runx-2 and osterix (OSX), along with genes encoding several bone matrix proteins, including bone sialoprotein (BSP), Osteopontin (OPN), osteocalcin (OCN), and collagen-I (Coll-I) were assessed by qRT-PCR (C). *Runx-2*, *Bsp*, and *Opn* expression paralleled ERK 1/2 signaling. The expression of late osteogenic marker genes, *Ocn* and *Osx*, was upregulated in all PFA treated samples, and this upregulation was synergistically increased in samples receiving +βGP treatment (+βGP +D5 PFA and +βGP +D10 PFA). *Osx* expression was also increased with βGP treatment alone. *Coll-I* expression was decreased in +βGP +D5 PFA and +PFA samples compared to untreated samples. Data are from one representative experiment of two with similar results. n=3-4, Box-Cox transformation, two-way ANOVA, #p<0.05, ##p<0.01, ###p<0.001 compared to untreated, *p<0.05, **, p<0.01, ***p<0.005 compared to both +βGP and +βGP +D10 PFA, ^p<0.05 compared to +βGP, +p<0.05, +++p<0.005 for marked comparison.

Protein level markers of osteogenic differentiation in differentiating EBs

To further assess the osteogenic phenotype of EBs induced by CaP precipitates at the protein level, alkaline phosphatase activity and the production of several osteogenic proteins, including matrix molecules and growth factors, were assayed from EBs with and without βGP treatment. Extracellular matrices derived from osteogenic cell types are known to promote the osteogenic differentiation of exogenous cells seeded onto them [74, 75, 78]. As such, the endogenous production of an osteogenic matrix, including associated mineral deposition and osteoinductive growth factors, may promote the further osteogenic differentiation of cells within the EB microenvironment. Conditioned media and cell pellets were collected at day 14 from βGP treated and untreated EBs and were assayed for overall osteogenic differentiation via alkaline phosphatase activity, a functional assay, as well as for the production of the bone extracellular matrix molecules osteopontin and osteoprotegrin to evaluate the osteogenic phenotype at the protein level [206, 207]. Alkaline phosphatase (ALP) activity was detected in all EB samples regardless of treatment but was increased with βGP treatment compared to untreated EBs ($p<0.005$) (Fig. 5.9 A). Osteoprotegrin (OPG) and osteopontin (OPN) protein secretion into conditioned media was detectable by ELISA in both treated and untreated samples (Fig. 5.9 B), but OPG was increased whereas OPN was decreased with βGP compared to untreated ($p<0.001$), suggesting osteogenic proteins are differentially regulated by microenvironmental changes resulting from phosphate treatment and CaP precipitation.

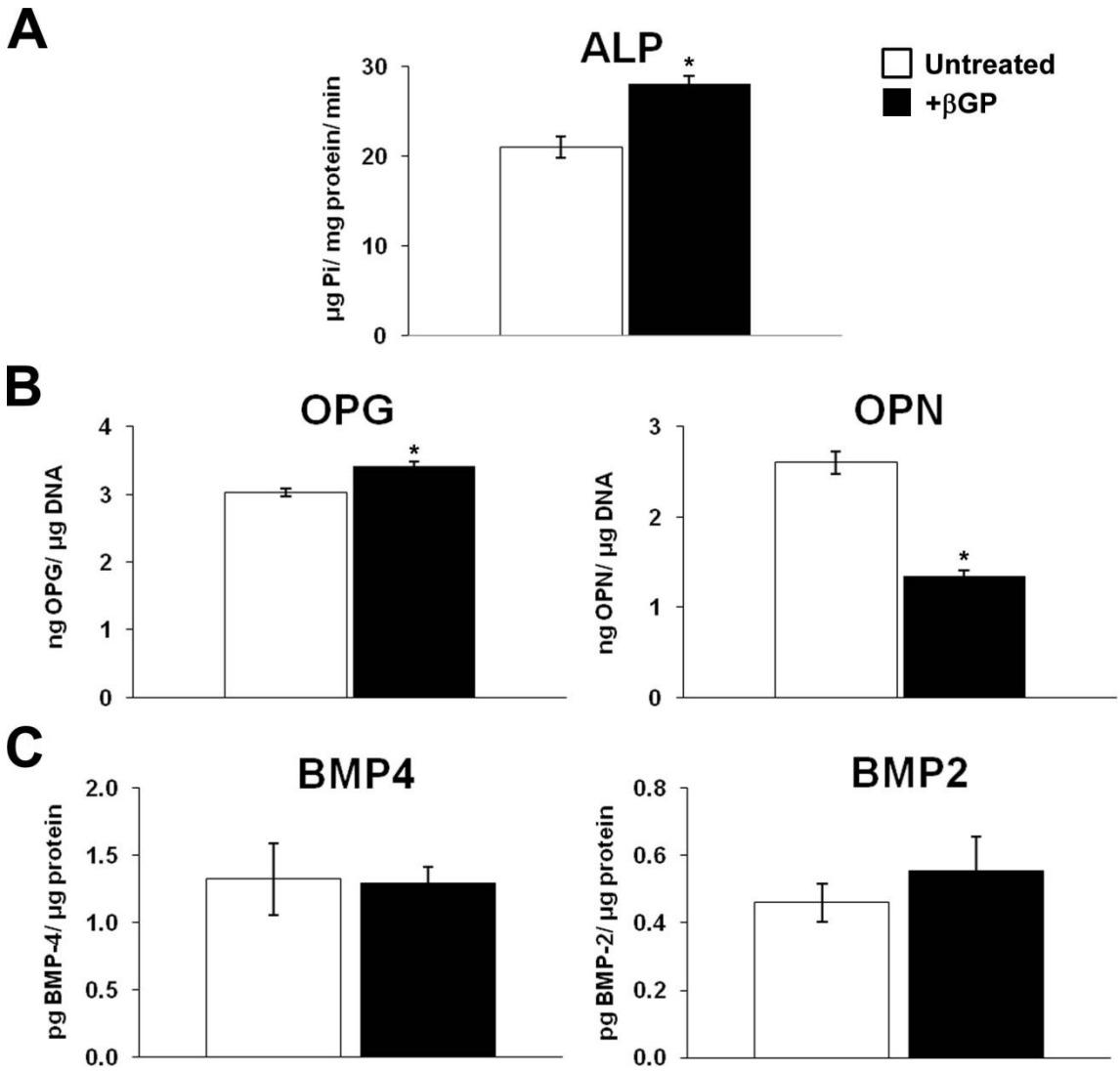

Figure 5.9. Osteogenic protein analyses. Alkaline phosphatase (ALP) activity, a marker of mature osteogenic differentiation, was assayed at day 14 (A) and was increased with βGP treatment. Osteoprotegrin (OPG) and osteopontin (OPN), two matrix proteins secreted by osteoblasts, were assayed by ELISA (B). OPG was increased and OPN was decreased with βGP treatment compared to untreated samples. Day 14 EB cell pellets contained equivalent amounts of BMP-2 and BMP-4 regardless of βGP treatment (C). n=6 samples for ALP, OPG and OPN, n=5 samples for BMP4 and BMP2, t-test, * $p<0.005$.

To quantify EB growth factor content, EBs with and without βGP treatment were analyzed at day 14 of differentiation for BMP-4 and BMP-2. The retention of these osteoinductive factors within the EB microenvironment, potentially in association with CaP precipitates, may account for the observed CaP precipitate induced osteogenic differentiation [208, 209]. No differences in BMP-2 or BMP-4 content were observed with βGP treatment. Treated EBs contained 0.55 ± 0.10 pg BMP-2/μg total protein and 1.29 ± 0.12 pg BMP-4/μg total protein, whereas untreated EBs contained 0.45 ± 0.06 pg BMP-2/μg total protein and 1.32 ± 0.27 pg BMP-4/μg total protein (Fig. 5.9 C).

Finally, because interactions with a collagenous matrix promote osteogenic differentiation [9, 10], the presence of collagen within EBs was assessed by Masson's Trichrome stain and immunofluorescence staining for collagen-I and collagen-II. EBs did not contain readily apparent staining for collagen, which stains in blue by Masson's Trichrome stain, regardless of phosphate treatment (Fig. 5.10 A), which was in agreement with observations by TEM that mineral deposits were not associated with organized collagen fibers present in bone (Fig. 5.5). Immunofluorescence staining for both collagen-I (Fig. 5.10 B) and collagen-II (Fig. 5.10 C) confirmed these findings, though collagen-I was enhanced when EBs were cultured with ascorbic acid. Taken together, these stains demonstrated that while EBs produce osteogenic matrix molecules and growth factors, these molecules are not associated with the production of a collagenous matrix as in mature bone.

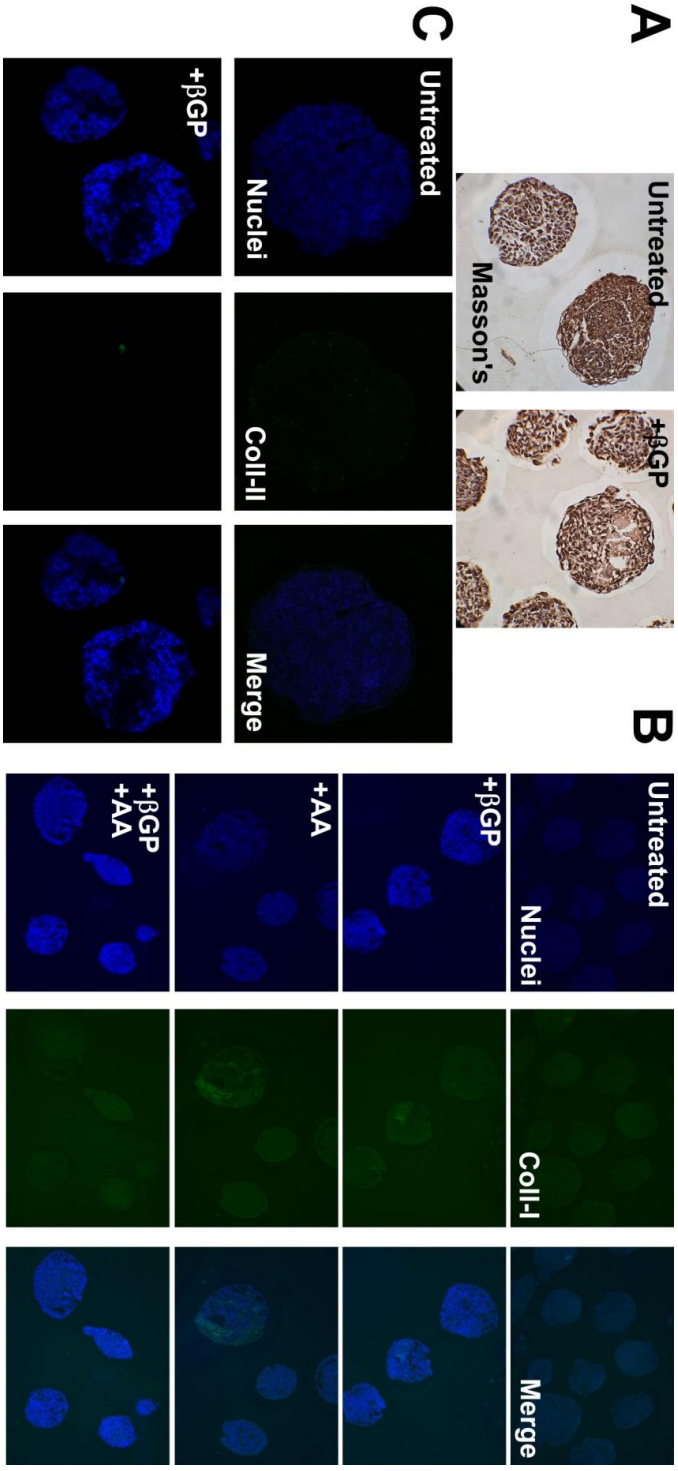

Figure 5.10. EB collagen content. Day 14 EBs were stained by Masson's Trichrome stain and immunofluorescence for collagen-I and collagen-II. EBs contained little positive staining for collagen (stained in blue) regardless of phosphate treatment (A). Immunofluorescence demonstrated little collagen-I, though there was an increase in positive staining in EBs treated with ascorbic acid (B). Staining for collagen-II also demonstrated little presence of the matrix protein.

In total, EBs differentially regulated the production and secretion of proteins in response to βGP treatment. In parallel with observed enhancements at the mRNA expression level, βGP treatment enhanced protein level markers of osteogenic differentiation, including osteogenic extracellular matrix molecule production, and this effect was directly associated with the formation of CaP precipitates. Additionally, even untreated EBs produced osteogenic and osteoinductive molecules endogenously, including osteogenic matrix proteins and growth factors, as they spontaneously differentiated to cells from all three germ lineages, including bone forming osteoblasts. Overall, these data suggest that not only did EBs produce CaP mineral deposits, given the minimal substrate (βGP), but changes in the EB micronenvironment resulting from CaP precipitate formation induced ERK signaling and subsequent osteogenic differentiation at the gene and protein levels.

Discussion

This study presented evidence that mineral deposits, which may be formed endogenously within EBs by culture with βGP, induced osteogenic differentiation of mouse ESCs, demonstrated at the gene and protein levels. Additionally, the mineral accumulation was formed from CaP precipitates, was quantifiable by multiple metrics, and induced activation of ERK 1/2 signaling and osteogenic differentiation. Previous work in our lab has demonstrated that alterations in the extracellular EB micrcoenvironment by controlled presentation and delivery of materials and soluble factors within EBs lead to phenotypic changes and differentiation [99, 102, 197]. Here, to understand the relationship between mineral formation and osteogenic differentiation, the EB microenvironment was manipulated by the introduction of endogenously formed CaP

precipitates. Though the directed osteogenic differentiation of mouse ESCs has often been achieved by addition of a combination of soluble factors, including, βGP, ascorbic acid, dexamethasone [103, 110, 198], or $1\alpha,25(OH)_2D_3$ vitamin D [105], βGP alone was necessary for the development of mineral deposits within EBs (Fig. 5.1 A). Additionally, uniformly sized EBs, formed by forced aggregation, were used in order to reduce variability that may arise in EB differentiation due to variation in EB size within the starting population [97, 203, 204].

CaP precipitates were found to form endogenously within EBs upon the addition of βGP and to increase over the course of EB differentiation in a quantifiable manner (Fig 5.2, 5.3, 5.4). During histological evaluation of the CaP precipitates formed in EBs, regions of positive von Kossa staining that did not correspond with positive Alizarin red staining of adjacent sections were noted (Fig. 5.3). This discrepancy may have been attributed to several possible explanations. The contrast between positive staining and cell nuclei was greater with von Kossa staining, allowing for better resolution by eye of EBs containing positive staining by an observer evaluating the stain. Because of this difference, μCT was used to provide more reliable and less observer biased quantification of the CaP precipitates within EBs. Perhaps more importantly, though often used interchangeably to demonstrate mineralization, these two stains do not actually demonstrate the same thing. Whereas Alizarin red stain chelates calcium, von Kossa staining actually demonstrates phosphate. Alizarin red staining has its caveats, too, as in addition to CaP mineralization, calcium binding proteins and proteoglycans stain positively for Alizarin red as well. As described in detail by Bonewald et al, neither stain, nor μCT, can truly demonstrate true matrix mineralization, as observed in native bone,

with hydroxyapatite, collagen-I fibrils, and matrix vesicles [37], motivating more detailed material characterization.

Though observed to be the same by gross examination used to quantify mineralization in this study, EB mineral deposits were not the same in structure and composition as ones observed in other osteogenic cell types and native bone and were found to be precipitates of CaP (Fig. 5.5), nucleated by cellular debris within EBs (Fig. 5.6, 5.7). These material differences were not apparent based solely upon histological and μCT techniques often used to characterize bone formation and mineralization *in vitro* and *in vivo.* Additionally, the induction of osteogenic gene expression by these precipitates represents a reversal of expected relationship of mineralization and differentiation based on development [105]. These findings underscored the need to carefully characterize the apparent phenotype and mineral deposit formation of osteogenic cells generated *in vitro* [37, 75, 131]. Transmission electron microscopy of mineral deposits within EBs did not suggest the presence collagen-I mediated mineralization observed from osteoblasts *in vitro* and *in vivo*, including clear collagen fibril formation with matrix vesicles [6, 37], but demonstrated both intra-and extracellular accretions. Additionally, SEM, EDS, FTIR, and XRD suggested the presence of poorly crystalline calcium phosphate, distinct in elemental content and crystal structure from hydroxyapatite found in mature bone (Fig. 5.5). The findings of this study suggested a different mineralization process than that observed in mature bone formation, but it supported gene level analysis, in which *collagen-I* gene expression was not upregulated at day 14 with βGP treatment. Mason's Trichrome staining and immunofluorescence for both collagen-I and collagen- II proteins also did not provide evidence of abundant collagen within either treated or untreated EB

populations (Fig. 5.10). *Collagen-I* expression has been shown to be only transiently increased in embryonic and mesenchymal stem cells undergoing osteogenic differentiation [105, 113, 210], while other studies have demonstrated downregulation of *collagen-I* expression in MC3T3-E1 pre-osteoblast cells upon treatment with inorganic phosphate [211].

Based on TEM, staining for cellular debris within precipitates, and the ability of non-viable EBs to form precipitation, CaP mineral deposits were suggested to have formed by nucleation of crystal formation on celluar debris within EBs (Fig. 5.5. 5.6, 5.7). During embryogenesis, the mineralization of the collagenous extracellular matrix is a cell mediated process involving CaP deposition from matrix vesicles as hydroxyapatite [6, 37]. However, in addition to being an active, cell mediated process in mineralizing tissues, mineralization is a process that is actively inhibited by non-mineralizing tissues. Mineral precipitation onto non-viable cells can occur under physiologic conditions because the cells are no longer actively producing PPi, a potent inhibitor of CaP crystal formation [47]. Additionally, non-viable cell CaP precipitation has been demonstrated to occur to a greater extent and with different structure and composition from CaP precipitation produced in the setting of viable cells [131]. Comparisons of CaP precipitates in vascular smooth muscle cells with CaP precipitation in non-viable, fixed cells found that the precipitates formed were of different composition and structure by EDS, XRD, and TEM. Additionally less precipitation was present in live cells than non-viable cells, suggesting that though initiated through the same passive process, viable cells modulate the CaP precipitate accumulation by controlling precipitation rate [131]and through templating provided by cell-produced osteogenic matrix molecules

[212]. Based on these findings, one may hypothesize a mechanism by which CaP precipitation occurs within the EB microenvironment. PPi was cleaved by alkaline phosphatase, whose activity was maintained within EBs through day 14 of differentiation regardless of βGP treatment (Fig 5.9 A). The removal of PPi thus created a microenvironment permissive of CaP precipitation, especially in the setting of media containing elevated levels of inorganic phosphate, which was also liberated from βGP by alkaline phosphatase.

Regardless of their mechanism of formation, composition, or structure, CaP precipitates were found to induce osteogenic differentiation of ESCs, paralleling findings previously reported in more mature cell types [130-132], and confirmed by studies blocking the formation of precipitates by PFA treatment (Fig. 5.8). Previous studies have found that phosphate treatment of MC3T3-E1 cells induces ERK 1/2 activation [107, 116], which regulates Runx-2 activation and downstream osteogenic gene expression [205].The same ERK 1/2 pathway was activated in response to βGP treatment of EBs, leading to osteogenic differentiation (Fig 4.5). Both phosphate-induced mineralization and differentiation of MC3T3-E1 cells have been inhibited by treatment with PFA, thought to inhibit phosphate transport into cells, specifically through Type III Na,Pi co-transporter PiT-1, suggesting that phosphate needed to enter the cell for phenotypic changes to happen. However, more recent electrophysiological studies of PiT-1 expressed exogenously in *Xenopus* oocytes have found that its transport of Pi was not actually blocked by PFA treatment at the concentrations typically used (0.5 mM), pointing towards another mechanism of action [128]. PFA is also an analogue of PPi, which, as described above, directly interferes with CaP crystal formation [129]. Recent work

performed has demonstrated that both endogenously formed and exogenously provided CaP precipitates induced osteogenic differentiation independent of phosphate concentration and transport and that the induction occured via ERK 1/2 activation [130-132]. In light of the recent findings, the mechanism of PFA inhibition of phosphate-induced osteogenic differentiation observed previously may be reevaluated.

In the current EB study, ERK 1/2 signaling was activated in the presence of CaP precipitates within EBs and was correlated with increases in osteogenic gene expression, including early osteoblast transcription factor *Runx-2* and osteogenic matrix proteins *Bsp* and *Opn* (Fig. 5.8 B, C). Taken together these findings suggested that phosphate-induced osteogenic differentiation of EBs was actually induced by CaP precipitates and not by blocking of phosphate uptake by cells. This conclusion was further supported by the observation that ERK activation was still induced in PFA treated EBs when precipitate formation was allowed to occur before the initiation of PFA treatment (+βGP +D10 PFA).

Not all osteogenic genes evaluated appeared to have been regulated through this mechanism. Interestingly, transcription of late osteoblast marker genes encoding osteocalcin and osterix were actually increased with PFA treatment (Fig 5.8 C). Additionally, *coll-I* expression at day 14 and *Runx-2* expression at day 10 were significantly decreased with PFA treatment alone, pointing towards the ability of PFA to affect cell phenotype by itself. This highlighted the possibility that PFA may affect cell phenotype in multiple ways including inhibition of CaP precipitation, blocking phosphate uptake via PiT-1, and other as yet unidentified mechanisms. Furthermore, the role of phosphate transport by PiT-1 in promoting osteogenic differentiation cannot be

completely discounted either. PiT-1 expression at the protein level was required for BMP-2 induced matrix mineralization of MC3T3-E1 [119] and vascular smooth muscle cells [120]. Also in vascular smooth muscle cells, siRNA blocking of PiT-1 protein expression reduced phosphate induced osteogenic gene expression [124]. For future studies, in order to circumvent the ambiguity in PFA action, other agents to block CaP precipitation can be used, such as phosphocitrate [132], or the exogenous introduction of CaP in the form of microparticles [213] or nanocrystals [130] may be investigated. Though the precise mechanism still remains a point of contention, even in more committed and extensively studied cell types than ESCs, this study demonstrated a conservation of phosphate-induced osteogenic differentiation by activation of ERK signaling that has been reported in a variety of cells, including osteoblasts [116], dental pulp cells [133], and vascular smooth muscle cells[134].

In addition to the increases in gene expression, increases in protein markers of osteogenic differentiation were also observed in EBs with CaP precipitates, and some proteins were expressed at high levels regardless of treatment, which may provide a clue to how the extracellular microenvironment, including matrix molecules, growth factors, and CaP precipitates, and differentiation could be interrelated. Though the mechanism by which cells sense and respond to CaP precipitates and how that leads to osteogenic differentiation remain to be elucidated [130-132], it would be reasonable to hypothesize that this effect is mediated through interactions of the CaP material with osteogenic and osteoinductive molecules produced within the cellular microenvironment. Osteogenic cells themselves produce extracellular matrices that have been demonstrated promote osteogenic differentiation of exogenous cells re-seeded on them [74, 75, 78], suggesting

the creation of a feedback loop within EBs between differentiating cells and their self-produced osteoinductive extracellular environment. In addition to osteogenic matrix protein production, osteoinductive growth factors BMP-2 and BMP-4 were both produced by EBs (Fig 5.9). Based on previous studies of EBs, mesoderm differentiation was expected to be enhanced by day 5, when βGP treatment was initiated [184], and since BMP-4 is critical during embryonic development and mesoderm formation [36], it was not surprising that it was present in large amounts in EBs regardless of treatment. CaP precipitates may have the ability to bind and retain these growth factors within the EB microenvironment, either serving as a local reservoir or presenting the growth factors in a manner that can promote osteoinduction of cells within EBs. In fact, CaP coated microparticles have been proposed for the delivery of BMPs because of CaP affinity for binding proteins [213].

Osteogenic differentiation induced by CaP may also depend on surface characteristics of the precipitates and how they modulate osteoinductive protein entrapment or binding. CaP containing material surface geometry has been found to alter the dissolution and re-precipitation of CaP, leading to entrapment of organic material, including growth factors such as BMPs, which in turn may impart osteoinductivity [208, 209]. Within the microenvironment of osteogenic cells, CaP containing materials with the appropriate surface characteristics have been suggested to be modified by proteins secreted by differentiating osteogenic cells. This cell-altered surface is in turn able to promote the osteogenic differentiation of additional neighboring cells. In a study of osteoinduction by calcium phosphate-containing materials, material implanted in the abdominal muscle of baboons induced new bone formation when its surface contained

concavities of specific geometry [214]. It was suggested that through an inductive feedforward loop, surfaces with specific topography interacted with soluble osteoinductive cues, which in turn induced osteogenic cells at the material surface to produce more osteoinductive molecules, ultimately inducing downstream bone formation. Additionally, osteoblastic differentiation of MG63 osteosarcoma cells and mesenchymal stem cells on titanium surfaces has been found to be modulated in response to surface, micron-scale roughness and nanoscale features in a similar manner [215, 216]. Material stiffness has also been suggested to effect cell differentiation, with more rigid surfaces promoting osteogenic differentiation of mesenchymal stem cells [217].

This study presented the novel opportunity to interrogate the relationship between mineralization and differentiation by embryonic stem cells, cells present during the earliest stages of development. The paradigm has traditionally been that osteogenic differentiation *in vitro* parallels intramembranous and endochondral ossification *in vivo* with osteogenic differentiation preceding mineralization [105].The current study, as well as recent studies cited above, suggest that this process might be able to occur in reverse, with mineralization inducing differentiation by the creation of an osteoinductive microenvironment within EBs, establishing a feedback loop between mineralization and differentiation.

Conclusions

In conclusion, markers of osteogenic differentiation in ESCs were responsive to the subtle manipulation of the culture environment achieved through introduction of endogenously formed CaP precipitates, created by the addition of just an organic

phosphate substrate, βGP. CaP precipitate-induced differentiation resulted in osteogenic gene expression and protein production by EBs and occurred via activation of the ERK 1/2 signaling, a response conserved across multiple cell types. The current study established an EB model for studying the endogenous differentiation capacity harbored by differentiating ESCs, with minimal exogenous cues, allowing for the identification of more subtle processes and interactions that may be occurring within the cellular microenvironment of differentiating cells. Such a model provided a window to probe the interrelationship between differentiation and mineralization during the earliest stages of development and established a test bed for future mechanistic studies of osteogenic differentiation. This work not only provided insights into the physiology of calcified tissues but also raised the possibility devising a strategy to capture or mimic the cues present within this embryonic-like milieu for bone tissue engineering or regenerative medicine applications.

CHAPTER 6

DEVITALIZED EMBRYOID BODY-DERIVED MATERIAL INDUCES BONE FORMATION IN VIVO

Introduction

Acellular matrix-derived therapies are attractive because of improved handling characteristics and stability over fresh tissue and may be derived by a variety of techniques, including chemical and physical treatments. The resultant acellular materials lack viable cells but retain natural ECM components, such as structural adhesive proteins, glycosaminoglycans and bioactive growth factors embedded within the native matrix from the tissue of origin [70-73]. One such acellular matrix in use commonly for clinical, bone regenerative applications is demineralized freeze-dried bone allograft, also commonly referred to as demineralized bone matrix (DBM). While autograft bone is the gold standard for bone repair, its use is limited by significant donor site morbidity and limited source of material [218]. An alternative, therefore, is the use of cadaveric-sourced, allograft tissue, such as DBM [22]. Extraction of the mineral phase of bone by acid treatment yields a demineralized matrix comprised of mostly collagen, along with non-collagenous matrix proteins and associated growth factors. Extracellular matrix associated growth factors may additionally have increased bioavailability after demineralization, due to an increased hydration state [49] and unmasking of regions of matrix obscured and entrapped beneath mineralization [219]. Increased growth factor bioavailability after demineralization may therefore account for the observation that,

Modified from:
K Sutha, SL Hyzy, Z Schwartz, BD Boyan, and TC McDevitt, *Devitalized Embryoid Body-Derived Material Induces Bone Formation In Vivo,* **in preparation**.

when implanted in an ectopic site *in vivo*, DBM is osteoinductive while non-demineralized bone matrix is not osteoinductive [50]. Factors found to be present in DBM include primarily bone morphogenetic proteins (BMPs), which impart DBM its osteoinductivity, in combination with, but to a far lesser extent, other factors, including vascular endothelial growth factor (VEGF) [31, 51].

Since its first description in the 1960's, the osteoinductivity of DBM has long been known to be due mostly to its BMP-2 content [22-24]. BMP-2 is directly osteoinductive, and as such, recombinant human BMP-2 is employed clinically as a single factor therapy used to promote bone growth and regeneration, although at supraphysiologic doses in the milligram range [InFUSE; Medtronic Sofamor Danek, Memphis, TN] compared to the nanogram amounts present within clinical doses of DBM [25]. DBM also contains VEGF, which is vital to osteoinductivity, as it is required for endochondral bone formation and promotes neovascularization allowing for the recruitment of the mesenchymal progenitor cells that are acted upon by the BMP to form new bone [5, 27, 28]. Another osteoinductive factor of interest but not abundant in adult bone-derived DBM is BMP-4. Like BMP-2, BMP-4 is directly osteoinductive, due to their high level of homology [31]. During endochondral ossification *in vivo*, knockout of either *Bmp2* or *Bmp4* is rescued by endogenous expression of the other, allowing for normal bone formation, suggesting interchangeable roles during osteogenesis; however, removal of both BMP-2 and BMP-4 together completely inhibits osteoblast differentiation and long bone development *in vivo* [32]. However, BMP-4 is also critical during earlier stages of development and necessary for gastrulation and mesoderm formation [36]. With respect to DBM osteoinductivity, *in vivo* intramuscular

osteoinductivity has been found to be correlated with the amount of BMP-4 extractable from DBM, measured *in vitro* [61] though it has also been reported to be undetectable in DBM by other studies [25, 51].

The osteoinductivity of DBM preparations is often evaluated i*n vivo*, by intramuscular implantation into the hindlimb of nude athymic mice [53]. This model is widely used for the evaluation of DBM [64, 220, 221] and is accepted as the ASTM standard for the evaluation of osteoinductivity of materials [62]. In the intramuscular model, it is believed that DBM particles recruit MSCs to the implantation site before inducing the formation of a cartilage intermediate and eventual bone, in a manner analogous to endochondral bone formation [26]. The osteoinductive factors within DBM can be inactivated by heating, and so inactive DBM may be used as a carrier for the evaluation of growth factors, which may modify the osteoinductivity of DBM [222]. For example, the approach of co-delivering a single,soluble growth factor with inactive DBM has been used to evaluate BMP-2 [24] and platelet derived growth factor (PDGF) [63], but the same technique can also be employed to deliver more complex mixtures and materials [223].

The use of DBM comes with its own caveats though. The *in vivo* osteoinductivity of DBM has been found to vary manufacturer to manufacturer and even batch to batch from the same manufacturer [53]. As with any cadaveric-sourced, allograft tissue, there is limited donor availability, as well as little control over donor characteristics, such as age, or environmental exposures, such as pharmaceutical use, that may impact the quality and osteoinductivity of DBM, which in turn leads to donor to donor and batch to batch

variability [2, 25, 51, 54, 55]. These donor tissue limitations motivate the identification of a more homogeneous and controlled material source.

One approach that has been explored to overcome donor to donor tissue variability is the generation of extracellular matrix (ECM) and acellular biomaterials *in vitro* derived from a single, starting cell source. This method has been used to generate devitalized materials produced by MC3T3-E1 osteoblast-like cells [75] and mesenchymal stem cells (MSCs) [76, 78, 224] that were found to be osteoinductive when re-seeded with exogenous cell types *in vitro*. Though *in vitro* results were encouraging, when MSC-derived ECM osteoinductivity was evaluated *in vivo*, no new bone formation was observed [65]. The disparity between *in vitro* and *in vivo* results may be explained by the heterogeneity of cell types that are able to respond to the implant *in vivo* compared with the single, osteogenic cell type that was seeded *in vitro*. Additionally, as the ECM was already highly mineralized pre-implantation, the bioavailability of associated growth factors may have been reduced, blunting their osteoinductive capability. In the absence of strongly osteoinductive cues, or ones masked by mineralization, other cell types resident within the tissue exhibited a stronger response to the implanted material than the osteoprogenitor cell population, forming a fibrous capsule and hindering further progenitor cell recruitment and infiltration before new bone could be formed. The fibrous response to the MSC-derived material was similar to that previously observed to non-demineralized bone matrix [50]. For the given reasons, the MSCs used to generate the devitalized material, *in vitro*, may have had too mature an osteoblastic phenotype leading to a balance of ECM and osteoinductive cues that was not optimized to favor bone formation.

Pluripotent cells, including embryonic stem cells (ESCs), are an attractive alternative source of starting cells. Pluripotent ESCs, derived from the inner cell mass of blastocyst stage embryos, are capable of extensive self-renewal and differentiation into cell types comprising all three germ lineages (ectoderm, endoderm, and mesoderm) [89]. As such, these cells are capable of differentiating not only into osteogenic lineages, but also into associated cell types, such as endothelial and hematopoietic cells, that contribute to bone formation and maintenance [3, 105, 195]. Additionally, ESCs are capable of producing molecules that can affect the growth and injury response of somatic cells and tissues, a function that may be lost in mature cells [86]. ESCs may be differentiated as three dimensional cell aggregates, embryoid bodies (EBs), and devitalized EB material (EBM) may be derived from these cells by chemical[225, 226] and physical disruption techniques, including freeze-drying by lyophillization [69], while retaining bioactive factors. The use of an acellular therapy derived from devitalized ESCs, such as EBM, eliminates the risk of teratoma formation associated with the direct delivery of viable ESCs or EBs [87]. ESCs undergo osteogenic differentiation in response to a variety of different media supplements [103-105, 111], but previous studies presented here have looked specifically at osteogenic differentiation within EBs in response to β-glycerophosphate (βGP) treatment alone (see Chapter 4, 5). Cell lysates from EBs with and without βGP treatment have previously been found to contain physiologically relevant concentrations of growth factors known to contribute to DBM osteoinductivity: BMP-2, BMP-4, and VEGF (see Chapter 5).

Given the presence of osteoinductive factors within EBM, in particular BMP-2, BMP-4, and VEGF, the goal of this study was to evaluate whether or not this ESC-

derived material harbors osteoinductive potential. It was hypothesized that bioactive factors enriched within the embryonic-like microenvironment within EBs, in particular BMP-2 and BMP-4, would recruit and induce the differentiation of bone forming cells when implanted, *in vivo*, and that osteoinductive potential of EBM would be enhanced when derived from EBs undergoing osteogenic differentiation in response to phosphate stimulation. The use of a less mineralized material than investigated in previously unsuccessful MSC studies was expected to improve growth factor bioavailability and material osteoinductivity. The goals of the study were achieved by quantifying levels of BMP-2, VEGF, and BMP-2 extracted from EBM, and evaluating osteoinduction compared to active and inactive DBM *in vivo* by implantation into a nude athymic mouse hindlimb intramuscular implantation model. Osteoinductivity was measured by mineralization quantification, semi-quantitatitve bone induction score, and quantitative histomorphometric measurements of new bone formation.

Materials and Methods

Mouse ESC culture

Mouse embryonic stem cells (D3 cell line) were maintained in the undifferentiated state on 0.1% gelatin coated tissue culture dishes in ESC media containing DMEM (Mediatech, Herndon, VA) supplemented with 15% FBS (Hyclone, Logan, UT), 2mM L-glutamine (Mediatech), 1x non-essential amino acids (Mediatech), 100U/ml penicillin/ 100 μg/ml streptomyocin/ 0.25 μg/ml amphotericin (GIBCO, Carlsbad, CA), 0.1 mM β-mercaptoethanol (Fisher, Fairlawn, NJ), and 10^3 U/mL of leukemia inhibitory factor (LIF, Chemicon, Temecula, CA). Media was changed at least

every 2 days, and cells were passaged every 2-3 days before reaching 70% confluency with 0.05% trypsin (GIBCO).

EB formation and osteogenic differentiation

EBs were formed by the ultra-high throughput, forced aggregation method using Aggrewell™ inserts [148] with 1000 cells per well, as described in Chapter 3 – General Methods. EBs were either left untreated, or osteogenic differentiation was initiated by addition of 10 mM β-glycerophosphate (βGP, MP Biomedical, Solon, OH) beginning from day 5 of EB differentiation. For cell pellet growth factor analysis, EBs were cultured in 10 nM dexamethasone, 50 μg/ml ascorbic acid, and 10 mM βGP from day 5-10.

Characteristics of DBM used

DBM previously found to have high osteoinductive capacity was used as a positive control for bone formation (Musculoskeletal Transplant Foundation, Edison, NJ). DBM was derived from donated, human cadaveric tissue and processed by cleaning, de-fatting, and disinfecting of the cortical bone; grinding bone to yield particles of sizes between 400-1000 μm; demineralization of the bone particles in dilute hydrochloric acid solutions to result in a residual calcium content less than 8% per American Associate of Tissue Banks (AATB) standards; and freeze-drying of the final product. DBM from the same lot as that used for the positive control was heated at 105 °C for 24 hours to inactivate osteoinductive factors present within the DBM, and inactive DBM was then used as a negative control and as a vehicle for the delivery of EBM.

Characterization of EBM

Devitalized EB material (EBM) was isolated at day 5, 10, and 14 of EB differentiation by lyophillization, as described previously by Ngangan and McDevitt [69], from untreated EBs (-βGP) as well as EBs initiated to undergo osteogenic differentiation and mineralization (+βGP). Previous studies have demonstrated osteogenic differentiation and mineralization in response to βGP treatment administered from day 5 of differentiation (see Chapter 4). Briefly, cell spheroids in each group were harvested at day the day of isolation by gravity-induced sedimentation for ~5 minutes in a 50 ml conical tube for every five 100 mm dishes, and excess media was aspirated. Spheroids were washed twice in phosphate-buffered saline, resuspended in sterile, deionized water, and aliquoted into microcentrifuge (1.5 ml) tubes (~$2x10^3$ EBs per tube). After pelleting, tubes were frozen in water at -80°C overnight and then lyophilized overnight to generate devitalized material (Labconco, Kansas City, MO).

To assess gross morphology and characteristics, images of DBM and EBM were acquired using a dissecting stereomicroscope equipped with a digital camera (Nikon SMZ1500). EBM and DBM were also evaluated histologically. The materials were embedded in Histogel (Richard Allen Scientific, Kalamazoo, MI), dehydrated via an increasing series of ethanol and xylene rinses (Shandon Pathcentre Enclosed Processor), embedded in paraffin (Shandon Histocentre 2 Embedding System), cut into 5 μm-thick sections (Microm HM 355S Rotary Microtome), and placed on positively charged glass slides. Sections were stained by routine H&E (Leica AutoStainer XL).

To further evaluate for the presence of collagen within EBM, a modified Mallory's Aniline Blue (MMAB) staining protocol was used [227]. Aniline blue is a constituent of commonly used Masson's Trichrome stain protocols to demonstrate collagen. Briefly, deparaffinized slides were post-fixed in Bouin's fixative before staining in 0.125% acid fuschin solution, differentiation in 1% phosphotungsic acid solution, and staining of collagen by 0.5% aniline blue solution.

Growth factor retention within EBM and within EB cell pellets was evaluated by enzyme linked immunosorbent assays (ELISA) as described in Chapter 3 – General Methods. Unknown values were compared to a standard curve generated from known concentrations of individual proteins in Tissue Protein Extraction Reagent (TPER, Pierce). Though the antibodies used were directed against human isoforms of each growth factor, they were known to exhibit cross reactivity with their mouse counterparts as well.

Endotoxin assay

The end point chromogenic limulus amebocyte lysate (LAL) endotoxin test (Lonza, Walkersville, MD) was used to assay the levels of endotoxin present in EBM. Briefly, EBM samples were resuspended in 500 μL sterile PBS, placed on a rotisserie for 30 minutes at room temperature, and centrifuged for 5 minutes at 14,000 RPPM to remove particulates. Endotoxin testing was performed as described in the product manual. Briefly, test samples and endotoxin standards reacted with the LAL for 10 minutes, followed by the addition of a substrate solution and incubated for 6 minutes, and then the reaction was stopped with stop reagent (25% glacial acetic acid solution). The

entire reaction was performed at 37°C. Absorbance readings at 405nm were taken using a SpectraMax M2e plate reader, and the endotoxin concentration (EU/mL) was calculated using the standard curve generated using the endotoxin standard supplied with the kit.

Preparation of Implants

For intramuscular implantation, DBM and day 10 EBM were loaded into size 5 gelatin capsules (Torpac, Fairfield, NJ) that had previously been UV-sterilized overnight. Previous studies have demonstrated that gelatin capsules dissolve quickly and do not affect osteoinductivity [2, 53]. Capsules were loaded in a biological safety cabinet in order to maintain sterility. 15 mg of DBM (active or inactive) was loaded into each capsule for positive and negative controls respectively. For day 10 EBM groups (-βGP EBM, +βGP EBM), 7.5 mg of inactive DBM was first loaded, and then 7.5 mg of EBM was added. The two materials were mixed together inside the capsule using a spatula. To ensure sterility before implantation *in vivo*, capsules were further sterilized by UV light overnight. Prior evaluation of the positive control DBM was conducted using the same protocol, so any loss in osteoinductivity resulting from the sterilization procedure was accounted for. In a separate study, viable day 10 EBs (~10^3 EBs) with and without βGP treatment were implanted intramuscularly. EBs were resuspended in 100-200 μl of PBS and transferred into gelatin capsules immediately before surgical implantation.

Implantation Protocol

Material formulations were implanted according to a Georgia Institute of Technology Institutional Animal Care and Use Committee approved protocol. Sixteen

male athymic Nu/Nu mice (Harlan, Indianapolis, IN) were divided into four groups with four mice each (Active DBM, Inactive DBM, -βGP EBM, +βGP EBM). A nude mouse strain with reduced helper T cells was chosen to reduce the possibility that the observed response was immunological rather than due to the implanted materials themselves. Samples were implanted into the gastrocnemius with one implant per limb, and each mouse received two of the same implant, reducing systemic effects or influence of one implant type on the other, giving eight implants per sample. Previous studies have demonstrated that an implant in one limb may cause systemic effects that influence response to an implant of a different type in the contralateral limb [228].

Mice were anesthetized by inhalation of 5% isofluorane in O_2, and hind limb implantation sites on both legs were disinfected with isopropanol and chlorhexiderm. A 0.5 cm incision was made over each gastrocnemius, and a muscle pouch was created under each muscle by blunt dissection. Implants were inserted into the muscle pouch, and the incision was closed by wound clips before dissolution of the gelatin capsule. Mice were housed for 35 days under conditions suitable for their immunocompromised state and were given food and water *ad libitum*. Studies have previously demonstrated that 35 days is sufficient to demonstrate osteoinductive activity by this model [2, 53].

Evaluation of mineralization – X-ray and micro-computed tomography (μCT)

For evaluation of mineralization and new bone formation, animals were euthanized at 35 days post-implantation by carbon dioxide asphyxiation. Hind limbs were removed and fixed in 10% neutral buffered formalin, and limbs examined by X-ray to localize the site of implantation (Faxitron, Lincolnshire, IL). The number of limbs

containing mineralization detectable by X-ray was noted for each group, and mineralization at the site of implantation was then further evaluated by μCT. The samples were scanned in air using a μCT 40 (Scanco Medical, Brüttisellen, Switzerland) at 55 kVp, 145 μA, 200-ms integration time, and a voxel size of 30 μm in a 30 mm scanning tube. Evaluation of μCT scans used sigma, support and threshold values set at 3.3, 2, and 70, respectively. Mineral volumes are expressed as absolute volume of mineralization. A minimum threshold of percent total volume containing mineralization was established (0.05%), above which limbs were counted as being positive for mineralization by μCT. Limb measurements were obtained and used to obtain an estimate of total hindlimb volume for these calculations.

Histological evaluation

After mineralization analysis, hind limbs were decalcified in 14% EDTA in water (pH 7) for two weeks (Sigma), before paraffin embedding and sectioning, with the progression of decalcification monitored daily by X-ray. Three consecutive cross sections (5 μm) were collected per slide at three different levels in the region of the implant along the longitudinal axis of the limb and were stained by routine hematoxylin and eosin stains (Leica AutoStainer XL). Each level was at least 250 μm apart from one another, and adjacent sections at each of the three levels were also collected for additional staining. The mouse tibia and fibula were used as reference points to confirm the correct orientation of the sections as the implants may have shifted after surgery once mice began applying weight to their hind limbs. All stained sections were evaluated by light microscopy for the presence or absence of DBM particles and new bone formation. One

complete section (of the nine total) per implant exhibiting the greatest amount of ossicle formation and residual DBM was selected. Because the selected section was the one containing residual DBM and the most new bone, the results were positively biased toward success for each implant type. To further evaluate for the presence of residual EBM within the implant site, the MMAB staining protocol described above was also used on sections adjacent to the sections chosen for scoring and histomorphometric evaluation.

For osteoinduction scoring, the entire section was qualitatively evaluated by two independent observers blinded to implant type and graded according to the previously published semi-quantitative rating system [2, 53, 63]. A score of 0 was given when no residual DBM or EBM was observed within the entire section. A score of 1 was given when residual EBM or DBM particles were present without any new bone formation. A score of 2 indicated one ossicle was observed, a score of 3 indicated ossicle formation present at multiple sites, and a score of 4 indicated ossicle formation covering >70% of the entire limb section examined. Observer scoring was calibrated to an experienced scorer prior to the start of the experiment. In cases where observer scores disagreed, the disputed sections were evaluated and scored by a third observer (ZS). The overall grade for each implant type was obtained by averaging the eight scores for the samples in each group. Implants receiving a score of 1.5 or greater were considered osteoinductive.

The same histological sections used for osteoinduction scoring were also evaluated by quantitative histomorphometric analysis using Metamorph™ software (v. 7.5, Molecular Devices, Sunnyvale, CA). Images of the implant site in each section were captured at the appropriate magnification using a Nikon 80i Upright light Microscope equipped with an externally mounted digital camera (Spot Flex, Diagnostic Instruments,

Sterling Heights, MI). Calibrations of distance were performed according to manufacturer instructions accompanying the software. The areas of total ossicle formation (marrow space and associated new bone), new bone, and new bone marrow alone (distinct from DBM and limb bones) were measured. The semi-quantitative score indicated both whether osteoinduction occurred and the number of ossicles formed, whereas the quantitative histomorphometry provided an assessment of the total amount of new bone formed but not whether it was located as one large ossicle or as multiple smaller ossicles.

Statistical analysis

Results are presented as mean and standard error of the mean for each variable, with n being the number of implant sites (n=8), unless otherwise noted. In cases where the entire data set for a given measurement did not approximate a normal distribution when first examined by exploratory data analysis, including examination of box and whisker plots, the data were transformed by Box-Cox transformations before further statistical analyses [151]. For histomorphometry data, data were not normally distributed even after transformation, so Kruskal-Wallis, non-parametric analysis of variance (ANOVA) with Tukey's post-hoc test was used to determine significant differences [229] and were performed using MATLAB (Mathworks, Natick, MA). Otherwise, statistically significant differences were determined by one-way ANOVA followed by Tukey's post-hoc test using Systat 12 (Chicago, IL). $p<0.05$ was considered significant.

Results

DBM and EBM characterization

DBM and EBM were characterized prior to implantation for general structure, composition, and extractable growth factor content. By gross, macroscopic examination, DBM was identified as a hard, dense, and particulate material, comprised of distinct granular pieces with rough edges. In contrast, EBM had a "cottonball" appearance that was loosely packed with handling characteristics similar to that of a dry powder and still had the ultrastructure of individual EBs identifiable (Fig. 6.1 A left panel). These differences in material architecture between DBM and EBM were also observed at the microscopic level, as revealed by H&E staining. DBM was comprised of solid, eosinophilic particles on the size range of 400-1000 μm, whereas EBM had a looser structure, again with the architechture of individual EBs still intact (Fig. 6.1 A center panel). EBM macro- and microscopic structures and staining were unchanged regardless of day of isolation and βGP treatment and were similar to previously published data [69]. MMAB staining revealed abundant, positive collagen staining (blue stain) of DBM, while EBM was apparently devoid of collagen, based on the lack of positive aniline blue staining.

ELISA was used to quantify the extractable amounts of several key growth factors within EBM and DBM known to be important in bone development and repair: BMP-2, BMP-4, and VEGF. All three growth factors could be extracted from EBM and were present at significantly higher levels than could be extracted from DBM by TPER buffer in this study ($p<0.005$, Fig. 6.1 B). Osteogenic differentiation of EBs under βGP treatment did not alter the amounts of any of these three growth factors at day 10 or day 14, though the production of BMP-2 and BMP-4 were temporally regulated over the course of EB differentiation. More BMP-2 was produced and retained within +βGP EBM

isolated at day 14 compared to day 5 untreated EBM ($p<0.05$), and BMP-4 was reduced in day 14 +βGP EBM compared to day 5 and day 10 isolated EBMs. In a separate experiment to evaluate the influence of other commonly used osteogenic supplements on BMP-2 and BMP-4 production, EBs were cultured from day 5 to 10 with βGP along with dexamethasone and ascorbic acid. The addition of these other factors did not change levels of BMP-2 produced in EBs but significantly increased BMP-4 production compared to untreated samples ($p<0.05$). However, this increase was only 1.4 fold compared to untreated EBs and 1.7 fold compared to +βGP EBs ($p<0.005$) (Fig. 6.2).

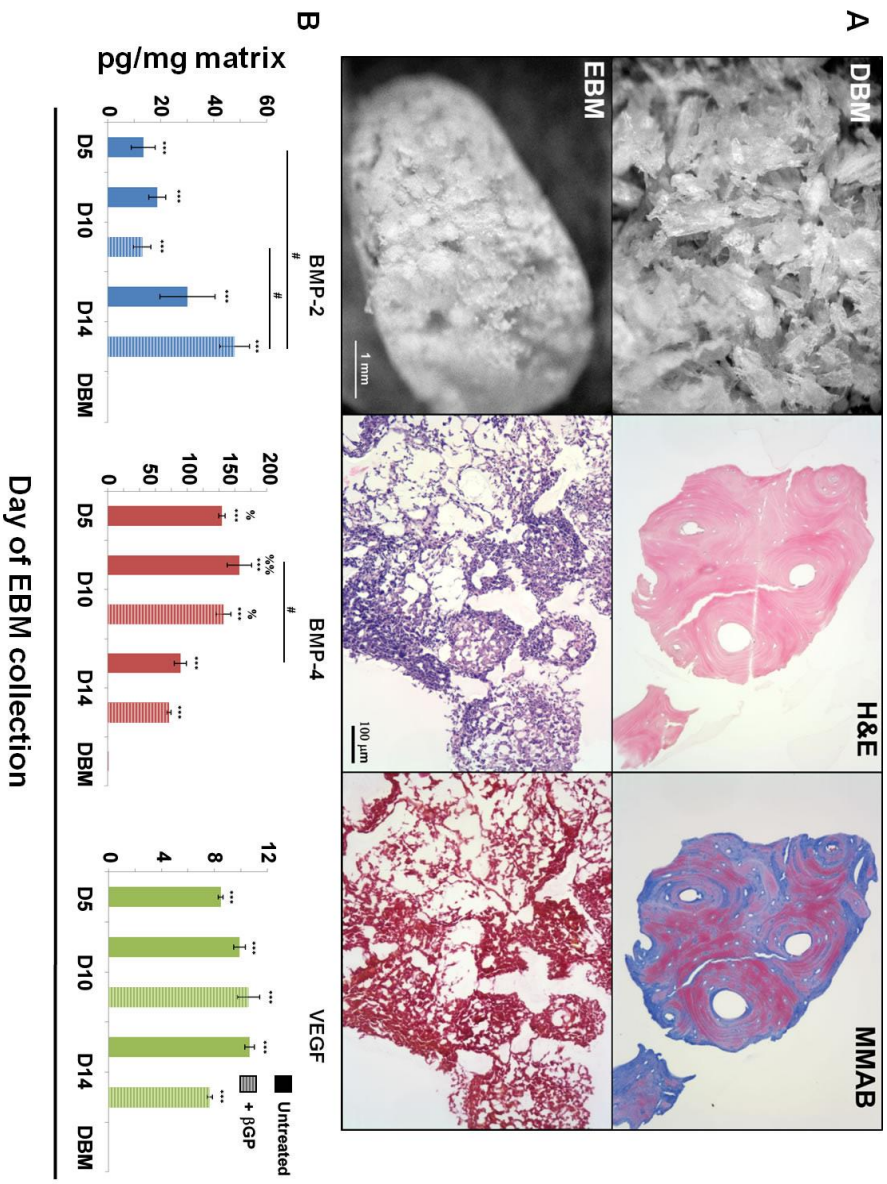

Figure 6.1. Characterization of DBM and EBM. DBM and EBM structure and composition were examined macroscopically (left) and microscopically revealing different material architectures (center, H&E) and collagen content (right, modified Mallory's Aniline Blue (MMAB)) (A). Growth factors extracted from both materials were quantified by ELISA. More BMP-2, VEGF, and BMP-4 were extracted from EBM than from DBM (B). n=3 samples, Box-Cox transformation, ANOVA, Tukey's post-hoc test, ***$p<0.005$ compared to DBM, #$p<0.05$ for marked comparison, %$p<0.05$, %%$p<0.01$ compared to Day 14 + βGP EBM.

For subsequent *in vivo* evaluation, EBM was isolated at day 10 of differentiation. Since EBM formulations were all found to contain BMP-2, BMP-4, and VEGF levels on the same order of magnitude regardless of day of isolation, this time point was chosen based not only on the growth factor content, but on the presence of mineral deposits within EBs. In previous studies, βGP-induced mineral accumulation began by day 10 and increased through day 14 (see Chapter 4). Because mineral volume was used as an assessment in this study, the day 10 time point was chosen for isolation of EBM to avoid biasing these measurements. Additionally, the variability in EBM yield was decreased at day 10 compared to day 14. Furthermore, highly mineralized matrices may have decreased bioavailability of growth factors compared to less mineralized matrices because of decreased hydration and masking of growth factors by the mineralization [49, 219]. After selection of culture day, the endotoxin levels of EBM prepared for implantation were assayed. The amounts of endotoxin contained within –βGP and +βGP EBM samples were found to be 0.18 ± 0.05 and 0.23 ± 0.08 EU/ml, which were less than the FDA guideline of 0.5 EU/mL (Fig 6.2) [230]. Taken together, EBM selected for implantation contained acceptably low endotoxin levels while maintaining factors known to impart osteoinductivity, BMP-2, BMP-4, and VEGF.

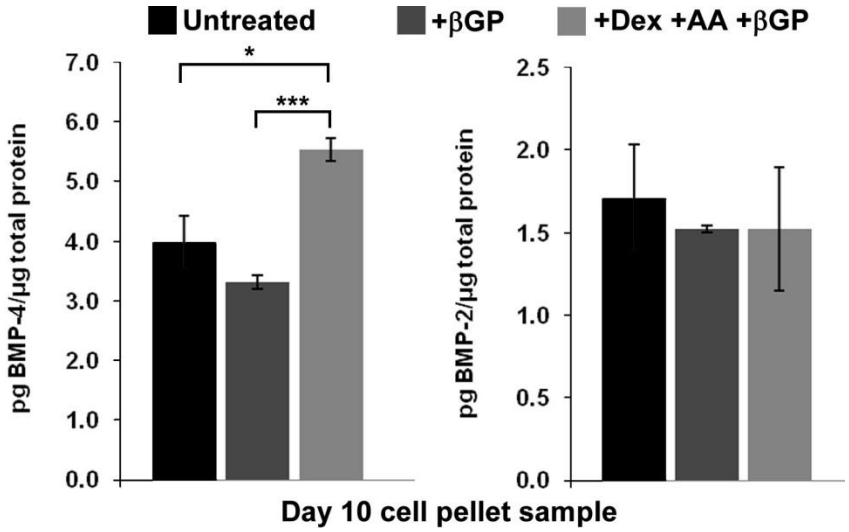

Figure 6.2. EB BMP production. BMP4 and BMP-2 produced by EBs undergoing osteogenic differentiation were quantified from EB cell pellets by ELISA. At day 10, EBs treated with a combination of dexamethasone (Dex), ascorbic acid (AA) and βGP produced equal amounts of BMP-2 and more BMP-4 than EBs treated with βGP alone ($p<0.005$) or left untreated ($p<0.05$). n=3 samples, ANOVA, Tukey's post-hoc test, ***$p<0.005$. *$p<0.05$ for marked comparison.

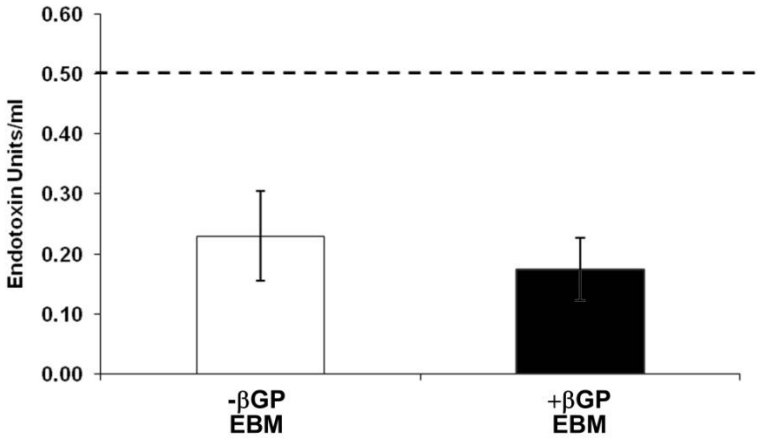

Figure 6.3. EBM endotoxin levels. EBM was evaluated for the presence of endotoxin by LAL assay. –βGP and +βGP EBM preparations were found to contain the same amount of endotoxin, which was below the FDA guideline level of 0.5 endotoxin units/ml. n=3 samples, ANOVA.

Validation of the nude mouse muscle-implantation assay

The DBM used in the study was osteoinductive (osteoinduction score = 2.75 ± 0.16), with an identical semi-quantitative score to that derived by previous studies using the same batch (Fig. 6.6 B). Heat inactivation resulted in a loss of this osteoinductivity (score = 1.13 ± 0.13), $p<0.005$ between inactive and active DBM). The quantitative histomorphometric measurements of osteoinduction (ossicle, marrow space, and new bone areas) were in agreement with the semi-quantitative score, demonstrating osteoinductivity by increases in each of these measures in response to active DBM compared to inactive DBM ($p<0.5$, Fig. 6.8). No evidence of pathological changes were present, such as infection of muscle wasting, with surrounding tissues normal and no signs of fibrosis in the sections. Additionally, the existing long bones had a normal histological appearance. These observations indicate that the model was valid and that the osteoinductive effects of EBM preparations could be assessed from the results.

Viable EB implantation

In a separate study, day 10 EBs, both with and without βGP treatment, were implanted in the same nude athymic mouse intramuscular ectopic osteoinduction model. By 21 - 28 days post-implantation, all mice receiving viable EBs were found to have masses in their hindlimbs of varying sizes and were sacrificed early (Fig. 6.4 A). When the limbs were excised and evaluated by H&E staining, cells of all three germ lineages (endoderm, mesoderm, ectoderm) were identified, suggesting teratoma formation.

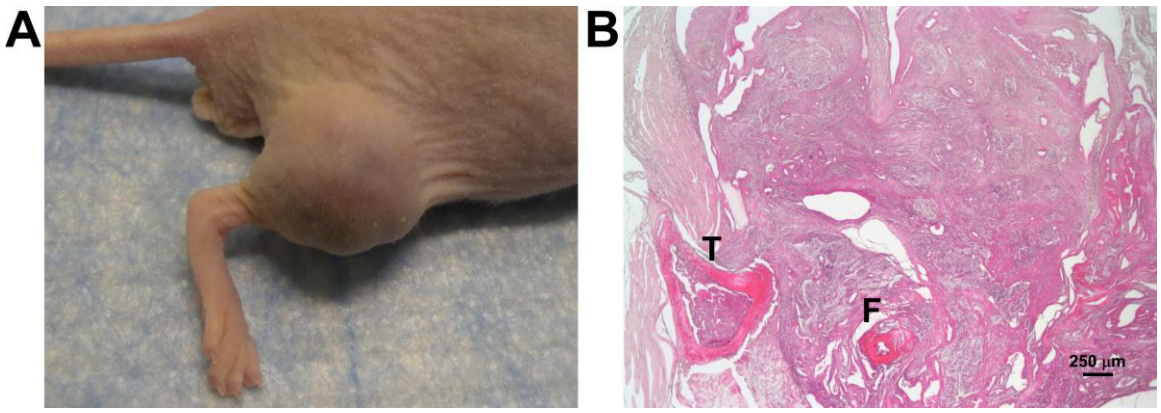

Figure 6.4. Viable EB Implantation. Viable day 10 EBs alone, with and without βGP treatment, were implanted in mouse hindlimbs. Large masses in the hindlimbs were formed by 28 days post-implantation (A), and when evaluated histologically, the masses were determined to be teratomas comprised of all cells from all three germ lineages (B). Tibia (T), Fibula (F), Scale bar in B = 250 µm.

In vivo osteoinductivity of EBM – mineralization analysis

35 days post implantation, mineralization associated with the DBM and EBM implant sites was detectable by X-ray (Figure 6.5 A, top panel). Multiple areas of mineralization were present throughout active DBM implanted samples. In contrast, fewer but more tightly localized areas of mineralization were observed in EBM implanted samples. 8 out of 8 limbs implanted with active DBM and 7 out of 8 limbs implanted with +βGP EBM exhibited mineralization that could be visualized by X-ray compared with 3 out of 8 limbs and 1 out of 8 limbs for -βGP EBM and inactive DBM, respectively. As expected, X-ray and µCT results matched one another, with the same limbs with mineralization detectable by X-ray exhibiting mineral detectable by µCT (>0.05% total limb volume, 0.10 mm^3) (Fig. 6.5 A, bottom). Comparing the average mineral volume for each group, including limbs with no mineralization, active DBM (3.59 ± 1.20 mm^3) and +βGP EBM (0.93 ± 0.47 mm^3) had increased amounts of

mineralization compared to inactive DBM alone (0.06 ± 0.04 mm^3, $p<0.005$, $p<0.05$). Additionally, active DBM had significantly more mineralization than –βGP EBM samples (0.41 ± 0.19 mm^3, $p<0.005$). Based on the combined mineralization analyses, +βGP EBM induced the formation of a larger volume of mineralized tissue than inactive DBM alone.

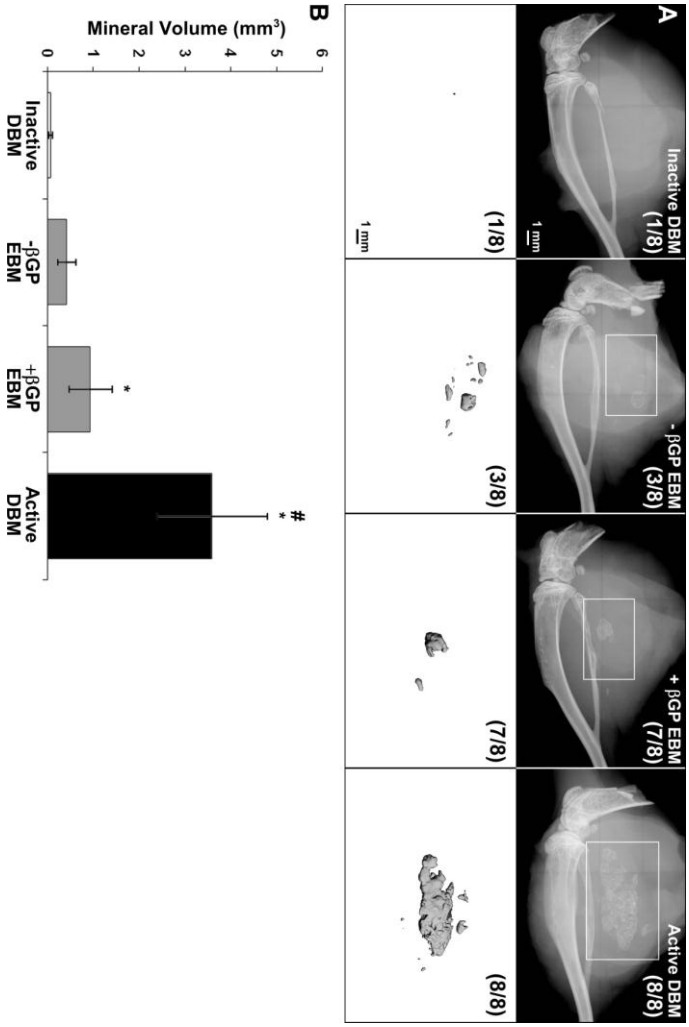

Figure 6.5. Evaluation of mineralization *in vivo*. DBM and EBM formulations were evaluated in a mouse intramuscular osteoinduction model. Mineralization associated with the material implant sites was visualized by X-ray predominantly in limbs treated with active DBM (8/8 limbs) and + βGP EBM (7/8 limbs) (# of limbs with mineralization detectable by x-ray/total number of limbs per group) (A, top). Mineralization was further visualized and quantified by μCT and was also found predominantly in active DBM (8/8 limbs) and + βGP EBM (7/8 limbs) (# of limbs with mineralization detectable by μCT (mineral volume > 0.05% of total limb volume (0.10 mm^3))/total number of limbs per group) (A, bottom). The total mineral volume per limb, quantified by μCT, was also found to be increased in active DBM and + βGP EBM implanted limbs (B). n=8 samples, Box-Cox transformation, ANOVA, Tukey's post-hoc test, *$p<0.05$ compared to inactive DBM alone, #$p<0.05$ compared to –βGP EBM.

In vivo osteoinductivity of EBM – histological assessments and new bone formation

Because mineralization can occur in the absence of new bone formation and new bone formation can occur in the absence of mineralization, further histological assessments were undertaken as the definitive determination of the osteoinductivity of these materials. H&E stained sections from each implant site were evaluated for the formation of ossicles, which are characterized by the presence of new bone formation, amalgamation of new bone with residual DBM at their interface, and associated new marrow space.(Fig. 6.6 A, Fig, 6.7 A). Sections evaluated from both EBM implanted groups were often found to have a single large ossicle per section, sometimes larger than the 0.78 mm^2 field of view at 10x, while sections from the active DBM group tended to have multiple smaller ossicles, located within a larger area of residual DBM (Fig. 6.6 A). Additionally, regions of mineralization in both EBM implanted sample groups corresponded directly with new bone formation as evaluated histologically. When sections were taken directly at the location of mineralization, determined by X-ray and μCT, ossicle formation was observed at that site in all EBM samples that contained mineralization. Conversely, the size and distribution of ossicles observed in the active DBM group did not always appear to match directly the mineral volume measurements. After localization of ossicles, the EBM implanted limbs were further examined for signs of the presence of residual EBM.

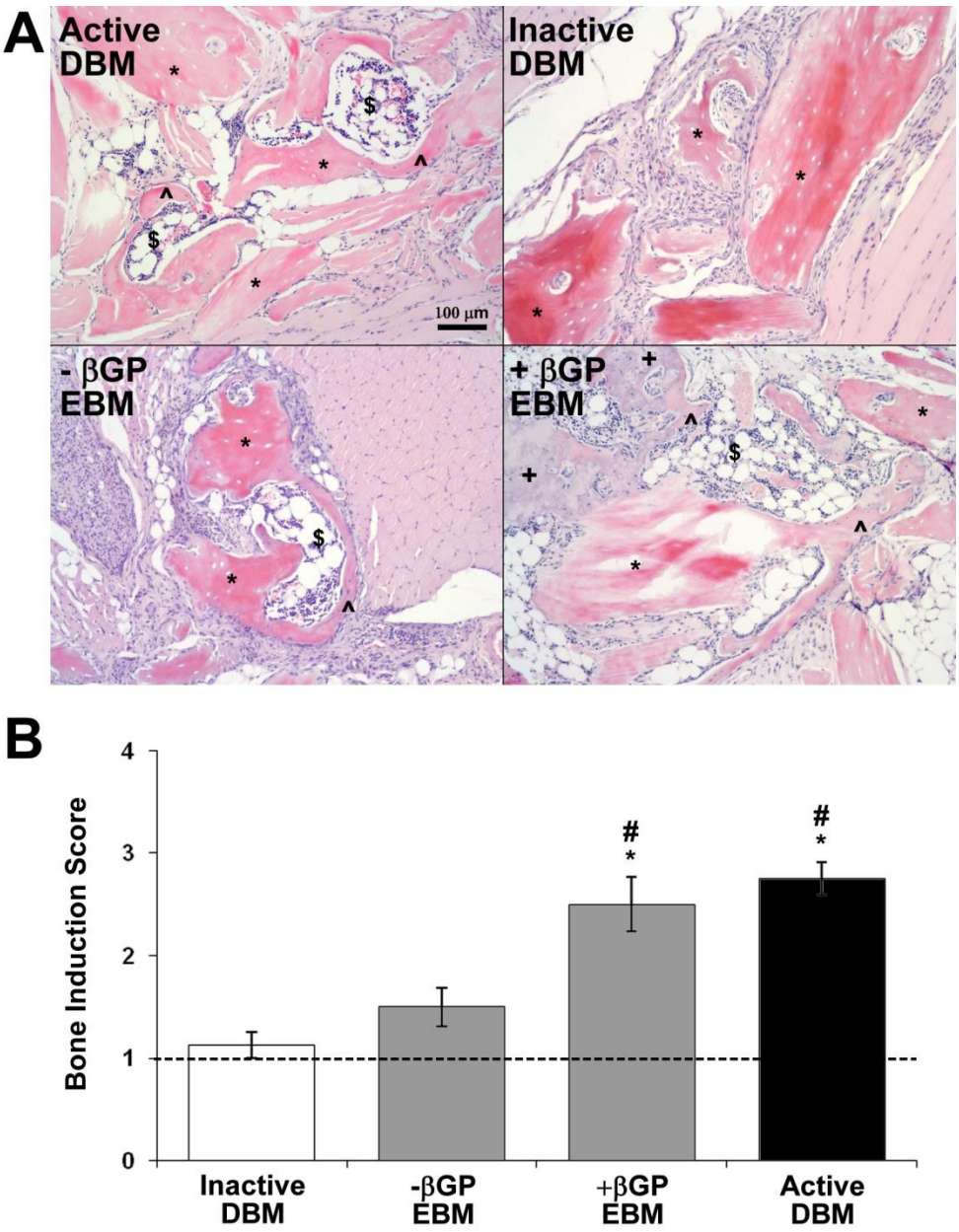

Figure 6.6. New bone induction and osteoinduction score. H&E stained sections obtained from DBM and EBM implanted limbs were evaluated and scored for the presence of ossicles and new bone formation, with the presence of residual DBM (*), new bone (^), and marrow space ($) identified in active DBM and both EBM implanted limbs. Residual EBM (+) was also noted in EBM implanted samples (A). Bone induction scores were based on a semi-quantitative assessment of ossicle formation in the H&E stained sections, with 1 representing an implant with no osteoinductivity (B). Active DBM and +βGP EBM were found to be osteoinductive (score >1.5, 95% confidence interval) and to have significantly higher scores than both Inactive DBM and –βGP EBM. ANOVA, Tukey's post-hoc test, *$p<0.05$ compared to inactive DBM alone, #$p<0.05$ compared to –βGP EBM.

Though the EBM was not labeled prior to implantation, areas within or immediately adjacent to some of the large ossicles observed in both EBM groups contained material not present in any of the active or inactive DBM samples, either in areas of DBM, associated with ossicles, or within any normal tissue throughout the rest of the tissue section (Fig. 6.7 A, top). The observed material was identified as EBM based on its observation in only EBM implanted limbs, its location within the implant site in relation to residual DBM and new bone formation, and its unique H&E staining pattern. The EBM was found to be amalgamated with the new bone, with new bone integrating along the EBM boundaries in direct apposition to the material, similar in appearance to what was observed at the interface of new bone with residual DBM. Some EBM was observed embedded within newly formed bone within the large ossicles and was further distinguished from new bone by its speckled staining pattern (Fig. 6.7 B, top). Based on previous studies of EB matrix composition and staining pre-implantation, including low collagen-I expression by EBs (see Chapters 4, 5) and lack of positive Aniline blue staining in pre-implantation EBM (Figure 6.1 A), EBM did not contain much collagen. Because new bone and residual DBM are rich in collagen, additional stains were undertaken to distinguish the EBM by this difference in collagen content. MMAB stain was used to identify collagen rich materials within the ossicle regions (Fig. 6.7 A, bottom). As expected, DBM (active and inactive) and new bone both stained blue by MMAB, demonstrating a composition rich in collagen. However, the distinct regions of EBM identified by H&E were largely devoid of collagen, further supporting the material's identification as residual EBM (Fig. 6.7 B, bottom).. Taken together, the combination of stains used demonstrated ossicle formation and the presence of residual

EBM in EBM implanted samples, along with the physical association of EBM with new bone formation. Based on the H&E stained sections, semi-quantitative measurements accounting for the number of limbs exhibiting ossicle formation and the number of ossicles formed were then undertaken to compare the osteoinductivity of each group.

Based on semi-quantitative osteoinduction score, +βGP EBM and active DBM induced new bone formation by 35 days post implantation, whereas inactive DBM did not (Fig. 6.6 B). The +βGP EBM group was osteoinductive (score = 2.50 ± 0.27), with a higher semi-quantitative osteoinduction score than both inactive DBM negative control ($p>0.005$) and -βGP EBM ($p<0.01$) and no difference in osteoinduction score compared to the active DBM positive control. Though -βGP EBM was not found to be osteoinductive (score = 1.50 ± 0.37, mean score ± 95% confidence interval), with no difference in its score compared to inactive DBM, large ossicles were also formed in 4 out of 8 -βGP EBM implanted limbs, including all three that demonstrated mineralization by x-ray and μCT analyses (Fig. 6.8 A).

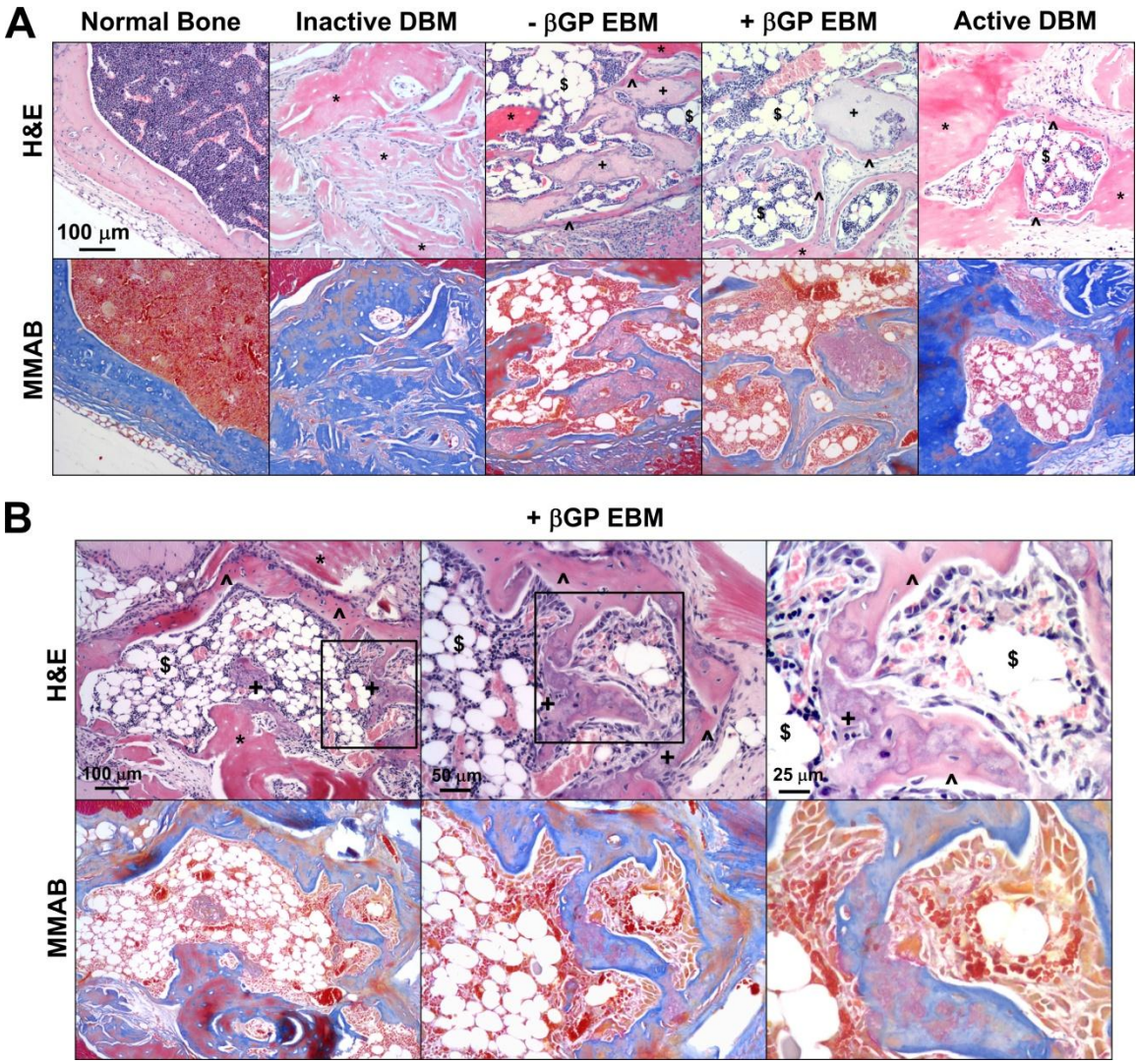

Figure 6.7. Presence of residual EBM. Representative H&E stained sections from each implant group were compared with adjacent sections stained by modified Mallory's Aniline Blue (MMAB) stain, which demonstrates collagen in blue (A). Higher magnification images from a +βGP EBM implanted limb revealed that residual EBM stained differently by both H&E and MMAB than both residual DBM and newly formed bone and that EBM was embedded within the newly formed bone in EBM implanted limbs (B). Residual DBM (*), new bone (^), and marrow space ($), residual EBM (+).

Quantitative measurement of new bone formation was increased in the +βGP EBM group compared to inactive DBM, with no difference compared to the active DBM positive control. All limbs that demonstrated mineralization by X-ray and μCT exhibited ossicle formation when evaluated histologically (Fig 6.8 A). Based on histomorphometry, measures of ossicle area, new bone, and marrow space area were increased with +βGP EBM implants compared to inactive DBM ($p<0.05$), similar to measures observed in the active DBM implanted limbs ($p<0.05$ between active and inactive DBM) (Fig. 6.8 B-C). No difference was found in any of these measures for either +βGP EBM or active DBM when compared to -βGP EBM implants. In summary, mineralization quantification, semi-quantitative osteoinduction scoring, and histomorphometric evaluations of new bone formation, including quantification of ossicle, marrow space, and new bone areas, all confirmed the finding that +βGP EBM was osteoinductive *in vivo*, at a level equal to that of the positive control, active DBM.

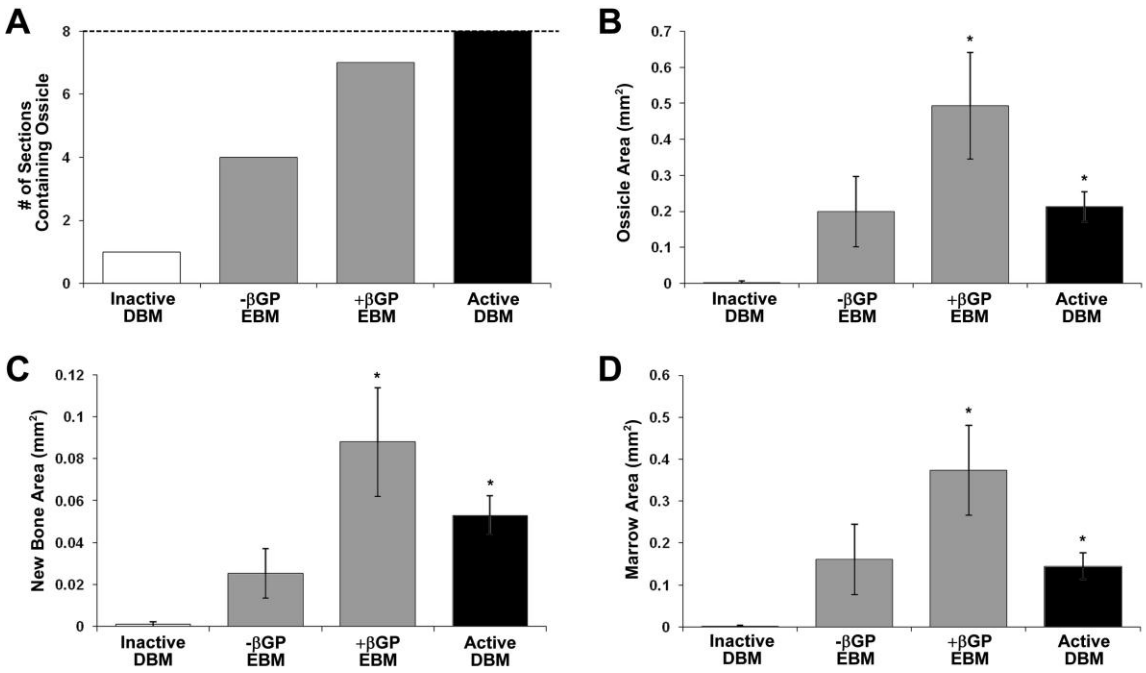

Figure 6.8. Quantitative histomorphometry. One H&E-stained section was evaluated per limb for osteoinduction scoring and histomorphometric measurements, for a total of 8 sections per group (dotted line, A). Total ossicle area (B), new bone area (C), and new marrow space area (D) were measured in all sections from each implant group. Ossicle, new bone, and marrow space areas were increased in +βGP EBM and active DBM implanted groups compared to inactive DBM. n=8 samples, Kruskal-Wallis non-parametric ANOVA, Tukey's post-hoc test, *$p<0.05$ compared to inactive DBM.

Discussion

The results of this study demonstrated osteoinductivity of EBM when implanted *in vivo*, which may have been attributed to retention of several osteoinductive growth factors, BMP-2, VEGF, and BMP-4, at levels similar to or well above those found in DBM. Due to the potential for teratoma formation associated with the implantation of viable EBs (Fig 6.4), acellular delivery growth factors produced by EBs, as in EBM, was the only safe method for transferring the osteoinductive potential harbored within the EB microenvironment to *in vivo* applications. The osteoinductivity of BMP-2 has been well characterized [22, 24]. VEGF has been found to be necessary for cartilage remodeling during endochondral ossification [27], the mechanism by which new bone was formed within the intramuscular model used in this study[26, 63]. One osteoinductive factor abundant in EBM but largely devoid in DBM was BMP-4. In addition to being directly osteoinductive [31], BMP-4 may have served to prime endogenous, host cell populations that are responsive to osteoinduction. BMP-4 treatment promoted osteogenic differentiation of MSCs expanded *ex vivo* under low serum conditions, which then formed bone when implanted *in vivo* [231], and low doses of BMP-4 increased the survival and stemness of adipose derived stem cells, *in vitro* [232]. Lastly, these factors may have acted in a synergistic manner. Delivery of condensed DNA plasmids for BMP-4, VEGF, and bone marrow stromal cells synergistically increased bone formation *in vivo* compared to delivery of any single component or any combination of two [233].

The amounts of BMP-2 and VEGF extracted from EBM in this study were similar on a per mass basis to those described in DBM, while an order of magnitude higher amount of BMP-4 was present in EBM than has been reported to be in DBM. Previous

studies have found variable amounts of each of these growth factors within DBM, varying both manufacturer to manufacturer and batch to batch [25, 52]. Levels of BMP-2 have been measured from 2 – 120 pg/mg DBM [25, 52, 59, 234], while BMP-4 has ranged from completely undetectable to at most 8 pg/mg DBM depending on the study [25, 51, 59, 61, 234]. In this study, different EBM preparations were found to contain extractable BMP-2 levels ranging 13 – 48 pg/mg EBM and BMP-4 levels ranging 77 – 166 pg/mg EBM, depending on day of isolation and osteogenic differentiation (Fig. 6.1 B). The EBM implanted *in vivo* in this study (day 10) contained 20 times more BMP-4 than the highest reported amount in DBM [61]. VEGF has been reported to vary from 0.04-0.39 pg/μg total protein between three different manufacturer formulations of DBM [51],which were similar to levels measured in EBs within this study (0.03-0.05 pg/μg total protein in EBM) (Fig. 6.1 B). The amount of growth factor extracted from DBM has varied with extraction method employed, accounting for the underestimation of these growth factors from DBM within this study, which used a mild detergent and salt solution, TPER. Based on ELISA results for growth factors extracted from EBM, these three osteoinductive factors were all present in EBM, regardless of day of isolation or osteogenic differentiation with βGP, motivating evaluation of EBM osteoinductive potential.

When evaluated *in vivo*, +βGP EBM was osteoinductive with respect to mineralization, osteoinduction score, and histomorphometric measurements of new bone formation. +βGP EBM also performed the same as active DBM by the same measurements, but some differences were noted in the distribution and localization of mineralization observed and new bone formed. In all groups, limbs demonstrating

mineralized tissue by X-ray and μCT also exhibited ossicle formation (Fig. 6.5 A, 6.8). However, regions of mineralization were present in active DBM samples that did not directly correspond to ossicle formation by histological assessments. Re-mineralization of DBM may occur in the absence of new bone formation under physiological conditions [235, 236]. In +βGP EBM samples, new bone tended to form as one large ossicle compared to multiple smaller ossicles found in the active DBM group. Though the total marrow area per section was not increased, isolated, larger ossicles in EBM implanted limbs were also associated with more new marrow space per each individual ossicle. The development of marrow space to support the newly formed bone is important for its maintenance, as it provides a pool of mesenchymal and osteoprogenitor cells for continued remodeling of the bone, but the establishment of marrow is also dependent upon the formation of new bone first [237, 238]}.

Examination of similarities and differences between DBM and EBM that may favor new bone formation in response to one material or the other may reveal clues to differential mechanisms of osteoinduction. Favoring osteoinductivity of EBM, EBM contained more BMP-4 than does DBM, as mentioned above. BMP-4 has been found to be interchangeable during osteogenesis *in vivo* with BMP-2 [32], the primary osteoinductive factor contained within DBM [22]. Aniline blue staining both pre- and post-implantation also demonstrated that DBM was rich in collagen whereas EBM was devoid of it. The observed lack of collagen within the EBM was consistent with previous studies demonstrating low levels of *collagen-I* gene expression, regardless of osteogenic differentiation, along with little to no apparent collagen at the protein level (see Chapters 4, 5). The lack of a dense collagenous matrix in EBM may have facilitated vascular in

growth, migration of osteoprogenitor cells into the material, and easier remodeling. This potential difference in remodeling may explain formation of single, large ossicle in EBM samples instead of multiple smaller ossicles in the active DBM group, where residual DBM took longer to be remodeled and resorbed [63, 237]. Additionally, the less compacted EBM may have allowed for greater bioavailability of contained growth factors, which was supported by the ease of growth factor extraction in TPER, a mild detergent and salt solution, from EBM compared to DBM in this study. Complete protein extractions from DBM have been typically achieved under harsher conditions, such as digestion by collagenase [61] or solubilization in guanidine HCl [51].

Conversely, the dearth of collagen may be viewed as disfavoring osteoinduction by EBM. Interactions between osteoblasts and the collagen-rich bone matrix surrounding them are known to be important in bone development and remodeling. Osteoblast adhesion to collagen-I fibrils promotes osteoblastic differentiation and is mediated via $\alpha 2\beta 1$ integrin binding of collagen [9, 10, 239]. In this study, this difference was circumvented by delivery of EBM with inactive DBM, potentially providing a template for remodeling and allowing osteoblast binding to occur around the EBM without directly altering the EBM composition itself. Delivery of EBM with inactive DBM not only eliminated this potential limitation of EBM but also facilitated its localization. Preliminary studies delivering EBM alone, without inactive DBM, showed mineralization by X-ray, suggestive of osteoinductivity, but were hindered by difficulty in localizing the smaller implant site and lack of previous data on how EBM may have been remodeled after 5 weeks *in vivo*. Future studies may eliminate the need for inactive DBM as a source of collagen by delivery of EBM within a collagen sponge.

–βGP EBM was not found to be osteoinductive or to have increased bone formation when compared to inactive EBM but was also not significantly decreased compared to +βGP EBM. Additionally, in isolated –βGP samples that exhibited new ossicle formation histologically (4 of 8 limbs), histomorphometric measurements of new bone formed were still similar to those obtained for +βGP samples, just observed in fewer limbs. Both –βGP and +βGP EBM were found to have the same content of the three growth factors assayed, so it would be expected that each would have similar osteoinductivity; however, the results indicated that growth factor content alone was not the sole determinant of osteoinductivity. Some ossicles were formed in response to – βGP EBM, with residual EBM visible and associated with new bone, suggesting the growth factors that remained present were still capable of inducing bone formation. This observation may suggest that the osteoinductive growth factors were not being retained at the implant site in –βGP EBM.

The potential difference in growth factor retention may have been accounted for by differences in mineral composition between –βGP and +βGP EBM. Prior to EBM isolation at day 10, calcium phosphate containing mineralization was present within EBs after βGP treatment (see Chapters 4, 5). The mineralization, generated within EB *in vitro*, may have increased osteogenesis in response to implanted EBM by binding and retaining growth factors, particularly BMPs, which had been produced within EBs during osteogenic differentiation. Studies in both osteoblasts and vascular smooth muscle cells have demonstrated osteogenic differentiation in response to exogenously administered calcium phosphate precipitates via extracellular-signal regulated kinase (ERK 1/2) pathway activation [131, 132], the same pathway suggested to mediate phosphate

treatment-induced osteogenic differentiation in EBs (see Chapter 5). The phenomenon of calcium phosphate osteoinduction, *in vitro,* was likely dependent upon protein interactions at the surface of formed calcium phosphate within the microenvironment of osteogenic EBs [214] and not due to intrinsic osteoinductive properties of calcium phosphate materials in general. Calcium phosphate microparticles have also been proposed for the delivery of BMPs because of their protein binding ability [213], and so calcium phosphate deposits formed *in vitro* within EBs may have prolonged the retention of BMPs when +βGP EBM was implanted, *in vivo*.

Though the exact mechanism of calcium phosphate osteoinductivity observed *in vitro* remains to be elucidated, surface characteristics and how they modulate osteoinductive protein production, entrapment, and binding appear to be important. In a series of *in vivo* intramuscular studies of calcium phosphate-containing materials in goats, surface geometry was found to alter the dissolution and re-precipitation of calcium phosphate and entrapment of organic material, including growth factors such as BMPs, which in turn was hypothesized to lead to observed changes in osteoinduction [208, 209]. In another study of osteoinduction by calcium phosphate-containing materials, materials with specific surface topography that may have entrapped osteoinductive factors induced bone formation, *in vivo* [214]. Additionally, osteoblastic differentiation of MSCs and MG63 osteosarcoma cells on titanium surfaces has been found to be modulated in response to surface, micron-scale roughness [215, 216]. One final explanation for the difference in EBM osteoinductivities could be differential expression of other growth factors, inhibitors, or osteogenic matrix molecules that might be present but were not

tested for. For example, BMP-7 is also known to be osteoinductive in isolation and is used clinically to induce bone formation [Stryker Biotech, Hopkinton, MA].

Though the most likely candidates and mechanisms have been discussed, further studies and characterization may elucidate the mechanism by which EBM osteoinductivity occurs. Additional work is also required to optimize EBM formulation to maximize osteoinductivity, including day of differentiation, dosing, and osteogenic differentiation supplements used. BMP-2 content and calcium phosphate mineralization are increased at day 14 of differentiation with βGP treatment though BMP-4 is reduced. Though only one dosage of EBM was investigated in this study, half of the mass dose used for the DBM positive control, EBM still performed as well as active DBM by all metrics assessed, suggesting a higher per mass potency of EBM, promoting equal, perhaps more sustainable new bone formation, based on the associated marrow space formed [238]. The difference in potency may be explained by differences in matrix composition, as DBM is comprised primarily of collagen, which is lacking in EBM. Equivalent dosing of EBM and DBM will allow for more direct comparisons of material potency and osteoinductivity. Additionally, in this study, only βGP was used to promote osteogenic differentiation of EBs, so the investigation of EBM derived from ESCs differentiated with other osteogenic supplements, such as dexamethasone, may be explored. It may, however, be preferable to have a more, immature, embryonic-like matrix. MSC-derived osteogenic matrix that was found to be osteoinductive *in vitro* failed to demonstrate osteoinductivity when evaluated *in vivo* [65, 78]. These results also raise the possibility of deriving EBM from ESCs directed to differentiate towards other cell lineages to yield tissue specific, regenerative materials for other applications.

Conclusions

In this study, ESC-derived material harbored bioactive, osteoinductive factors (BMP-2, BMP-4, VEGF) and was osteoinductive when evaluated *in vivo* by a nude athymic mouse intramuscular osteoinduction model. Additionally, osteoinductivity was enhanced in EBM derived from cells undergoing osteogenic differentiation. EBM osteoinductivity, measured by amount of mineralization induced, semi-quantitative osteoinduction score, and quantitative histomorphometry, was found to be at a level equal to that of DBM, a commercially available and widely used osteoinductive material, and interestingly, the same osteoinductivity was observed even though half the mass of EBM was delivered as active DBM, suggesting a higher potency of EBM, which may be attributed to its higher per mass BMP-4 content. The use of EBM presents the possibility of removing donor to donor and batch to batch variability that confounds the utility of cadaveric sourced DBM, while also suggesting the derivation of a myriad of other tissue specific, ESC-derived materials.

CHAPTER 7

FUTURE CONSIDERATIONS

In this work, the osteogenic differentiation of mouse embryonic stem cells (ESCs) was investigated in response to phosphate treatment, and the mechanism by which phosphate induced osteogenic differentiation was examined. Subsequently, the osteoinductive embryoid body (EB) microenvironment induced by phosphate treatment was harnessed as an acellular material and evaluated for its *in vivo* osteoinductivity. Osteogenic differentiation was enhanced with phosphate treatment at the gene, protein, and functional levels and was accompanied by changes in expression and responsiveness of two $1\alpha,25(OH)_2D_3$ receptors. Mineral deposits formed within EBs in response to phosphate treatment were characterized to be calcium phosphate (CaP) precipitates, and the presence of CaP precipitates within the EB microenvironment was associated with enhanced osteogenic differentiation via activation of ERK 1/2 signaling. Finally, the microenvironment within EBs undergoing osteogenic differentiation, promoted by phosphate treatment, was captured as devitalized EB material (EBM) and was found to be osteoinductive *in vivo*, inducing new bone formation at a level equal to that of a commercially available and clinically utilized acellular, osteoinductive biomaterial, demineralized bone matrix (DBM).

Previous studies in more committed cell types, including osteoblasts [116], chondrocytes [121, 122], dental pulp cells [133], and vascular smooth muscle cells[134], have found phosphate treatment to regulate processes of growth and differentiation in mineralizing cell types. Additionally, both osteoblasts and undifferentiated ESCs have

high levels of alkaline phosphatase expression and activity, such that alkaline phosphatase has been used as a marker to identify both cell types from other cell populations. The commonality of high alkaline phosphatase activity suggested that the handling of phosphate was important to vital functions or characteristics of both ESCs and osteogenic cell types. Based on these findings, the first goal was to investigate if phosphate induced signaling and osteogenic differentiation, an effect previously found to be mediated through ERK 1/2 activation, was conserved in ESCs differentiated as EBs (Chapter 4). Methods typically used for directed osteogenic differentiation of ESCs have included a cocktail of factors including either $1\alpha,25(OH)_2D_3$ [105] or dexamethasone along with ascorbic acid and βGP [103, 106]. However, as the aim of this study was to investigate phosphate induced differentiation and not necessarily to isolate a purified population of osteogenic cells, βGP treatment alone was used to promote osteogenic differentiation. Another major difference between the current study and those previously reported in the literature was that, here, ESCs were maintained as EBs for the entire duration of differentiation. Typical methods of directed osteogenic differentiation have involved either plating of cells at day 5 after EB formation [103, 105] or maintaining ESCs in monolayer culture throughout the differentiation time course [240]. EB differentiation promotes mesoderm differentiation [184], a prerequisite for responsiveness to osteoinductive stimuli [105, 241], so future studies may seek to investigate the effects of phosphate upon cells grown from plated EBs as the formation of CaP precipitates may be altered in monolayer culture compared to the three dimensional environment within EBs. It also remains to be determined whether phosphate treatment alone can induce osteogenic differentiation of human ESCs as well since the transfer of

differentiation protocols from mouse to human cells has proven more challenging due to species differences. Further understanding of the biology of osteogenic responses to phosphate treatment in ESCs has broader impacts not only in the field of tissue engineering, where the use and control of osteogenic cell types is desired in the development of bone regenerative therapies, but also mineralization occurring within pathologic settings, such as vascular smooth muscle and valvular calcification, where cells may sense and respond to phosphate treatment through the same conserved mechanisms investigated in the current study.

Additionally, the osteogenic differentiation study identified that the osteogenic differentiation of EBs induced by phosphate treatment was accompanied by changes in the expression and responsiveness of two $1\alpha,25(OH)_2D_3$ receptors, Pdia3 and VDR (Chapter 4). The presence and differential regulation of these two receptors during EB differentiation indicated an important role of $1\alpha,25(OH)_2D_3$ signaling in bone differentiation and development in general. Each receptor's exact function during the early stages of development modeled by EB culture may be further investigated. For example, though Pdia3 -/- knockout is embryonically lethal by day E10.5 [190], ESCs may be derived from knockout mice, allowing for further examination of the receptor's role in early development using the EB differentiation model to determine at what stage during development $1\alpha,25(OH)_2D_3$ activation of PDIA3 is necessary for osteogenic differentiation and other important developmental processes.

The effects of phosphate treatment on osteogenic differentiation were attributed directly to the formation of CaP precipitates within EBs based on studies that CaP precipitates, independent of phosphate concentration and either administered

exogenously or formed endogenously under conditions promoting CaP precipitation, could induce the effects previously thought to be due to phosphate transport into cells [130-132]. The mechanism by which these precipitates might be sensed by cells is not clear but likely dependent upon how the precipitates are modified within the cellular microenvironment, including remodeling by cells and interactions with matrix proteins and growth factors. Osteogenic cell-modified surfaces may then in turn promote further osteogenic differentiation of neighboring cells [214]. Additional material characterization of the CaP precipitates formed within EBs, particularly in isolation instead of within a mixture of cellular material, would provide further information about their structure, composition, and protein binding. Also, because of the the exact mechanism of PFA inhibition of differentiation remains unclear, for future studies, CaP formation could be blocked with other agents known to inhibit crystal formation, including pyrophosphate [130] or phosphocitrate [132]; however, though such agents may not have the same potential effect on phosphate transport as PFA, they can have other effects on cell phenotype [47]. Studies of the direct administration of CaP precipitates in pre-osteoblast and vascular smooth muscle cells motivates the evaluation of ERK signaling and osteogenic differentiation in response to the direct administration of exogenously formed CaP to EBs. Such a study would also aid in discrimination between the effects of the increased Pi compared to those of the CaP deposits themselves and is currently being investigated in ESCs by our lab, using hydroxyapatite microparticles [213]. However this approach requires incorporation the CaP from the time of EB formation, whereas for the current study βGP treatment was initiated at day 5. As discussed above, ESCs must undergo initial mesodermal differentiation before they are responsive to osteogenic

differentiation cues, which does not occur until approximately day 5 within EBs [184]. As a result, the difference in the onset of treatment motivates the investigation of the incorporation of CaP particles in mesenchymal stem cell (MSC) spheroids as well. More differentiated MSCs already have an increased propensity for osteogenic differentiation than less differentiated ESCs, so MSCs may begin in a state more responsive to differentiation cues induced by the CaP particles than ESCs.

Whether phosphate induced differentiation is mediated through Pi uptake by cells, the simple presence of CaP in the microenvironment, or some combination of the two, it is clear from this work that ERK 1/2 signaling is activated as a result (Chapter 4, 5); however further elucidation of the cues or factors directly activating ERK signaling is required to understand the biological importance of phosphate or CaP sensing by cells undergoing osteogenic differentiation. The mechanism and pathways by which phosphate treatment induces ERK signaling, and therefore osteogenic differentiation, is still not completely understood, even in more committed cell types. ERK signaling is a common pathway activated by many cues and signals, so multiple mechanisms of activation may be responsible for its induction by phosphate. In this study, BMPs were found to be enriched within the EB microenvironment and suggested to participate in the observed osteogenic differentiation. In addition to Smad pathway induced effects of BMPs on osteogenic differentiation [8, 26], BMP induced osteoblast differentiation is known to require non-Smad pathway signaling as well, including activation of ERK 1/2. BMP-2 activates ERK signaling in mesenchymal progenitor [135] and C2C12 cells [125], and this BMP induced activation leads to both Runx-2 [127] and osterix transcriptional activity[136]. Additionally, $1\alpha,25(OH)_2D_3$ binding of PDIA3 also stimulates a rapid ERK

activation [126], so potential interaction of CaP precipitate and $1\alpha,25(OH)_2D_3$ signals may also exist. It is likely that a combination of this myriad of signals is having a synergistic effect by converging at ERK activation, therefore inducing osteogenic differentiation.

Given recent setbacks in the translation of ESC based cell therapies to clinical use, the further development of acellular approaches to harness the regenerative potential of ESCs are more attractive than ever. After establishing that CaP precipitates created an *in vitro* osteoinductive microenvironment within EBs, we demonstrated the ability to harness the osteoinductive potential of these EBs by implantation *in vivo*, suggesting promising future clinical applicability of this or similar approaches (Chapter 6). The *in vivo* osteoinduction and *in vitro* differentiation are likely to share common mechanisms, as the *in vivo* studies evaluated factors all also present *in vitro*. Consequently, the same questions remain regarding how the presence of CaP in EBs enhances the osteoinductive microenvironment, so further elucidation of the mechanism by which EBM induces the formation of new bone is required. Since EBM is a mixture of devitalized cells and ECM, it is not clear whether the growth factors were originally associated with the matrix or sequestered within the cells and only liberated upon devitalization of the cells. However, difference in growth factor location also cannot be distinguished from the measurements of growth factor content within cell pellets. The presence of inhibitors of osteogenic differentiation within –βGP EBM may explain why –βGP EBM, while containing equivalent amounts of growth factors, was not found to be osteoinductive. Since BMPs are thought to be the factors responsible for the osteoinduction, the evaluation of potential inhibitory factors, such as Noggin, is also needed. In addition to its enrichment in growth

factor content, EBM may have had unique matrix and material properties that lead to its osteoinductivity. It was suggested by the reduced collagen content and the larger ossicle formation that EBM was more easily remodeled than DBM. Further evaluation for the presence of osteoclast remodeling of the EBM may clarify this possibility. Additionally, given the formation of larger marrow spaces with EBM implantation, the enhancement of factors promoting establishment of the bone marrow niche, such as stromal derived factor-1 (SDF-1/CXCL12), are also of interest for further investigation [242]. SDF-1 is a potent hematopoetic stem cell (HSC) chemoattractant that promotes homing and engraftment, and it has been demonstrated to be produced at low levels by mouse ESCs that increased with EB differentiation [243]. SDF-1 not only stimulates HSC transmigration from circulation into extravascular bone marrow space but also promotes HSC survival. However, its production may simply be a consequence of increased bone formation, as seen in response to EBM, as bone formation is important for marrow regeneration [237, 238], and it is produced by a variety of cells associated with bone, including endosteal osteoblasts and endothelial cells. However if SDF-1 is actually enriched within EBM itself, potential therapies to enhance bone marrow engraftment after transplantation could be a possibility through adjunct delivery of EBM.

Optimization of the derivation, preparation, and delivery of EBM or related ESC-derived factors may also be investigated. Only one osteogenic differentiation condition and one time point were evaluated in the present study. Preparations derived at different days would capture earlier more embryonic-like states and later more committed ones. Additionally, EBM derived under different osteogenic differentiation methods, including culture with $1\alpha,25(OH)_2D_3$ [105], dexamethasone, and ascorbic acid [103], could be used

to evaluate whether material from a more homogeneously differentiated population is preferable or if the presence of factors produced by multiple types of cells present within EBs is needed. Multiple cell types participate in the formation of bone *in vivo* with the signals directing its formation arising not just from the osteoblasts themselves but also from other cells, including endothelial cells and chondrocytes [3]. Consequently, the more embryonic, less differentiated state of EBs and their ability to generate cues to direct the formation of all different types of cells is what makes them a novel and attractive material source. Additionally, the osteoinductity of extracellular matrices from more differentiated and more homogeneous cell populations have already been investigated, using osteogenically differentiated MSCs. Though those studies demonstrated osteoinductivity *in vitro* [78], the MSC generated matrix was not osteoinductive when evaluated *in vivo* [65], likely because osteoinductive cues harbored within the matrix were masked by mineralization produced by the more mature and differentiated osteogenic cell type. Thus, the heterogeneity of EB differentiation and the more embryonic-like environment it recapitulates are its advantages when compared to acellular therapies derived from more differentiated cells or tissues.

The optimal dosage of EBM delivered and ratio of EBM to inactive DBM, including delivery of EBM alone, should be further explored in future studies. An equal mixture of active and inactive DBM (7.5 mg and 7.5 mg) would provide a more fair comparison than the positive control of active DBM alone (15 mg) used in this study as such a formulation would contain an equivalent mass of "active" material as implanted in the EBM samples (7.5 mg). Two preliminary studies were initially performed delivering lower mass doses of EBM (~2.5 mg) and without inactive DBM vehicle, and these

studies did demonstrate signs of mineralization with EBM implantation by x-ray in both studies and μCT in one, though substantially less than in the current study, however technical difficulties with histology limited the ability to draw conclusions about new bone formation in both. Based on mineralization analyses alone, these observations suggest that the investigation of lower doses (< 5mg) would yield decreased new bone formation. Higher doses of EBM are needed for more direct comparisons with DBM at the dose used for the positive control (15 mg). Varying the amount of inactive DBM used as a vehicle would also provide insights into the balance between growth factor and extracellular matrix binding-induced signaling required for osteogenic differentiation [74, 244]. In addition to facilitating location of the implant site histologically, inactive DBM provides a collagenous matrix absent in EBM, which itself is an important part of osteogenic differentiation. Integrin mediated binding of collagen-I has been shown to regulate early osteoblast differentiation and control the expression of key genes in osteoblastogenesis [9, 10]. Therefore, it is expected that some inactive DBM is required in order for the osteoinductive effects of EBM to be seen. As an alternative to inactive DBM, EBM could be delivered within a synthetic scaffold, eliminating the need for the use of any allograft tissue altogether.

The isolation of factors from or produced by differentiating osteogenic EBs in a soluble form may be an attractive alternative therapeutic approach to the delivery of EBM, as injectable therapies are minimally invasive. Extraction of proteins, particularly growth factors, may be prepared from tissues or acellular materials, such as EBM. The extraction in Tissue Protein Extraction Reagent (TPER) used to quantify growth factor content in this study demonstrated that growth factors were more readily extractable from

EBM than DBM, without collagenase digestion or harsh ionic agents that may disrupt growth factor bioactivity. The ease of growth factor extraction from EBM suggested that growth factors were less tightly sequestered within the ECM present in EBM than growth factors in DBM, thus increasing bioavailability of osteoinductive factors in EBM. Also, conditioned media from differentiating EBs may be directly injected. However, the caveat for both of these aforementioned approaches to deliver factors in a soluble form is the short half life of growth factors *in vivo* as they may easily diffuse away from the site of injection. To overcome this limitation, biomaterials may be used to bind these bioactive factors. The capture and delivery of ESC secreted factors using a self assembled nanofiber gel has been reported for *in vivo* applications [245], and such a technique could be used to harness EB derived conditioned media or extractions. Such injectable or engineered delivery approaches may lose any beneficial effects of the delivery of the natural extracellular matrix itself, which can bind and stabilize growth factors, prolonging half life, or provide patterning required for processes such as mineralization [74, 212]. In the case of osteogenic EBM in particular, the novel osteoinductive effect may be lost by such methods since the CaP precipitates themselves may be playing a role in stabilizing the BMPs within EBs.

Though viable EBs undergoing osteogenic differentiation may be implanted for therapeutic purposes, for several reasons, the characteristics of EBM make it more attractive for translation to clinical practice. Viable cells may be advantageous for some applications because they can directly participate in osteogenesis themselves, in cases where host cells may have a reduced capacity to respond to osteoinductive cues, as is known to occur with aging. However, such a therapy necessitates preparation

immediately at the time of implantation to maintain cell viability, losing the handling and storage advantages of novel acellular materials, such as EBM, that allow them to be prepared in advance. In addition, when using an ESC source, the danger always remains that if even a small population of undifferentiated cells persists, teratoma formation is possible, as was observed in preliminary EBM studies that also investigated implanting viable day 10 EBs. Thus, to reap the therapeutic benefits of the regenerative, embryonic-like microenvironment created by ESCs, development of an acellular therapy derived from ESCs, such as EBM, is the safest approach.

The novel findings here of EBM osteoinductivity motivate the further evaluation of EBM for use in bone tissue engineering and other regenerative applications. Materials for bone tissue engineering, such as DBM, have been evaluated for their ability to heal critical sized defects in bones that do not have the ability to close on their own [246]. Therefore, the delivery of osteogenic EB-derived EBM, by itself, with DBM, or embedded within a synthetic scaffold, could be evaluated for its ability to promote closure of critical sized defects. EBM has also been evaluated in our lab for its ability to promote dermal wound healing and angiogenesis. Both of these studies, however, used spontaneously differentiating EBs as the cell source for EBM. The current study represents the first use of EBM for a tissue specific application by material derivation from ESCs undergoing directed differentiation towards the cell type of that tissue. The directed differentiation of ESCs to endothelial cell phenotypes by pre-conditioning with fluid shear has been recently demonstrated by our lab, with upregulation of VEGF production enhanced when EBs formed from pre-conditioned ESCs were further cultured under low oxygen conditions. This increase in endothelial cell and VEGF production

could be exploited to yield EBM that may exhibit increased angiogenic potency, which in concert with βGP treatment, may yield even greater osteoinductive potential than seen in the current study, due to potential enrichment and capture of BMPs and VEGF. This approach to increase angiogenic potential could also be used in the absence of βGP treatment, to yield VEGF enriched EBM for delivery to other tissues requiring angiogenesis, such as ischemic myocardium. However, due to the observation of ossicle formation in isolated -βGP EBM implanted samples, one caveat is the potential for ectopic bone formation with the use of EBM for non-bone inductive applications, due to its high BMP content. The intramuscular implantation site used to evaluate osteoinductivity in this study is an ectopic bone formation site, one where bone does not normally form on its own. Similarly, any other implantation site for other applications in the body where EBM may be used could serve as an ectopic bone formation site as well, other than within bone itself. However, integrin mediated interactions with the collagen-I matrix, in combination with the osteoinductive factors present, are known play an important role osteogenic differentiation [9, 10] and would be absent when EBM is not delivered with inactive DBM. Additionally, untreated EB-derived EBM would also not contain the CaP precipitates proposed to have locally collected and enriched BMP content during EB differentiation.

The derivation of similar materials from human cell sources, including induced pluripotent stem cells, would eliminate the potential for cross species immunological interactions which may hinder the translation of the currently evaluated, mouse-derived EBM to clinical application. However, xenografts and xeno-derived acellular materials are already in use clinically, and after devitalization, xeno-derived acellular therapies

have improved safety and efficacy compared to xenografts [247, 248]. In comparison with DBM and other cadaveric sourced tissues, the further development of cell-derived biomaterials motivated by the current studies of EBM may one day reduce or even eliminate the need for donor allograft tissue, an end goal long promised by tissue engineering and regenerative medicine strategies, while providing the added benefit of also removing donor variability that may limit current therapy. Given a growing shortage organ and tissue donors, this potential advantage, as demonstrated in this study by EBM, is particularly exciting and brings that promise one step closer to fruition.

In conclusion, this work has demonstrated that the biological effects of phosphate treatment reported in a variety of other cell types are conserved in ESCs, and therefore potentially important in the further understanding of bone development. Furthermore it expands upon previous work established within our lab, developed to deliver the therapeutic benefits of stem cells in a cell free form, by demonstrating that the osteoinductive environment of differentiating ESCs may be harnessed as an acellular, osteoinductive biomaterial. This exciting finding demonstrates that through directed differentiation a tissue specific biomaterial can be derived that stimulates directed *in vivo* tissue response and formation, capturing the regenerative potential of ESCs and opening the door for the further development of ESC-derived materials for other applications. Future work will continue to elucidate the mechanisms of these effects, allowing for refinement of this novel approach and the development of other tissue specific therapies for regenerative medicine.

REFERENCES

1. Doll, B., et al., Evidence for a cellular and molecular decline in bone healing with age. Operative Techniques in Orthopaedics, 2002. **12**(2): p. 72-77.

2. Schwartz, Z., et al., Ability of commercial demineralized freeze-dried bone allograft to induce new bone formation is dependent on donor age but not gender. J Periodontol, 1998. **69**(4): p. 470-8.

3. Olsen, B.R., A.M. Reginato, and W. Wang, Bone development. Annu Rev Cell Dev Biol, 2000. **16**: p. 191-220.

4. Cowles, E., et al., Mineralization and the expression of matrix proteins during in vivo bone development. Calcif Tissue Int, 1998. **62**(1): p. 74-82.

5. Dai, J. and A. Rabie, VEGF: an essential mediator of both angiogenesis and endochondral ossification. Journal of dental research, 2007. **86**(10): p. 937.

6. Gerstenfeld, L., et al., Collagen expression, ultrastructural assembly, and mineralization in cultures of chicken embryo osteoblasts. J Cell Biol, 1988. **106**(3): p. 979-989.

7. Carvalho, R., et al., Selective adhesion of osteoblastic cells to different integrin ligands induces osteopontin gene expression. Matrix Biology, 2003. **22**(3): p. 241-249.

8. Suzawa, M., et al., Stimulation of Smad1 transcriptional activity by Ras-extracellular signal-regulated kinase pathway: a possible mechanism for collagen-dependent osteoblastic differentiation. Journal of Bone and Mineral Research, 2002. **17**(2): p. 240-248.

9. Jikko, A., et al., Collagen integrin receptors regulate early osteoblast differentiation induced by BMP-2. J Bone Miner Res, 1999. **14**(7): p. 1075-83.

10. Xiao, G., et al., Role of the alpha2-integrin in osteoblast-specific gene expression and activation of the Osf2 transcription factor. J Biol Chem, 1998. **273**(49): p. 32988-94.

11. Giachelli, C. and S. Steitz, Osteopontin: a versatile regulator of inflammation and biomineralization. Matrix Biology, 2000. **19**(7): p. 615-622.

12. Huang, W., et al., Osteopontin is a negative regulator of proliferation and differentiation in MC3T3-E1 pre-osteoblastic cells. Bone, 2004. **34**(5): p. 799-808.

13. Ducy, P., et al., Increased bone formation in osteocalcin-deficient mice. Nature, 1996. **382**(6590): p. 448-452.

14. Wan, M., et al., Transcriptional mechanisms of bone morphogenetic protein-induced osteoprotegrin gene expression. J Biol Chem, 2001. **276**(13): p. 10119-25.

15. Gordon, J., et al., Bone sialoprotein expression enhances osteoblast differentiation and matrix mineralization in vitro. Bone, 2007. **41**(3): p. 462-473.

16. Litvin, J., et al., Expression and function of periostin-isoforms in bone. Journal of Cellular Biochemistry, 2004. **92**(5): p. 1044-1061.

17. Kundu, A. and A. Putnam, Vitronectin and collagen I differentially regulate osteogenesis in mesenchymal stem cells. Biochemical and Biophysical Research Communications, 2006. **347**(1): p. 347-357.

18. El-Amin, S., et al., Extracellular matrix production by human osteoblasts cultured on biodegradable polymers applicable for tissue engineering. Biomaterials, 2003. **24**(7): p. 1213-1221.

19. Globus, R., et al., Fibronectin is a survival factor for differentiated osteoblasts. 1998. p. 1385-1393.

20. Hunter, G., et al., Nucleation and inhibition of hydroxyapatite formation by mineralized tissue proteins. Biochemical Journal, 1996. **317**(Pt 1): p. 59.

21. Urist, M.R., et al., Bone regeneration under the influence of a bone morphogenetic protein (BMP) beta tricalcium phosphate (TCP) composite in skull trephine defects in dogs. Clin Orthop Relat Res, 1987(214): p. 295-304.

22. Urist, M.R., Bone: formation by autoinduction. Science, 1965. **150**(698): p. 893-9.

23. Urist, M.R. and B.S. Strates, Bone morphogenetic protein. J Dent Res, 1971. **50**(6): p. 1392-406.

24. Schwartz, Z., et al., Addition of human recombinant bone morphogenetic protein-2 to inactive commercial human demineralized freeze-dried bone allograft makes an effective composite bone inductive implant material. J Periodontol, 1998. **69**(12): p. 1337-45.

25. Bae, H., et al., Intervariability and intravariability of bone morphogenetic proteins in commercially available demineralized bone matrix products. Spine, 2006. **31**(12): p. 1299.

26. Reddi, A.H., Initiation of fracture repair by bone morphogenetic proteins. Clin Orthop Relat Res, 1998(355 Suppl): p. S66-72.

27. Gerber, H.P., et al., VEGF couples hypertrophic cartilage remodeling, ossification and angiogenesis during endochondral bone formation. Nat Med, 1999. **5**(6): p. 623-8.

28. Schipani, E., et al., Regulation of Osteogenesis-Angiogenesis Coupling by HIFs and VEGF. Journal of Bone and Mineral Research, 2009. **24**(8): p. 1347-1353.

29. Mayr-Wohlfart, U., et al., Vascular endothelial growth factor stimulates chemotactic migration of primary human osteoblasts. Bone, 2002. **30**(3): p. 472-7.

30. Emad, B., et al., Vascular endothelial growth factor augments the healing of demineralized bone matrix grafts. Int J Surg, 2006. **4**(3): p. 160-6.

31. Cheng, H., et al., Osteogenic activity of the fourteen types of human bone morphogenetic proteins (BMPs). J Bone Joint Surg Am, 2003. **85-A**(8): p. 1544-52.

32. Bandyopadhyay, A., et al., Genetic Analysis of the Roles of BMP2, BMP4, and BMP7 in Limb Patterning and Skeletogenesis. PLoS Genet, 2006. **2**(12): p. e216.

33. Nakase, T., et al., Transient and localized expression of bone morphogenetic protein 4 messenger RNA during fracture healing. J Bone Miner Res, 1994. **9**(5): p. 651-9.

34. Yoshimura, Y., et al., Colocalization of noggin and bone morphogenetic protein-4 during fracture healing. J Bone Miner Res, 2001. **16**(5): p. 876-84.

35. Tsuji, K., et al., BMP4 is dispensable for skeletogenesis and fracture-healing in the limb. J Bone Joint Surg Am, 2008. **90 Suppl 1**: p. 14-8.

36. Winnier, G., et al., Bone morphogenetic protein-4 is required for mesoderm formation and patterning in the mouse. Genes Dev, 1995. **9**(17): p. 2105-16.

37. Bonewald, L.F., et al., von Kossa staining alone is not sufficient to confirm that mineralization in vitro represents bone formation. Calcif Tissue Int, 2003. **72**(5): p. 537-47.

38. Randle, W.L., et al., Integrated 3-dimensional expansion and osteogenic differentiation of murine embryonic stem cells. Tissue Eng, 2007. **13**(12): p. 2957-70.

39. El-Sabban, M.E., et al., Xenogenic bone matrix extracts induce osteoblastic differentiation of human bone marrow-derived mesenchymal stem cells. Regen Med, 2007. **2**(4): p. 383-90.

40. Katagiri, T., et al., Bone morphogenetic protein-2 converts the differentiation pathway of C2C12 myoblasts into the osteoblast lineage. J Cell Biol, 1994. **127**(6 Pt 1): p. 1755-66.

41. Garreta, E., et al., Osteogenic differentiation of mouse embryonic stem cells and mouse embryonic fibroblasts in a three-dimensional self-assembling peptide scaffold. Tissue Eng, 2006. **12**(8): p. 2215-2227.

42. Glowacki, J., Cellular reactions to bone-derived material. Clin Orthop Relat Res, 1996(324): p. 47-54.

43. Jono, S., et al., Phosphate regulation of vascular smooth muscle cell calcification. Circ Res, 2000. **87**(7): p. E10-7.

44. Fleisch, H. and S. Bisaz, Isolation from urine of pyrophosphate, a calcification inhibitor. Am J Physiol, 1962. **203**: p. 671-5.

45. Johnson, K., et al., Linked deficiencies in extracellular PP(i) and osteopontin mediate pathologic calcification associated with defective PC-1 and ANK expression. J Bone Miner Res, 2003. **18**(6): p. 994-1004.

46. Tenenbaum, H.C., M. Torontali, and B. Sukhu, Effects of bisphosphonates and inorganic pyrophosphate on osteogenesis in vitro. Bone, 1992. **13**(3): p. 249-55.

47. Addison, W.N., et al., Pyrophosphate inhibits mineralization of osteoblast cultures by binding to mineral, up-regulating osteopontin, and inhibiting alkaline phosphatase activity. Journal of Biological Chemistry, 2007. **282**(21): p. 15872.

48. Osathanon, T., C.M. Giachelli, and M.J. Somerman, Immobilization of alkaline phosphatase on microporous nanofibrous fibrin scaffolds for bone tissue engineering. Biomaterials, 2009. **30**(27): p. 4513-21.

49. Pietrzak, W., The Hydration Characteristics of Demineralized and Nondemineralized Allograft Bone: Scientific Perspectives on Graft Function. Journal of Craniofacial Surgery, 2006. **17**(1): p. 120.

50. Lohmann, C.H., et al., Tissue response and osteoinduction of human bone grafts in vivo. Arch Orthop Trauma Surg, 2001. **121**(10): p. 583-90.

51. Wildemann, B., et al., Quantification of various growth factors in different demineralized bone matrix preparations. J Biomed Mater Res A, 2007. **81**(2): p. 437-42.

52. Bae, H., et al., Variability Across Ten Production Lots of a Single Demineralized Bone Matrix Product. The Journal of Bone and Joint Surgery, 2010. **92**(2): p. 427.

53. Schwartz, Z., et al., Ability of commercial demineralized freeze-dried bone allograft to induce new bone formation. Journal of periodontology, 1996. **67**(9): p. 918.

54. Eppley, B.L., W.S. Pietrzak, and M.W. Blanton, Allograft and alloplastic bone substitutes: a review of science and technology for the craniomaxillofacial surgeon. J Craniofac Surg, 2005. **16**(6): p. 981-9.

55. Pietrzak, W., J. Woodell-May, and N. McDonald, Assay of Bone Morphogenetic Protein-2,-4, and-7 in Human Demineralized Bone Matrix. Journal of Craniofacial Surgery, 2006. **17**(1): p. 84.

56. Urist, M.R., S. Kovacs, and K.A. Yates, Regeneration of an enchondroma defect under the influence of an implant of human bone morphogenetic protein. J Hand Surg [Am], 1986. **11**(3): p. 417-9.

57. Swiontkowski, M., et al., Recombinant human bone morphogenetic protein-2 in open tibial fractures. A subgroup analysis of data combined from two prospective randomized studies. The Journal of Bone and Joint Surgery, 2006. **88**(6): p. 1258.

58. Badylak, S.F., et al., Small intestional submucosa: a rapidly resorbed bioscaffold for augmentation cystoplasty in a dog model. Tissue Eng, 1998. **4**(4): p. 379-87.

59. Katz, J., et al., Demineralized bone matrix as an osteoinductive biomaterial and in vitro predictors of its biological potential. Journal of Biomedical Materials Research Part B: Applied Biomaterials, 2009(1).

60. Glowacki, J., A review of osteoinductive testing methods and sterilization processes for demineralized bone. Cell Tissue Bank, 2005. **6**(1): p. 3-12.

61. Honsawek, S., R. Powers, and L. Wolfinbarger, Extractable bone morphogenetic protein and correlation with induced new bone formation in an in vivo assay in the athymic mouse model. Cell and tissue banking, 2005. **6**(1): p. 13-23.

62. WK16591, A., Guide for the in vivo assessment of demineralized bone materials. 2007, ASTM International: West Conshohocken, PA.

63. Ranly, D.M., et al., Platelet-derived growth factor inhibits demineralized bone matrix-induced intramuscular cartilage and bone formation. A study of immunocompromised mice. J Bone Joint Surg Am, 2005. **87**(9): p. 2052-64.

64. McMillan, J., et al., Osteoinductivity of demineralized bone matrix in immunocompromised mice and rats is decreased by ovariectomy and restored by estrogen replacement. Bone, 2007. **40**(1): p. 111-21.

65. Pham, Q., et al., Analysis of the osteoinductive capacity and angiogenicity of an in vitro generated extracellular matrix. Journal of Biomedical Materials Research Part A, 2009(2).

66. Gilbert, T.W., T.L. Sellaro, and S.F. Badylak, Decellularization of tissues and organs. Biomaterials, 2006.

67. Jackson, D.W., et al., Freeze dried anterior cruciate ligament allografts. Preliminary studies in a goat model. Am J Sports Med, 1987. **15**(4): p. 295-303.

68. Jackson, D.W., et al., The effects of in situ freezing on the anterior cruciate ligament. An experimental study in goats. J Bone Joint Surg Am, 1991. **73**(2): p. 201-13.

69. Ngangan, A.V. and T.C. McDevitt, Acellularization of embryoid bodies via physical disruption methods. Biomaterials, 2009. **30**(6): p. 1143-9.

70. Badylak, S.F., Xenogeneic extracellular matrix as a scaffold for tissue reconstruction. Transpl Immunol, 2004. **12**(3-4): p. 367-77.

71. Voytik-Harbin, S.L., et al., Identification of extractable growth factors from small intestinal submucosa. J Cell Biochem, 1997. **67**(4): p. 478-91.

72. McDevitt, C.A., G.M. Wildey, and R.M. Cutrone, Transforming growth factor-beta1 in a sterilized tissue derived from the pig small intestine submucosa. J Biomed Mater Res A, 2003. **67**(2): p. 637-40.

73. Hodde, J.P., D.M. Ernst, and M.C. Hiles, An investigation of the long-term bioactivity of endogenous growth factor in OASIS Wound Matrix. J Wound Care, 2005. **14**(1): p. 23-5.

74. Suzawa, M., et al., Extracellular matrix-associated bone morphogenetic proteins are essential for differentiation of murine osteoblastic cells in vitro. Endocrinology, 1999. **140**(5): p. 2125-33.

75. Evans, N., et al., Extracellular matrix-mediated osteogenic differentiation of murine embryonic stem cells. Biomaterials, 2010.

76. Thibault, R.A., et al., Osteogenic differentiation of mesenchymal stem cells on pregenerated extracellular matrix scaffolds in the absence of osteogenic cell culture supplements. Tissue Eng Part A, 2010. **16**(2): p. 431-40.

77. Thibault, R.A., A.G. Mikos, and F.K. Kasper, Protein and mineral composition of osteogenic extracellular matrix constructs generated with a flow perfusion bioreactor. Biomacromolecules, 2011. **12**(12): p. 4204-12.

78. Datta, N., et al., Effect of bone extracellular matrix synthesized in vitro on the osteoblastic differentiation of marrow stromal cells. Biomaterials, 2005. **26**(9): p. 971-7.

79. Quarto, R., D. Thomas, and C. Liang, Bone progenitor cell deficits and the age-associated decline in bone repair capacity. Calcified tissue international, 1995. **56**(2): p. 123-129.

80. Bellantuono, I., A. Aldahmash, and M. Kassem, Aging of marrow stromal (skeletal) stem cells and their contribution to age-related bone loss. BBA-Molecular Basis of Disease, 2009. **1792**(4): p. 364-370.

81. Becerra, J., et al., Demineralized bone matrix mediates differentiation of bone marrow stromal cells in vitro: effect of age of cell donor. Journal of bone and mineral research: the official journal of the American Society for Bone and Mineral Research, 1996. **11**(11): p. 1703.

82. Christiansen, M., et al., CBFA1 and topoisomerase I mRNA levels decline during cellular aging of human trabecular osteoblasts. Journals of Gerontology Series A: Biological and Medical Sciences, 2000. **55**(4): p. 194-200.

83. Longaker, M.T., et al., Fetal fracture healing in a lamb model. Plast Reconstr Surg, 1992. **90**(2): p. 161-71; discussion 172-3.

84. McCullagh, J.J., P. Gill, and D.J. Wilson, Repair of cartilaginous fractures during chick limb development. J Orthop Res, 1990. **8**(1): p. 127-31.

85. Shahinian, H., et al., Programmed healing of membranous bone in the fetal lamb. Ann Plast Surg, 2005. **54**(1): p. 79-84.

86. Wan, D.C., et al., Global age-dependent differences in gene expression in response to calvarial injury. J Craniofac Surg, 2008. **19**(5): p. 1292-301.

87. Evans, M.J. and M.H. Kaufman, Establishment in culture of pluripotential cells from mouse embryos. Nature, 1981. **292**(5819): p. 154-6.

88. Martin, G.R., Isolation of a pluripotent cell line from early mouse embryos cultured in medium conditioned by teratocarcinoma stem cells. Proc Natl Acad Sci U S A, 1981. **78**(12): p. 7634-8.

89. Doetschman, T.C., et al., The in vitro development of blastocyst-derived embryonic stem cell lines: formation of visceral yolk sac, blood islands and myocardium. J Embryol Exp Morphol, 1985. **87**: p. 27-45.

90. Thomson, J.A., et al., Isolation of a primate embryonic stem cell line. Proc Natl Acad Sci U S A, 1995. **92**(17): p. 7844-8.

91. Thomson, J.A., et al., Pluripotent cell lines derived from common marmoset (Callithrix jacchus) blastocysts. Biol Reprod, 1996. **55**(2): p. 254-9.

92. Thomson, J.A., et al., Embryonic stem cell lines derived from human blastocysts. Science, 1998. **282**(5391): p. 1145-7.

93. Reubinoff, B.E., et al., Embryonic stem cell lines from human blastocysts: somatic differentiation in vitro. Nature Biotechnology, 2000. **18**(4): p. 399-404.

94. Takahashi, K., et al., Induction of pluripotent stem cells from adult human fibroblasts by defined factors. Cell, 2007.

95. Yu, J., et al., Induced pluripotent stem cell lines derived from human somatic cells. Science, 2007. **318**(5858): p. 1917.

96. Meissner, A., M. Wernig, and R. Jaenisch, Direct reprogramming of genetically unmodified fibroblasts into pluripotent stem cells. Nature Biotechnology, 2007. **25**(10): p. 1177-1181.

97. Park, I., et al., Reprogramming of human somatic cells to pluripotency with defined factors. 2007.

98. Belmonte, J., et al., Induced pluripotent stem cells and reprogramming: seeing the science through the hype. Nature Reviews Genetics, 2009.

99. Bratt-Leal, A.M., R.L. Carpenedo, and T.C. McDevitt, Engineering the embryoid body microenvironment to direct embryonic stem cell differentiation. Biotechnol Prog, 2009. **25**(1): p. 43-51.

100. Desbaillets, I., et al., Embryoid bodies: an in vitro model of mouse embryogenesis. Exp Physiol, 2000. **85**(6): p. 645-51.

101. Hopfl, G., M. Gassmann, and I. Desbaillets, Differentiating embryonic stem cells into embryoid bodies. Methods Mol Biol, 2004. **254**: p. 79-98.

102. Carpenedo, R.L., et al., Homogeneous and organized differentiation within embryoid bodies induced by microsphere-mediated delivery of small molecules. Biomaterials, 2009. **30**(13): p. 2507-15.

103. Buttery, L.D., et al., Differentiation of osteoblasts and in vitro bone formation from murine embryonic stem cells. Tissue Engineering, 2001. **7**(1): p. 89-99.

104. Phillips, B.W., et al., Compactin enhances osteogenesis in murine embryonic stem cells. Biochem Biophys Res Commun, 2001. **284**(2): p. 478-84.

105. zur Nieden, N.I., G. Kempka, and H.J. Ahr, In vitro differentiation of embryonic stem cells into mineralized osteoblasts. Differentiation, 2003. **71**(1): p. 18-27.

106. Bielby, R., et al., In vitro differentiation and in vivo mineralization of osteogenic cells derived from human embryonic stem cells. Tissue Engineering, 2004. **10**(9-10): p. 1518-1525.

107. Conrads, K.A., et al., A combined proteome and microarray investigation of inorganic phosphate-induced pre-osteoblast cells. Mol Cell Proteomics, 2005. **4**(9): p. 1284-96.

108. Jaiswal, N., et al., Osteogenic differentiation of purified, culture-expanded human mesenchymal stem cells in vitro. J Cell Biochem, 1997. **64**(2).

109. Liu, P., et al., Regulation of osteogenic differentiation of human bone marrow stromal cells: interaction between transforming growth factor-ß and 1, 25 (OH) 2 vitamin D 3 in vitro. Calcified tissue international, 1999. **65**(2): p. 173-180.

110. Shimko, D.A., et al., Comparison of in vitro mineralization by murine embryonic and adult stem cells cultured in an osteogenic medium. Tissue Eng, 2004. **10**(9-10): p. 1386-98.

111. Bielby, R.C., et al., Enhanced derivation of osteogenic cells from murine embryonic stem cells after treatment with ionic dissolution products of 58S bioactive sol-gel glass. Tissue Eng, 2005. **11**(3-4): p. 479-88.

112. Kawaguchi, J., P.J. Mee, and A.G. Smith, Osteogenic and chondrogenic differentiation of embryonic stem cells in response to specific growth factors. Bone, 2005. **36**(5): p. 758-69.

113. Handschel, J., et al., Induction of osteogenic markers in differentially treated cultures of embryonic stem cells. Head Face Med, 2008. **4**: p. 10.

114. Tielens, S., et al., Effect of 17beta-estradiol on the in vitro differentiation of murine embryonic stem cells into the osteogenic lineage. In Vitro Cell Dev Biol Anim, 2008. **44**(8-9): p. 368-78.

115. Beck, J., GR, B. Zerler, and E. Moran, Phosphate is a specific signal for induction of osteopontin gene expression. Proc Natl Acad Sci U S A, 2000. **97**(15): p. 8352-57.

116. Beck, G.R. and N. Knecht, Osteopontin regulation by inorganic phosphate is ERK1/2-, protein kinase C-, and proteasome-dependent. Journal of Biological Chemistry, 2003. **278**(43): p. 41921.

117. Stein, G., et al., Runx2 control of organization, assembly and activity of the regulatory machinery for skeletal gene expression. Oncogene, 2004. **23**: p. 4315-4329.

118. Nielsen, L.B., F.S. Pedersen, and L. Pedersen, Expression of type III sodium-dependent phosphate transporters/retroviral receptors mRNAs during osteoblast differentiation. Bone, 2001. **28**(2): p. 160-166.

119. Suzuki, A., et al., Enhanced Expression of the Inorganic Phosphate Transporter Pit 1 Is Involved in BMP 2–Induced Matrix Mineralization in Osteoblast Like Cells. Journal of Bone and Mineral Research, 2006. **21**(5): p. 674-683.

120. Li, X., H.Y. Yang, and C.M. Giachelli, BMP-2 promotes phosphate uptake, phenotypic modulation, and calcification of human vascular smooth muscle cells. Atherosclerosis, 2008. **199**(2): p. 271-7.

121. Kimata, M., et al., Signaling of extracellular inorganic phosphate up-regulates cyclin D1 expression in proliferating chondrocytes via the Na+/Pi cotransporter Pit-1 and Raf/MEK/ERK pathway. Bone, 2010. **47**(5): p. 938-947.

122. Denison, T.A., et al., Inorganic phosphate modulates responsiveness to 24,25(OH)2D3 in chondrogenic ATDC5 cells. J Cell Biochem, 2009. **107**(1): p. 155-62.

123. Guicheux, J., et al., A novel in vitro culture system for analysis of functional role of phosphate transport in endochondral ossification. Bone, 2000. **27**(1): p. 69-74.

124. Li, X., H.Y. Yang, and C.M. Giachelli, Role of the sodium-dependent phosphate cotransporter, Pit-1, in vascular smooth muscle cell calcification. Circ Res, 2006. **98**(7): p. 905-12.

125. Gallea, S., et al., Activation of mitogen-activated protein kinase cascades is involved in regulation of bone morphogenetic protein-2-induced osteoblast differentiation in pluripotent C2C12 cells. Bone, 2001. **28**(5): p. 491-8.

126. Chen, J., et al., Protein-disulfide isomerase-associated 3 (Pdia3) mediates the membrane response to 1,25-dihydroxyvitamin D3 in osteoblasts. J Biol Chem, 2010. **285**(47): p. 37041-50.

127. Jun, J.H., et al., BMP2-activated Erk/MAP kinase stabilizes Runx2 by increasing p300 levels and histone acetyltransferase activity. J Biol Chem, 2010. **285**(47): p. 36410-9.

128. Ravera, S., et al., Deciphering PiT transport kinetics and substrate specificity using electrophysiology and flux measurements. Am J Physiol Cell Physiol, 2007. **293**(2): p. C606-20.

129. Villa-Bellosta, R. and V. Sorribas, Phosphonoformic acid prevents vascular smooth muscle cell calcification by inhibiting calcium-phosphate deposition. Arterioscler Thromb Vasc Biol, 2009. **29**(5): p. 761-6.

130. Sage, A.P., et al., Hyperphosphatemia-induced nanocrystals upregulate the expression of bone morphogenetic protein-2 and osteopontin genes in mouse smooth muscle cells in vitro. Kidney Int, 2011. **79**(4): p. 414-22.

131. Villa-Bellosta, R., A. Millan, and V. Sorribas, Role of calcium-phosphate deposition in vascular smooth muscle cell calcification. American Journal of Physiology- Cell Physiology, 2010.

132. Khoshniat, S., et al., Phosphate-dependent stimulation of MGP and OPN expression in osteoblasts via the ERK1/2 pathway is modulated by calcium. Bone, 2011. **48**(4): p. 894-902.

133. Tada, H., et al., Phosphate increases bone morphogenetic protein-2 expression through cAMP-dependent protein kinase and ERK1/2 pathways in human dental pulp cells. Bone, 2011. **48**(6): p. 1409-16.

134. Speer, M.Y., et al., Smooth muscle cells give rise to osteochondrogenic precursors and chondrocytes in calcifying arteries. Circulation research, 2009: p. CIRCRESAHA. 108.183053 v1.

135. Lou, J., et al., Involvement of ERK in BMP-2 induced osteoblastic differentiation of mesenchymal progenitor cell line C3H10T1/2. Biochem Biophys Res Commun, 2000. **268**(3): p. 757-62.

136. Choi, Y.H., et al., Osterix is regulated by Erk1/2 during osteoblast differentiation. Biochem Biophys Res Commun, 2011. **415**(3): p. 472-8.

137. Jurutka, P.W., et al., Vitamin D receptor: key roles in bone mineral pathophysiology, molecular mechanism of action, and novel nutritional ligands. J Bone Miner Res, 2007. **22 Suppl 2**: p. V2-10.

138. Khanal, R.C. and I. Nemere, The ERp57/GRp58/1,25D3-MARRS receptor: multiple functional roles in diverse cell systems. Curr Med Chem, 2007. **14**(10): p. 1087-93.

139. Boyan, B.D., et al., Plasma membrane requirements for 1alpha,25(OH)2D3 dependent PKC signaling in chondrocytes and osteoblasts. Steroids, 2006. **71**(4): p. 286-90.

140. Zanello, L.P. and A. Norman, 1alpha,25(OH)2 vitamin D3 actions on ion channels in osteoblasts. Steroids, 2006. **71**(4): p. 291-7.

141. Breen, E.C., et al., In vivo occupancy of the vitamin D responsive element in the osteocalcin gene supports vitamin D-dependent transcriptional upregulation in intact cells. Proc Natl Acad Sci U S A, 1994. **91**(26): p. 12902-6.

142. Kraichely, D.M. and P.N. MacDonald, Transcriptional activation through the vitamin D receptor in osteoblasts. Front Biosci, 1998. **3**: p. d821-33.

143. Zanello, L.P. and A.W. Norman, Electrical responses to 1alpha,25(OH)2-Vitamin D3 and their physiological significance in osteoblasts. Steroids, 2004. **69**(8-9): p. 561-5.

144. Baran, D.T., Nongenomic actions of the steroid hormone 1 alpha,25-dihydroxyvitamin D3. J Cell Biochem, 1994. **56**(3): p. 303-6.

145. Wali, R.K., et al., Vitamin D receptor is not required for the rapid actions of 1,25-dihydroxyvitamin D3 to increase intracellular calcium and activate protein kinase C in mouse osteoblasts. J Cell Biochem, 2003. **88**(4): p. 794-801.

146. Schwartz, Z., et al., Differential regulation of prostaglandin E2 synthesis and phospholipase A2 activity by 1,25-(OH)2D3 in three osteoblast-like cell lines (MC-3T3-E1, ROS 17/2.8, and MG-63). Bone, 1992. **13**(1): p. 51-8.

147. Carpenedo, R.L., C.Y. Sargent, and T.C. McDevitt, Rotary suspension culture enhances the efficiency, yield, and homogeneity of embryoid body differentiation. Stem Cells, 2007. **25**(9): p. 2224-34.

148. Ungrin, M.D., et al., Reproducible, ultra high-throughput formation of multicellular organization from single cell suspension-derived human embryonic stem cell aggregates. PLoS ONE, 2008. **3**(2): p. e1565.

149. Pfaffl, M.W., A new mathematical model for relative quantification in real-time RT-PCR. Nucleic Acids Res, 2001. **29**(9): p. e45.

150. Yeung, Y.G. and E.R. Stanley, A solution for stripping antibodies from polyvinylidene fluoride immunoblots for multiple reprobing. Anal Biochem, 2009. **389**(1): p. 89-91.

151. Spitzer, J.J., A primer on Box-Cox estimation. The Review of Economics and Statistics, 1982. **64**(2): p. 307-313.

152. Nelson, T.J., A. Martinez-Fernandez, and A. Terzic, Induced pluripotent stem cells: developmental biology to regenerative medicine. Nat Rev Cardiol, 2010. **7**(12): p. 700-10.

153. Kitagawa, M. and T. Era, Differentiation of mesodermal cells from pluripotent stem cells. Int J Hematol, 2010. **91**(3): p. 373-83.

154. Yamada, T., et al., In vitro differentiation of embryonic stem cells into hepatocyte-like cells identified by cellular uptake of indocyanine green. Stem Cells, 2002. **20**(2): p. 146-54.

155. Cohen, S., et al., Repair of full-thickness tendon injury using connective tissue progenitors efficiently derived from human embryonic stem cells and fetal tissues. Tissue Eng Part A, 2010.

156. Kong, C.W., F.G. Akar, and R.A. Li, Translational potential of human embryonic and induced pluripotent stem cells for myocardial repair: Insights from experimental models. Thromb Haemost, 2010. **104**(1).

157. Kane, N.M., et al., Derivation of endothelial cells from human embryonic stem cells by directed differentiation: analysis of microRNA and angiogenesis in vitro and in vivo. Arterioscler Thromb Vasc Biol, 2010. **30**(7): p. 1389-97.

158. Lee, H., et al., Directed differentiation and transplantation of human embryonic stem cell-derived motoneurons. Stem Cells, 2007. **25**(8): p. 1931-9.

159. Doevendans, P.A., et al., Differentiation of cardiomyocytes in floating embryoid bodies is comparable to fetal cardiomyocytes. J Mol Cell Cardiol, 2000. **32**(5): p. 839-51.

160. Sargent, C.Y., et al., Hydrodynamic modulation of embryonic stem cell differentiation by rotary orbital suspension culture. Biotechnol Bioeng, 2010. **105**(3): p. 611-26.

161. Coucouvanis, E. and G.R. Martin, Signals for death and survival: a two-step mechanism for cavitation in the vertebrate embryo. Cell, 1995. **83**(2): p. 279-87.

162. Keller, G.M., In vitro differentiation of embryonic stem cells. Curr Opin Cell Biol, 1995. **7**(6): p. 862-9.

163. Conley, B.J., et al., Derivation, propagation and differentiation of human embryonic stem cells. Int J Biochem Cell Biol, 2004. **36**(4): p. 555-67.

164. Kurosawa, H., Methods for inducing embryoid body formation: in vitro differentiation system of embryonic stem cells. J Biosci Bioeng, 2007. **103**(5): p. 389-98.

165. Furedi-Milhofer, H., et al., Interactions of matrix proteins from mineralized tissues with octacalcium phosphate. Connect Tissue Res, 1994. **30**(4): p. 251-64.

166. Golub, E.E. and K. Boesze-Battaglia, The role of alkaline phosphatase in mineralization. Current Opinion in Orthopaedics, 2007. **18**(5): p. 444-448 10.1097/BCO.0b013e3282630851.

167. Porter, R.M., W.R. Huckle, and A.S. Goldstein, Effect of dexamethasone withdrawal on osteoblastic differentiation of bone marrow stromal cells. J Cell Biochem, 2003. **90**(1): p. 13-22.

168. Castano-Izquierdo, H., et al., Pre-culture period of mesenchymal stem cells in osteogenic media influences their in vivo bone forming potential. J Biomed Mater Res A, 2007. **82**(1): p. 129-38.

169. Heng, B.C., et al., Strategies for directing the differentiation of stem cells into the osteogenic lineage in vitro. J Bone Miner Res, 2004. **19**(9): p. 1379-94.

170. van Leeuwen, J.P., et al., Vitamin D control of osteoblast function and bone extracellular matrix mineralization. Crit Rev Eukaryot Gene Expr, 2001. **11**(1-3): p. 199-226.

171. Kuske, B., V. Savkovic, and N.I. zur Nieden, Improved media compositions for the differentiation of embryonic stem cells into osteoblasts and chondrocytes. Methods Mol Biol, 2011. **690**: p. 195-215.

172. St-Arnaud, R., The direct role of vitamin D on bone homeostasis. Arch Biochem Biophys, 2008. **473**(2): p. 225-30.

173. Paredes, R., et al., Bone-specific transcription factor Runx2 interacts with the 1alpha,25-dihydroxyvitamin D3 receptor to up-regulate rat osteocalcin gene expression in osteoblastic cells. Mol Cell Biol, 2004. **24**(20): p. 8847-61.

174. Hwang, Y.S., et al., The use of murine embryonic stem cells, alginate encapsulation, and rotary microgravity bioreactor in bone tissue engineering. Biomaterials, 2008.

175. Langenbach, F., et al., Osteogenic Differentiation Influences Stem Cell Migration Out of Scaffold-Free Microspheres. Tissue Eng Part A, 2010. **16**(2): p. 759.

176. Alfred, R., et al., Serum-free scaled up expansion and differentiation of murine embryonic stem cells to osteoblasts in suspension bioreactors. Biotechnol Bioeng, 2010. **106**(5): p. 829-40.

177. Taiani, J.T., et al., Reduced differentiation efficiency of murine embryonic stem cells in stirred suspension bioreactors. Stem Cells Dev, 2010. **19**(7): p. 989-98.

178. Takahashi, N., et al., Regulatory mechanism of osteoclastogenesis by RANKL and Wnt signals. Front Biosci, 2011. **16**: p. 21-30.

179. van den Bemd, G.J., et al., A central dinucleotide within vitamin D response elements modulates DNA binding and transactivation by the vitamin D receptor in cellular response to natural and synthetic ligands. J Biol Chem, 2002. **277**(17): p. 14539-46.

180. Martin, J.Y., et al., Proliferation, differentiation, and protein synthesis of human osteoblast-like cells (MG63) cultured on previously used titanium surfaces. Clin Oral Implants Res, 1996. **7**(1): p. 27-37.

181. Duplomb, L., et al., Concise review: embryonic stem cells: a new tool to study osteoblast and osteoclast differentiation. Stem Cells, 2007. **25**(3): p. 544-52.

182. Guldberg, R.E., et al., Analyzing bone, blood vessels, and biomaterials with microcomputed tomography. IEEE Eng Med Biol Mag, 2003. **22**(5): p. 77-83.

183. Guldberg, R., et al., 3D imaging of tissue integration with porous biomaterials. Biomaterials, 2008. **29**(28): p. 3757-3761.

184. Sargent, C.Y., G.Y. Berguig, and T.C. McDevitt, Cardiomyogenic differentiation of embryoid bodies is promoted by rotary orbital suspension culture. Tissue Engineering Part A, 2009. **15**(2): p. 331-342.

185. Duplomb, L., et al., Differentiation of osteoblasts from mouse embryonic stem cells without generation of embryoid body. In Vitro Cell Dev Biol Anim, 2007. **43**(1): p. 21-4.

186. Karp, J.M., et al., Cultivation of human embryonic stem cells without the embryoid body step enhances osteogenesis in vitro. Stem Cells, 2006. **24**(4): p. 835-43.

187. Kato, S., et al., In vivo function of VDR in gene expression-VDR knock-out mice. J Steroid Biochem Mol Biol, 1999. **69**(1-6): p. 247-51.

188. Lee, C.S., et al., Coordinated tether formation in anatomically distinct mice growth centers is dependent on a functional vitamin D receptor and is tightly linked to three-dimensional tissue morphology. Bone, 2011.

189. Tunsophon, S. and I. Nemere, Protein kinase C isotypes in signal transduction for the 1,25D3-MARRS receptor (ERp57/PDIA3) in steroid hormone-stimulated phosphate uptake. Steroids, 2010. **75**(4-5): p. 307-13.

190. Wang, Y., et al., Disruption of Pdia3 gene results in bone abnormality and affects 1alpha,25-dihydroxy-vitamin D3-induced rapid activation of PKC. J Steroid Biochem Mol Biol, 2010. **121**(1-2): p. 257-60.

191. Olivares-Navarrete, R., et al., Integrin alpha2beta1 plays a critical role in osteoblast response to micron-scale surface structure and surface energy of titanium substrates. Proc Natl Acad Sci U S A, 2008. **105**(41): p. 15767-72.

192. Schwartz, Z., et al., Beta-1 integrins mediate substrate dependent effects of 1alpha,25(OH)2D3 on osteoblasts. J Steroid Biochem Mol Biol, 2007. **103**(3-5): p. 606-9.

193. Wang, L., et al., Integrin beta1 silencing in osteoblasts alters substrate-dependent responses to 1,25-dihydroxy vitamin D3. Biomaterials, 2006. **27**(20): p. 3716-25.

194. Bain, G., et al., Embryonic stem cells express neuronal properties in vitro. Dev Biol, 1995. **168**(2): p. 342-57.

195. McCloskey, K.E., M.E. Gilroy, and R.M. Nerem, Use of embryonic stem cell-derived endothelial cells as a cell source to generate vessel structures in vitro. Tissue Eng, 2005. **11**(3-4): p. 497-505.

196. zur Nieden, N.I., et al., Induction of chondro-, osteo- and adipogenesis in embryonic stem cells by bone morphogenetic protein-2: effect of cofactors on differentiating lineages. BMC Dev Biol, 2005. **5**: p. 1.

197. Bratt-Leal, A.M., et al., Incorporation of biomaterials in multicellular aggregates modulates pluripotent stem cell differentiation. Biomaterials, 2011. **32**(1): p. 48-56.

198. Bourne, S., et al., Osteogenic differentiation of mouse embryonic stem cells: differential gene expression analysis by cDNA microarray and purification of osteoblasts by cadherin-11 magnetically activated cell sorting. Tissue Eng, 2004. **10**(5-6): p. 796-806.

199. Bellows, C.G., J.N.M. Heersche, and J.E. Aubin, Inorganic phosphate added exogenously or released from [beta]-glycerophosphate initiates mineralization of osteoid nodules in vitro. Bone and Mineral, 1992. **17**(1): p. 15-29.

200. Chung, C.H., et al., Mechanism of action of beta-glycerophosphate on bone cell mineralization. Calcif Tissue Int, 1992. **51**(4): p. 305-11.

201. Fleisch, H., R.G. Russell, and F. Straumann, Effect of pyrophosphate on hydroxyapatite and its implications in calcium homeostasis. Nature, 1966. **212**(5065): p. 901-3.

202. Demer, L.L. and Y. Tintut, Vascular calcification: pathobiology of a multifaceted disease. Circulation, 2008. **117**(22): p. 2938-48.

203. Bauwens, C.L., et al., Control of human embryonic stem cell colony and aggregate size heterogeneity influences differentiation trajectories. Stem Cells, 2008. **26**(9): p. 2300-10.

204. Niebruegge, S., et al., Generation of human embryonic stem cell-derived mesoderm and cardiac cells using size-specified aggregates in an oxygen-controlled bioreactor. Biotechnol Bioeng, 2009. **102**(2): p. 493-507.

205. Xiao, G., et al., MAPK pathways activate and phosphorylate the osteoblast-specific transcription factor, Cbfa1. J Biol Chem, 2000. **275**(6): p. 4453-9.

206. Lian, J., et al., Structure of the rat osteocalcin gene and regulation of vitamin D-dependent expression. Proc Natl Acad Sci U S A, 1989. **86**(4): p. 1143-1147.

207. Manolagas, S., D. Burton, and L. Deftos, 1, 25-Dihydroxyvitamin D3 stimulates the alkaline phosphatase activity of osteoblast-like cells. J Biol Chem, 1981. **256**(14): p. 7115-7117.

208. Habibovic, P., et al., 3D microenvironment as essential element for osteoinduction by biomaterials. Biomaterials, 2005. **26**(17): p. 3565-75.

209. Habibovic, P., et al., Osteoinduction by biomaterials--physicochemical and structural influences. J Biomed Mater Res A, 2006. **77**(4): p. 747-62.

210. Kundu, A., C. Khatiwala, and A. Putnam, Extracellular Matrix Remodeling, Integrin Expression, and Downstream Signaling Pathways Influence the Osteogenic Differentiation of Mesenchymal Stem Cells on Poly (Lactide-Co-Glycolide) Substrates. Tissue Eng Part A, 2008. **15**(2): p. 273-283.

211. Beck, G.R., Jr., E. Moran, and N. Knecht, Inorganic phosphate regulates multiple genes during osteoblast differentiation, including Nrf2. Exp Cell Res, 2003. **288**(2): p. 288-300.

212. Marsh, M.E., et al., Mineralization of bone-like extracellular matrix in the absence of functional osteoblasts. Journal of Bone and Mineral Research, 1995. **10**(11): p. 1635-1643.

213. Jongpaiboonkit, L., T. Franklin-Ford, and W.L. Murphy, Growth of hydroxyapatite coatings on biodegradable polymer microspheres. ACS Appl Mater Interfaces, 2009. **1**(7): p. 1504-11.

214. Ripamonti, U., et al., The induction of bone formation by smart biphasic hydroxyapatite tricalcium phosphate biomimetic matrices in the non-human primate Papio ursinus. J Cell Mol Med, 2008. **12**(6B): p. 2609-21.

215. Olivares-Navarrete, R., et al., Direct and indirect effects of microstructured titanium substrates on the induction of mesenchymal stem cell differentiation towards the osteoblast lineage. Biomaterials, 2010. **31**(10): p. 2728-35.

216. Gittens, R.A., et al., The effects of combined micron-/submicron-scale surface roughness and nanoscale features on cell proliferation and differentiation. Biomaterials, 2011. **32**(13): p. 3395-403.

217. Engler, A.J., et al., Matrix elasticity directs stem cell lineage specification. Cell, 2006. **126**(4): p. 677-89.

218. De Long, W.G., Jr., et al., Bone grafts and bone graft substitutes in orthopaedic trauma surgery. A critical analysis. J Bone Joint Surg Am, 2007. **89**(3): p. 649-58.

219. Sampath, T.K. and A.H. Reddi, Distribution of bone inductive proteins in mineralized and demineralized extracellular matrix. Biochem Biophys Res Commun, 1984. **119**(3): p. 949-54.

220. Boyan, B., et al., Potential of porous poly-D, L-lactide-co-glycolide particles as a carrier for recombinant human bone morphogenetic protein-2 during osteoinduction in vivo. Journal of biomedical materials research, 1999. **46**(1).

221. Carnes Jr, D., et al., Evaluation of 2 novel approaches for assessing the ability of demineralized freeze-dried bone allograft to induce new bone formation. Journal of periodontology, 1999. **70**(4): p. 353-363.

222. Boyan, B., D. Ranly, and Z. Schwartz, Use of growth factors to modify osteoinductivity of demineralized bone allografts: lessons for tissue engineering of bone. Dental Clinics of North America, 2006. **50**(2): p. 217-228.

223. Boyan, B.D., et al., Porcine fetal enamel matrix derivative enhances bone formation induced by demineralized freeze dried bone allograft in vivo. J Periodontol, 2000. **71**(8): p. 1278-86.

224. Pham, Q.P., et al., The influence of an in vitro generated bone-like extracellular matrix on osteoblastic gene expression of marrow stromal cells. Biomaterials, 2008. **29**(18): p. 2729-39.

225. Nair, R., A.V. Ngangan, and T.C. McDevitt, Efficacy of solvent extraction methods for acellularization of embryoid bodies. J Biomater Sci Polym Ed, 2008. **19**(6): p. 801-19.

226. Nair, R., S. Shukla, and T.C. McDevitt, Acellular matrices derived from differentiating embryonic stem cells. J Biomed Mater Res A, 2008.

227. Sterehi, D.L. and L.R. Keefer, Modified Mallory aniline blue stain for bone, cartilage, and other connective tissues. Journal of histotechnology, 1998. **21**(2): p. 129-133.

228. Schwartz, Z., et al., Effect of glass ceramic and titanium implants on primary calcification during rat tibial bone healing. Calcif Tissue Int, 1991. **49**(5): p. 359-64.

229. Kruskal, W.H. and W.A. Wallis, Use of ranks in one-criterion variance analysis. Journal of the American statistical Association, 1952: p. 583-621.

230. CfDEa, R., Guideline on Validation of the Limulus Amebocyte Lysate Test as an End-Product Endotoxin Test for Human and Animal Parenteral Drugs, Biological Products, and Medical Devices, in In:US Department of Health and Human Services FaDA, editor. 1997: Rockville, MD.

231. Cordonnier, T., et al., Consistent osteoblastic differentiation of human mesenchymal stem cells with bone morphogenetic protein 4 and low serum. Tissue Eng Part C Methods, 2011. **17**(3): p. 249-59.

232. Vicente Lopez, M.A., et al., Low doses of bone morphogenetic protein 4 increase the survival of human adipose-derived stem cells maintaining their stemness and multipotency. Stem Cells Dev, 2011. **20**(6): p. 1011-9.

233. Huang, Y.C., et al., Combined angiogenic and osteogenic factor delivery enhances bone marrow stromal cell-driven bone regeneration. J Bone Miner Res, 2005. **20**(5): p. 848-57.

234. Blum, B., et al., Measurement of bone morphogenetic proteins and other growth factors in demineralized bone matrix. Orthopedics(Thorofare), 2004. **27**(1).

235. Price, P.A., et al., Evidence for a serum factor that initiates the re-calcification of demineralized bone. J Biol Chem, 2004. **279**(18): p. 19169-80.

236. Hamlin, N.J. and P.A. Price, Mineralization of decalcified bone occurs under cell culture conditions and requires bovine serum but not cells. Calcif Tissue Int, 2004. **75**(3): p. 231-42.

237. Schwartz, Z., et al., Differential effects of bone graft substitutes on regeneration of bone marrow. Clin Oral Implants Res, 2008. **19**(12): p. 1233-45.

238. Amsel, S., et al., The significance of intramedullary cancellous bone formation in the repair of bone marrow tissue. Anat Rec, 1969. **164**(1): p. 101-11.

239. Reyes, C.D. and A.J. Garcia, Alpha2beta1 integrin-specific collagen-mimetic surfaces supporting osteoblastic differentiation. J Biomed Mater Res A, 2004. **69**(4): p. 591-600.

240. Hwang, Y.S., J.M. Polak, and A. Mantalaris, In vitro direct osteogenesis of murine embryonic stem cells without embryoid body formation. Stem Cells Dev, 2008. **17**(5): p. 963-70.

241. Hwang, Y.S., et al., Enhanced derivation of osteogenic cells from murine embryonic stem cells after treatment with HepG2-conditioned medium and modulation of the embryoid body formation period: application to skeletal tissue engineering. Tissue Eng, 2006. **12**(6): p. 1381-92.

242. Sharma, M., et al., Stromal-derived factor-1/CXCR4 signaling: indispensable role in homing and engraftment of hematopoietic stem cells in bone marrow. Stem Cells Dev, 2011. **20**(6): p. 933-46.

243. Guo, Y., et al., SDF-1/CXCL12 enhances survival and chemotaxis of murine embryonic stem cells and production of primitive and definitive hematopoietic progenitor cells. Stem Cells, 2005. **23**(9): p. 1324-32.

244. Xiao, G., et al., Bone morphogenetic proteins, extracellular matrix, and mitogen-activated protein kinase signaling pathways are required for osteoblast-specific gene expression and differentiation in MC3T3-E1 cells. J Bone Miner Res, 2002. **17**(1): p. 101-10.

245. Webber, M.J., et al., Capturing the stem cell paracrine effect using heparin-presenting nanofibres to treat cardiovascular diseases. J Tissue Eng Regen Med, 2010. **4**(8): p. 600-10.

246. Marden, L.J., et al., Recombinant human bone morphogenetic protein-2 is superior to demineralized bone matrix in repairing craniotomy defects in rats. J Biomed Mater Res, 1994. **28**(10): p. 1127-38.

247. Ginting, N., L. Tremblay, and J.B. Kortbeek, Surgisis(R) in the management of the complex abdominal wall in trauma: a case series and review of the literature. Injury, 2010. **41**(9): p. 970-3.

248. Luciani, G.B., F. Santini, and A. Mazzucco, Autografts, homografts, and xenografts: overview on stentless aortic valve surgery. J Cardiovasc Med (Hagerstown), 2007. **8**(2): p. 91-6.